Water-in-Oil Microemulsions: Counterion Effects in AOT Systems and New Fluorocarbon-based Microemulsion Gels

WATER-IN-OIL MICROEMULSIONS: COUNTERION EFFECTS IN AOT SYSTEMS AND NEW FLUOROCARBON-BASED MICROEMULSION GELS

A Dissertation Presented

by

XIAOMING PAN

Submitted to the Graduate School of the

University of Massachusetts Amherst in partial fulfillment

of the requirements for the degree of

DOCTOR OF PHILOSOPHY

February 2010

Chemical Engineering

WATER-IN-OIL MICROEMULSIONS: COUNTERION EFFECTS IN AOT SYSTEMS AND NEW FLUOROCARBON-BASED MICROEMULSION GELS

A Dissertation Presented

by

XIAOMING PAN

Approved as to style and content by:

Surita R. Bhatia, Committee Chair

Susan C. Roberts, Committee Member

Paul L. Dubin, Committee Member

T. J. Mountziaris, Department Head
Department of Chemical Engineering

DEDICATION

To my parents and my wife.

ACKNOWLEDGMENTS

It is time to say goodbye to my student life again. It has been 6 years since I decided to take this long adventure journey. “Life is a box of chocolate.” (Forrest Gump) It is true. Turning back to school after 8 years of working in industry, I collected more tastes of chocolates than before. Looking back to this long time journey that I didn’t give up, looking back to those desperate and exciting moments that I never experienced, I should thank a lot of people who have supported, encouraged, assisted, and even stimulated me to go through this way.

The first person I should thank is my thesis advisor, Prof. Surita R. Bhatia, who is always supportive to the students. I am fortunate to have her as my advisor. I thank her for leading me into this awesomely interesting research field of biomaterials with her great mentorship and guidance, thank her for generous support and kind considerations, the freedom and flexibility to be creativity.

I thank my dissertation committee members, Prof. Paul L. Dubin and Prof. Susan C. Roberts, for their precious time and great patience, especially their valuable advice that are very helpful and inspiring in my research.

I thank Hoagland/Dubin/Rothstein/Bhatia super group for providing me a nice environment to hone my presentation skills and providing me tremendous advice.

I thank Huber group and Ford group for welcoming me to participate into bio-oil field, which is so hot in recent years. I thank Prof. Huber and Prof. Ford for their generous support and open advice in research.

I thank Prof. Winter, Prof. Maroudas, Prof. Conner, Prof. Sun, Prof. Monson and Prof. Davis for their great instruction in classes. Thank Bobbie for her patient and considerate assistance. Thank Cheryl for her instructions and tips in resume and interview.

I was very lucky to have met one dozen groups of wonderful classmates and friends who shared class time, lab bench work, sports, travel, and life experience with me. They brought me a lot of fun. The memories are enjoyable.

I thank my labmates, Seo, Smitha, Hossein, Sarvesh, Soumitra, David, Neha, Paraveen, and Mark, for their support, assistance, encouragement, and travel fellowship.

I thank Bing, Eunyoung, Monica, Bernabe, Andres, Linda, Lin, Wei, Yan, Qi, Xilian (Jun), Lingling, Wenjun, Yingfeng, Xiaoying, Maohua, Zhongzhou, Shoujun, Ling, and other classmates, officemates and friends in chemical engineering, for their supporting, discussing, advising, and encouraging me.

I thank Xianbo, Zhixiang, Zhiyuan, Jianing, Jiafang, Jinbo, and Liming for listening, supporting, encouraging, and making me feel like at home while stay in USA.

I thank Bernabe, Yoan, Chin, Kim, Marty, and other soccer teammates for their organization and fellowship in soccer games, which has enriched my life in Amherst.

I thank Tianhong, Xiaoxia, Tao, Rong, Jincai, Yajuan, Cuihong, Yiming, and Rongsheng for great help with job hunting.

I cannot come here and stay here for so many years without the unconditional love and support from my family. They gave me strong wings to chase my dream and travel around the world. I know they are always watching and supporting me regardless of outcome. Especially thank my wife for coming here and keeping company with me through the whole tough life.

ABSTRACT

WATER-IN-OIL MICROEMULSIONS: COUNTERION EFFECTS IN AOT SYSTEMS AND NEW FLUOROCARBON-BASED MICROEMULSION GELS

FEBRUARY 2010

XIAOMING PAN, B.S., TSINGHUA UNIVERSITY

Ph.D., UNIVERSITY OF MASSACHUSETTS AMHERST

Directed by: Professor Surita R. Bhatia

Microemulsions have important applications in various industries, including enhanced oil recovery, reactions, separations, drug delivery, cosmetics and foods. We investigated two different kinds of water-in-oil microemulsion systems, AOT (bis(2-ethylhexyl) sulfosuccinate) microemulsions with various counterions and perfluorocarbon-based microemulsion gels with triblock copolymers. In the AOT systems, we investigated the viscosity and interdroplet interactions in $Ca(AOT)_2$, $Mg(AOT)_2$ and KAOT microemulsions, and compared our results with the commonly-studied NaAOT/water/decane system. We attribute the differences in behavior to different hydration characteristics of the counterions, and we believe that the results are consistent with a previously proposed charge fluctuation model. Perfluorocarbons (PFCs) are of interest in a variety of biomedical applications as oxygen carriers. We have used triblock copolymer Pluronic® F127 to modify the rheology of PFC-based microemulsions, we have been able to form thermoreversible PFOB (perfluorooctyl bromide)-based gels, and have investigated the phase stability, rheology, microstructure, interactions, and gelation mechanism using scattering, rheometry, and microscopy. Finally, we attempted to use these data to understand the relationship between rheology and structure in soft attractive colloids.

TABLE OF CONTENTS

LIST OF TABLES

Table Page

LIST OF FIGURES

CHAPTER 1

INTRODUCTION

My thesis work explores two different types of water-in-oil microemulsion systems. The first system involves a charged surfactant, AOT (bis(2-ethylhexyl) sulfosuccinate), which has commonly been used as a model system for the study of water-in-oil microemulsions. We have investigated the effect of counterion type on the solution interactions and viscosity, and have used our results to test a previously-proposed charge fluctuation model to describe interdroplet interactions in this system. The second microemulsion system we investigated utilizes a perfluorocarbon (PFC) as the oil. While other groups have reported stable PFC-based microemulsions, these systems have all been low-viscosity liquids. We wished to create stable, elastic gels containing PFCs. We used triblock copolymers to modify the rheology of the PFC microemulsion and form thermoreversible gels. We have attempted to use the results on this system to gain an understanding of the relationship between rheology and structure in soft attractive colloids.

This chapter gives a general overview of microemulsions, perfluorocarbons and fluorinated amphiphiles, polymer adsorption and triblock copolymers, and universal models and parameters in phase transitions in colloidal systems.

1.1 Microemulsions

The term “microemulsion” was first proposed by Schulman and coworkers in 1959 [1], who observed a transparent and stable formulation formed by adding a short chain

alcohol to a coarse macroemulsion stabilized by an ionic surfactant [2]. One of the best recent descriptions of microemulsions is given by Attwood [3]: "A microemulsion is a system of water, oil, and amphiphilic compounds (surfactant and co-surfactant) which is a transparent, single optically isotropic, and thermodynamically stable liquid."

The great potential for practical applications of microemulsions has stimulated a great deal of research in the field, especially for applications in enhanced oil recovery in the 1970s. Schulman and coworkers were the first to investigate these transparent liquids [1, 4-9]. The microstructure, size, shape, rheology and dynamics of microemulsions have been characterized by various techniques such as scattering, viscometry, rheometry, X-ray diffraction, ultracentrifugation, cryo-electron microscopy, electrical birefringence and nuclear magnetic resonance (NMR) [10]. One of the most significant developments in the field was a theoretical statistical-mechanical description of microemulsion systems, and the demonstration that microemulsions are thermodynamically stable phases because of their ultralow interfacial tension and highly flexible interfacial layer [11-18]. By contrast, emulsion systems are only kinetically stable and often phase separate after a short time. The other main differences between microemulsions and emulsions are the size and the shape of dispersed phase. Microemulsion droplets are nanoscale, typically 10-200 nm, much smaller than emulsion particles (1-20 μm) and also smaller than the wavelength of visible light, so that the microemulsion systems are transparent. The microstructure of microemulsions can evolve from droplet-like to bicontinuous structures, whereas emulsions consist of large coarse spherical droplets [19].

Due to these unique properties and characteristics, microemulsions have been used in various industries. Research on microemulsion-based flooding techniques in enhanced oil

recovery began in 1970s, however the potential of their use was overestimated because of the high expense of surfactant and current low oil prices [20-25]. Cheaper production of surfactants was needed to make this technique affordable [26-29]. Microemulsions can solubilize both hydrophilic and hydrophobic reactants at high concentration, so they have been used as a novel medium for chemical synthesis as "microreactors" or "nanoreactors", distinct from reactions in a bulk solvent [10]. The reaction parameters and chemical reactivity can be determined by the microstructure of microemulsion, the properties of solvent, surfactant and cosurfactant [30-35]. Microemulsion reaction systems have been used for spectroscopic analysis, preparations of mesoporous structure materials [36-38], synthesis of polymeric particles [37, 39-41], synthesis of ultrafine metal, metal oxide, and semiconductor particles [42-47], and even used in supercritical fluids [48-50] and enzyme-catalyzed reactions [51-53]. Due to their thermodynamic stability, bioavailability and topical penetration of poorly soluble drugs enhanced by the amphiphiles, microemulsions have gained an important role as drug delivery vehicles [19, 54-56] and in cosmetics [57-59]. This application has inspired research on the use of novel highly efficient and nontoxic surfactants and cosurfactants. The transparent nature and ability to solubilize large amounts of volatile organic compounds, like alcohol in fragrance formulations, make microemulsions an important precursor in cosmetic formulations, where they are sometimes referred to as microemulsion gels [60-62]. Some foods contain microemulsions naturally, and the preparation of foods nearly always requires the incorporation of lipids which exist as microemulsions in foods. Microemulsions can also be used as liquid membranes for separation due to their significantly large interfacial area and fast spontaneous separation, extracting organic substances, metal, or proteins from

dilute streams [63-69]. The ultralow interfacial tensions and the high solubilization power of both hydrophilic and hydrophobic substances make microemulsions an excellent medium in textile detergency [70-73].

In the above application processes, the rheological properties and structure are important factors. These impact the stability, reactivity, bioavailability, penetration, separation efficiency, fine particle quality, and so on. Viscosity is a macroscopically observable parameter, very important in oil recovery, drug delivery, reaction, cosmetics, and separations. The rheological properties, shape and size of microemulsion structure are basically determined by the surfactant and solvent. So the selection of surfactant and solvent is very important, attracting enormous interest of researchers on the factors of rheology and structure like chain length of solvent, ion size and charge of surfactant.

1.2 Perfluorocarbons and Fluorinated Amphiphiles

1.2.1 Perfluorocarbons (PFCs)

When the hydrogen atoms in hydrocarbons are replaced by fluorine completely, the products are called perfluorocarbons (PFCs), or simply fluorocarbons [74-76]. Hydrogenated amphiphiles can also be fluorinated fully or partially to form perfluorinated amphiphiles or partially fluorinated amphiphiles [74].

Due to its strong electronegativity, fluorine shows an unusually high potential of ionization and very low polarizability. Because the C-F bond is among the most stable single covalent bonds and its atom radius is much larger than hydrogen atom, most fluorocarbons are very stable and inert thermally, chemically and biologically [75, 76].

They also have a larger volume, a larger density and a much more stiff chain than their hydrogenated counterparts [74-79].

Because of the low polarizability of fluorine, both the van der Waals interactions between fluorinated chains and the cohesive energy densities in liquid fluorocarbons are very low, resulting in many valuable properties, such as high fluidity, low surface tension, low boiling point, low refractive indexes, low dielectric constant, high gas solubility, excellent spreading property, high vapor pressure, and high compressibility [75]. The high density, anti-friction properties, and magnetic susceptibility values close to that of the water in PFCs also are useful in biomedical applications [75]. Additionally, the perfluorinated chain offers larger surface area to enhance the hydrophobicity so that the chain is both hydrophobic and lipophobic. Fluorocarbons are even immiscible with their hydrogenated counterparts because of their different chain conformations. This phenomenon is still pending to be explained successfully and completely [75, 78].

1.2.2 Fluorinated Amphiphiles

Fluorinated amphiphiles can be classified into four types according to their functional groups on the backbone: anionic, cationic, amphoteric, and nonionic [74]. Because of strong hydrophobic interactions and low van der Waals interactions from the fluorinated chain, fluorinated amphiphiles tend to self-assemble in water and collect at interfaces, showing strong surface activity. They have much lower critical micellar concentrations (cmc) than their hydrogenated counterparts [74, 75]. An increase of the chain length will decrease the cmc, and branching of the backbone will increase the cmc [74].

Perfluorinated amphiphiles also have smaller cmc than their partially fluorinated counterparts [74, 75].

1.2.3 Applications of Fluorocarbons and Fluorinated amphiphiles

Because of their unique properties, fluorocarbons and fluorinated amphiphiles have a lot of applications in both biomedical research and industrial research. In biomedical research, typical applications involve oxygen transport, because of the exceptional oxygen solubility and biocompatibility displayed by PFCs [75, 76, 78]. It is reported that fluorocarbon-based systems can act as "liquid ventilation," temporary blood substitutes, and injectable oxygen carriers during surgery [74-76, 78]. Fluorocarbons can dissolve a large amount of gases, much more than hydrocarbons and water, displaying gas solubilities up to 25% higher than water [75, 76, 78]. The oxygen in fluorinated oil is not bound chemically to the fluorinated chain, so it may be easily transported to tissues. The fluorocarbon brings no risks of infection to tissues and body because there is no metabolite-related toxicity. Thus, fluorinated blood substitutes are very important in cases of blood shortage, rare blood type groups, on-site rescue, and so on [74-76, 78]. After Creutzfeldt-Jacob disease, also called "mad cow syndrome", was found, fluorinated microemulsions become more popular and competitive than the blood substitutes from bovine hemoglobin derivatives [78]. Fluorinated gels and microemulsions also have strong potentials for use in pulmonary drug delivery, controlled drug delivery, and ointments in pharmacy and ophthalmology to maintain gas exchange and acid-base status [74-76, 78]. They also work very well in retinal repair, replacement of the vitreous liquid, and treatment of articular disorders such as osteoarthritis and rheumatoid arthritis [75, 78].

In industrial research, fluorocarbons and their derivatives also can work as anticorrosive agents, antifriction components, flame retardants, sliding agents, water repellents, polymerization agents, metal working agents, and even uranium recovery agents [74, 75, 78].

Fluorinated amphiphiles can be used in protein extraction and other bioseparations [74, 75]. They are excellent wetting agents and foaming agents, and can be used in severely corrosive environments, especially where hydrocarbon-based amphiphiles would decompose [74, 75]. They can work as solvent-based adhesives, durable antifogging agents, antistatic agents, cement additives, cleaners for hard surfaces, coatings, crystal growth regulators, fire-fighting foams and powders. Also they are used in cosmetics as emulsifiers, lubricants, or oleophobic agents, and in electronics, electroplating, electropolishing, etching, emulsion polymerization, flotation of minerals, graphic imaging, herbicides and insecticides [74]. A limit to apply these fluorinated compounds is their cost. Thus, sometimes a mixture of fluorocarbon-based and hydrocarbon-based compounds will be used [74, 75].

1.3 Polymer Adsorption and Triblock Copolymers

Polymer adsorption has been a very effective tool to control and adjust the phase behavior and rheological properties of colloidal suspensions. Triblock copolymers, which consist of two endblocks and one midblock, are a significant class of macromolecules that have such attractive applications. Intuitively, the formation of bridges absorbing two surfaces on each end of the polymer will induce interparticle attractions, and the

formation of loops or brushes absorbing single surface on both of the ends will induce interparticle repulsion (Figure 1-1).

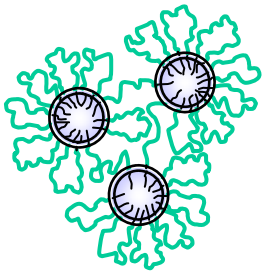

Figure 1-1. The triblock copolymers form loops and bridges on microemulsion droplets. Dark double circles indicate surfactant layer between two immiscible liquids.

These interactions lead to unusual phase behavior and rheological properties of emulsion systems containing triblock copolymers [80-88]. To understand the structure, dynamics, phase behavior and rheological properties of adsorbed layers of polymer or surfactant molecules in colloidal systems, numerous techniques have been used, such as scattering, magnetic resonance, spectroscopic, hydrodynamic and rheological techniques [82, 84-95]. For example, poly(ethylene oxide)/polyisoprene/poly(ethylene oxide) triblocks (PEO-PI-PEO) were investigated in microemulsion systems of AOT/water/decane [80, 81] and AOT/water/isooctane [89-95], forming highly associated solutions [80, 81, 89-95]. The phase behavior of AOT/water/decane is unusual with a gas-liquid transition due to an entropic gain with the conversion of loops to bridges. The viscoelastic moduli depend on concentration or volume fraction, conforming to theories of reversible networks or flowerlike micelle solutions [80]. SANS results of these systems showed that the equilibrium spacing of the droplets is independent of molecular weight and the number of polymers per droplet. The deviation between a power law

asymptote for *I(q)* at high *q* and Gaussian coils suggested chain swelling due to excluded volume effects of polymer layer [81].

The triblock poly(ethylene oxide)-poly(propylene oxide)-poly(ethylene oxide) (PEO-PPO-PEO) has attracted numerous interests for pharmaceutical applications such as drug delivery, gene therapy, and tissue engineering, because of its thermoreversible gelation around body temperature [96]. In our study, we will use PEO-PPO-PEO triblocks as rheology modifiers.

1.4 Universal Models for Phase Transitions and Rheology

Several authors have attempted to derive universal models to connect interparticle interactions to phase behavior and rheology in colloidal systems. In any colloidal dispersion system, the forces between components, usually expressed in terms of interparticle potential, play a significant role in the structure, phase stability and rheology of the system. Typical interparticle potentials have a repulsive component and an attractive component of depth Φ_{min}/kT, as despicted in Figure 1-2.

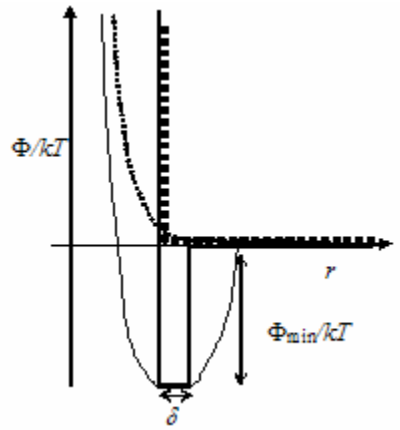

Figure 1-2. Typical pair potentials for colloids, showing hard sphere (▪▪▪), soft sphere (.....), attractive hard sphere(▬), and attractive soft sphere(——).

The dependence of solution rheology on the interparticle potential for dilute to moderately concentrated dispersions has been revealed by experiments, non-equilibrium theories, and simulations [89, 91, 93, 97-102]. Equilibrium phase transitions also are determined by the nature of the potentials. The transition of a crystalline solid from a disordered liquid at high concentrations is a typical example [103-105].

The liquid-gel transition between a liquid and a disordered viscoelastic solid, which is actively debated and studied, is suggested to occur through one of two mechanisms, attractive aggregation or formation of a glass. These two mechanisms also can be unified into "jamming transitions", a more general description [106].

Attractive aggregation in systems with interparticle attractions creates a fractal network of colloids in which the mass M within a radius r is given by $M \sim r^d$. Here d, a fractal dimension, can be measured using scattering techniques [105, 107]. The rheology of such systems can be described using percolation theory [108] and characterized by the particle volume fraction ϕ, with critical value of gelation, ϕ_c. The equilibrium modulus G_0 and the low shear viscosity η_0 are given by:

$$G_0 \sim \left(\frac{|\phi - \phi_c|}{\phi_c} \right)^t \text{ for } \phi > \phi_c \text{ and } \eta_0 \sim \left(\frac{|\phi - \phi_c|}{\phi} \right)^{-s} \text{ for } \phi < \phi_c \tag{1-1}$$

Near the critical gel point, G' and G'', the storage and loss modulus, have a power-law dependence on frequency [109, 110], with $G' \sim G'' \sim \omega^{\Delta}$ [111, 112].

G_0 can be scaled by considering energy stored in interparticle bonds [105]:

$$\frac{G_o}{kT} \sim \frac{\phi^2}{a^2} \left(-\frac{\Phi_{\min}}{kT} \right)^{3/2} \tag{1-2}$$

A disordered viscoelastic glass can be formed in both attractive and purely repulsive colloidal systems as first observed by Pusey and van Megen [103, 113]. For monodisperse hard sphere systems the liquid-glass transition occurs at ϕ_G=0.56-0.60 [113, 114]. Above the glass transition, *G'* starts to dominate over *G"* and becomes independent of frequency [115]. Colloidal glasses can also be formed in hard particles with short range attractions, such as colloids subject to depletion forces [116] and some polymeric micelles [117].

Jamming transitions are found to occur in a wide variety of attractive colloid systems and be able to unify the phenomena of gelation, aggregation, and the glass transition [106]. In these systems, the viscosity diverges as a critical volume fraction ϕ_c is approached, and *G'* develops a low frequency plateau [106].

The viscosity and modulus behaviors of jamming transitions can be described as [106]:

$$\eta = \eta_s(\phi_c - \phi)^{-a_\phi} \quad \text{and} \quad G_0 = G_\phi(\phi - \phi_c)^{-b_\phi} \tag{1-3}$$

where η_s is solvent viscosity, a_ϕ and b_ϕ are characteristic exponents, G_ϕ and ϕ_c depend on the interparticle attraction energy Φ_{min}/kT [106]. The viscosity and modulus have critical behavior at fixed ϕ as the attraction increases, leading to the following scaling [106]:

$$\eta = \eta_D\left(\Phi_{\min,c} - \Phi_{\min}\right)^{-a_\Phi} \quad \text{and} \quad G_o = G_\Phi\left(\Phi_{\min} - \Phi_{\min,c}\right)^{-b_\Phi} \tag{1-4}$$

where η_D is the dispersion viscosity, a_Φ and b_Φ are characteristic exponents, and G_Φ and $\Phi_{min,c}$ depend on ϕ.

It is important to note here that values for Φ_{min} were not measured, but were inferred based on models for the solution interactions [106]. Furthermore, the dependence of *G'* and *G"* on the frequency for the systems with different values of ϕ and Φ_{min}/kT can be

scaled into a universal curve [118]. Eq (1-3) and (1-4) are found to describe systems with relatively hard repulsions subject to a variety of attractive forces (depletions forces and van der Waals forces). Thus the onset of solid-like behavior can be controlled by either varying ϕ or strength of attraction.

The transition to a disordered solid, accompanied by an increase in *G'*, also occurs in colloids with soft repulsive forces, including dense emulsions, foams, multilamellar vesicles, and pastes. Theoretical efforts have demonstrated the universality of certain characteristics within these diverse systems.

Models for soft glasses have been developed to describe such systems in terms of a mean-field "noise temperature", x, with a glass transition occurring at x=1 [119, 120]:

$G'' \sim \omega$ for $2 < x$, $G'' \sim \omega^{x-1}$ for $1 < x < 2$

$G' \sim \omega$ for $3 < x$, $G' \sim \omega^{x-1}$ for $1 < x < 3$

For $x > 3$ the system is Maxwell-like at low frequencies; for $2 < x < 3$ there is an anomalous power law in the elastic modulus. For $1 < x < 2$, G' and G'' have a constant ratio, and both vary as ω^{x-1}. For $x \rightarrow 1$, G' and G'' approach some constant values [119, 120]. These models are able to qualitatively reproduce the rheology of a variety of systems. However, it is difficult to relate the parameters in these models to experimental measurable variables.

"Softness" is an important concept that needs to be addressed in these systems. This can be thought of as the "softness" of the repulsive portion of the potential. One of the definitions of softness is $S = (R_H - R_c)/R_c$ (R_H is hydrodynamic radius and Rc is core radius), which allows us to map results from hard sphere systems onto soft spheres using an appropriate scaling for ϕ. Because soft systems allow some degree of overlap and

compression, defining an effective volume fraction, ϕ_{eff}, is not straightforward. Vlassopoulus et al. [121] demonstrated that η_0 for soft polymer stars could be reduced into a master curve with data for hard spheres if ϕ_{eff} was defined based on the hydrodynamic radius, R_H, as determined from dynamic light scattering (DLS) [121]. The data overlap for $\phi_{eff} < 0.1$, however, deviations occur at higher volume fractions, with the viscosity for hard systems diverging much more rapidly near close-packing [121]. This suggests that an additional correction must be made to account for softness.

Bhatia et al. have examined the liquid-gel transition in a system of attractive polymeric micelles, which can be considered as "sticky" soft spheres, and find several rheological characteristics in common with those observed for glassy hard spheres [122]. As in the hard sphere system, they found that gelation can be controlled by either varying ϕ or Φ_{min}/kT (the latter is varied through addition of a surfactant which disrupts intermicellar association) [122]. The moduli are found to collapse onto a universal curve, again reminiscent of what is observed in the attractive hard sphere case. Moreover, after scaling the volume fraction using micellar parameters obtained from small-angle neutron scattering (SANS) and the hydrodynamic radius from DLS, Bhatia et al found that gelation occurs at $\phi_{eff} \sim 0.64$, similar to what would be expected for polydisperse hard spheres [123]. Thus, by using an appropriate scaling for ϕ_{eff}, it is possible to draw some connections between attractive hard spheres and soft spheres, although the soft nature of the repulsion should be fully considered.

1. 5 Summary of Dissertation

The remainder of this dissertation will be organized as follows. Chapter 2 focuses on the study of AOT systems with varying counterions, including background on this system, materials and methods, results and discussion, and conclusions. Chapter 3 describes the work on PFC-based microemulsions, including background on these systems, experimental methods, SANS data analysis, results and discussions, and conclusions. Finally, Chapter 4 describes some potential areas for future work.

Bibliography

[1] J. H. Schulman; W. Stoeckenius; L. M. Prince. *J. Phys. Chem.,* **1959**, 63, (10), p1677.

[2] T. P. Hoar; J. H. Schulman. *Nature,* **1943**, 152, p102.

[3] D. Attwood, Microemulsions. In *Colloidal Drug Delivery Systems*, Kreuter, J., Ed. Marcel Dekker, New York: **1994**.

[4] J. E. Bowcott; J. H. Schulman. *Zeitschrift Fur Elektrochemie,* **1955**, 59, (4), p283.

[5] C. E. Cooke; J. H. Schulman In *The effect of different hydrocarbons on the formation of microemulsions*, Surface Chemistry, Stockholm, 1964; Ekwall, P.; Groth, K.; Runnstrom-Reio, V., Eds. Academic Press, New York: Stockholm, 1964; pp 231.

[6] J. H. Schulman; J. A. Friend. *J. Colloid Sci.,* **1949**, 4, (5), p497.

[7] J. H. Schulman; D. P. Riley. *J. Colloid Sci.,* **1948**, 3, (4), p383.

[8] D. F. Sears; J. H. Schulman. *J. Phys. Chem.,* **1964**, 68, (12), p3529.

[9] Zlochowe.Ia; J. H. Schulman. *J. Colloid Interface Sci.,* **1967**, 24, (1), p115.

[10] P. Kumar; K. L. Mitta, *Handbook of Microemulsion Science and Technology.* **1999**, Marcel Dekker, New York.

[11] G. Gillberg; H. Lehtinen; S. Friberg. *J. Colloid Interface Sci.,* **1970**, 33, (1), p40.

[12] R. Muller; E. Gerard; P. Dugand; P. Rempp; Y. Gnanou. *Macromolecules,* **1991**, 24, (6), p1321.

[13] H. Saito; K. Shinoda. *J. Colloid Interface Sci.,* **1967**, 24, (1), p10.

[14] H. Saito; K. Shinoda. *J. Colloid Interface Sci.,* **1970**, 32, (4), p647.

[15] K. Shinoda. *J. Colloid Interface Sci.,* **1967**, 24, (1), p4.

[16] K. Shinoda. *J. Colloid Interface Sci.,* **1970**, 34, (2), p278.

[17] K. Shinoda; T. Ogawa. *J. Colloid Interface Sci.,* **1967**, 24, (1), p56.

[18] E. Sjoblom; S. Friberg. *J. Colloid Interface Sci.,* **1978**, 67, (1), p16.

[19] M. Kreilgaard. *Adv. Drug Deliv. Rev.,* **2002**, 54, pS77.

[20] J. L. Cayias; R. S. Schechter; W. H. Wade. *J. Colloid Interface Sci.,* **1977**, 59, (1), p31.

[21] M. Chiang; D. O. Shah. *Abstr. Pap. Am. Chem. Soc.,* **1980**, 179, (MAR), p147.

[22] M. Y. Chiang; K. S. Chan; D. O. Shah. *J. Can. Pet. Technol.,* **1978**, 17, (4), p61.

[23] R. N. Healy; R. L. Reed. *SPE J.,* **1974**, 14, (5), p491.

[24] R. N. Healy; R. L. Reed. *SPE J.,* **1977**, 17, (2), p129.

[25] M. J. Schwuger; K. Stickdorn; R. Schomacker. *Chem. Rev.,* **1995**, 95, (4), p849.

[26] M. Baviere; P. Glenat; V. Plazanet; J. Labrid. *SPE Reserv. Eng.,* **1995**, 10, (3), p187.

[27] J. D. Desai; I. M. Banat. *Microbiol. Mol. Biol. Rev.,* **1997**, 61, (1), p47.

[28] L. L. Schramm; D. B. Fisher; S. Schurch; A. Cameron. *Colloid Surf. A-Physicochem. Eng. Asp.,* **1995**, 94, (2-3), p145.

[29] E. C. Donaldson; G. V. Chilingarian; T. F. Yen, *Microbial Enhanced Oil Recovery.* **1989**, Elsevier, New York: p 9.

[30] C. A. Bunton; F. Nome; F. H. Quina; L. S. Romsted. *Accounts Chem. Res.,* **1991**, 24, (12), p357.

[31] A. Ceglie; K. P. Das; B. Lindman. *J. Colloid Interface Sci.,* **1987**, 115, (1), p115.

[32] S. J. Chen; D. F. Evans; B. W. Ninham; D. J. Mitchell; F. D. Blum; S. Pickup. *J. Phys. Chem.,* **1986**, 90, (5), p842.

[33] M. Fanun; M. Leser; A. Aserin; N. Garti. *Colloid Surf. A-Physicochem. Eng. Asp.,* **2001**, 194, (1-3), p175.

[34] F. M. Menger; A. R. Elrington. *J. Am. Chem. Soc.,* **1991**, 113, (25), p9621.

[35] V. K. Vanag; I. R. Epstein. *Phys. Rev. Lett.,* **2001**, 8722, (22).

[36] P. Y. Feng; X. H. Bu; G. D. Stucky; D. J. Pine. *J. Am. Chem. Soc.,* **2000**, 122, (5), p994.

[37] W. Meier. *Curr. Opin. Colloid Interface Sci.,* **1999**, 4, (1), p6.

[38] X. Zhang; F. Zhang; K. Y. Chan. *Mater. Lett.,* **2004**, 58, (22-23), p2872.

[39] M. Antonietti; R. Basten; S. Lohmann. *Macromol. Chem. Phys.,* **1995**, 196, (2), p441.

[40] W. Ming; F. N. Jones; S. K. Fu. *Macromol. Chem. Phys.,* **1998**, 199, (6), p1075.

[41] M. Antonietti; W. Bremser; D. Muschenborn; C. Rosenauer; B. Schupp; M. Schmidt. *Macromolecules,* **1991**, 24, (25), p6636.

[42] P. Y. Chow; J. Ding; X. Z. Wang; C. H. Chew; L. M. Gan. *Phys. Status Solidi A-Appl. Res.,* **2000**, 180, (2), p547.

[43] J. H. Clint; I. R. Collins; J. A. Williams; B. H. Robinson; T. F. Towey; P. Cajean; A. Khanlodhi. *Faraday Discuss.,* **1993**, p219.

[44] S. Eriksson; U. Nylen; S. Rojas; M. Boutonnet. *Appl. Catal. A-Gen.,* **2004**, 265, (2), p207.

[45] T. Hanaoka; H. Hayashi; T. Tago; M. Kishida; K. Wakabayashi. *J. Colloid Interface Sci.,* **2001**, 235, (2), p235.

[46] T. Masui; K. Fujiwara; Y. M. Peng; T. Sakata; K. Machida; H. Mori; G. Adachi. *J. Alloy. Compd.,* **1998**, 269, (1-2), p116.

[47] K. Zhang; C. H. Chew; S. Kawi; J. Wang; L. M. Gan. *Catal. Lett.,* **2000**, 64, (2-4), p179.

[48] N. Kometani; Y. Toyoda; K. Asami; Y. Yonezawa. *Chem. Lett.,* **2000**, (6), p682.

[49] H. Ohde; J. M. Rodriguez; X. R. Ye; C. M. Wai. *Chem. Commun.,* **2000**, (23), p2353.

[50] H. Ohde; C. M. Wai; H. Kim; J. Kim; M. Ohde. *J. Am. Chem. Soc.,* **2002**, 124, (17), p4540.

[51] Y. L. Khmelnitsky; R. Hilhorst; C. Veeger. *Eur. J. Biochem.,* **1988**, 176, (2), p265.

[52] A. Na; C. Eriksson; S. G. Eriksson; E. Osterberg; K. Holmberg. *J. Am. Oil Chem. Soc.,* **1990**, 67, (11), p766.

[53] H. Stamatis; A. Xenakis; M. Provelegiou; F. N. Kolisis. *Biotechnol. Bioeng.,* **1993**, 42, (1), p103.

[54] M. J. Lawrence; G. D. Rees. *Adv. Drug Deliv. Rev.,* **2000**, 45, (1), p89.

[55] J. M. Sarciaux; L. Acar; P. A. Sado. *Int. J. Pharm.,* **1995**, 120, (2), p127.

[56] T. F. Vandamme. *Prog. Retin. Eye Res.,* **2002**, 21, (1), p15.

[57] S. Magdassi. *Colloid Surf. A-Physicochem. Eng. Asp.,* **1997**, 123, p671.

[58] B. K. Paul; S. P. Moulik. *Curr. Sci.,* **2001**, 80, (8), p990.

[59] T. F. Tadros. *Intl. J. of Cosmetic Sci.,* **1992**, 14, (3), p93.

[60] F. Dreher; P. Walde; P. Walther; E. Wehrli. *J. Control. Release,* **1997**, 45, (2), p131.

[61] G. J. T. Tiddy. *Phys. Rep.-Rev. Sec. Phys. Lett.,* **1980**, 57, (1), p2.

[62] H. Wennerstrom; B. Lindman. *Phys. Rep.-Rev. Sec. Phys. Lett.,* **1979**, 52, (1), p1.

[63] N. N. Li Separating hydrocarbons with liquid membranes. US Pat. 3, 410, 794, **1968**.

[64] K. Naoe; T. Kai; M. Kawagoe; M. Imai. *Biochem. Eng. J.,* **1999**, 3, (1), p79.

[65] M. Saidi; H. Khalaf. *Hydrometallurgy,* **2004**, 74, (1-2), p85.

[66] V. E. Serga; L. D. Kulikova; B. A. Purin. *Sep. Sci. Technol.,* **1999**, 35, (2), p299.

[67] C. Tondre; A. Xenakis. *Faraday Discuss.,* **1984**, p115.

[68] S. W. Tsai; C. L. Wen; J. L. Chen; C. S. Wu. *J. Membr. Sci.,* **1995**, 100, (2), p87.

[69] J. M. Wiencek; S. Qutubuddin. *Sep. Sci. Technol.,* **1992**, 27, (10), p1211.

[70] N. Azemar; I. Carrera; C. Solans. *J. Dispersion Sci. Technol.,* **1993**, 14, (6), p645.

[71] R. L. Blum; M. H. Robbins; L. M. Hearn; S. L. Nelson Microemulsion dilutable cleaner. US Pat. 5, 854, 187, **1998**.

[72] C. Solans; J. G. Dominguez; S. E. Friberg. *J. Dispersion Sci. Technol.,* **1985**, 6, (5), p523.

[73] C. Toncumpou; E. J. Acosta; L. B. Quencer; A. F. Joseph; J. F. Scamehorn; D. A. Sabatini; S. Chavadej; N. Yanumet. *J. Surfactants Deterg.,* **2003**, 6, (3), p191.

[74] E. Kissa, *Fluorinated surfactants and repellents.* **2001**, Marcel Dekker, New York: Vol. 97.

[75] M. P. Krafft. *Adv. Drug Deliv. Rev.,* **2001**, 47, (2-3), p209.

[76] J. G. Riess. *Colloid Surf. A-Physicochem. Eng. Asp.,* **1994**, 84, (1), p33.

[77] C. Ceschin; J. Roques; M. C. Maletmartino; A. Lattes. *J. Chem. Tech. & Biotech. a-Chem. Tech.,* **1985**, 35, (2), p73.

[78] P. LoNostro; S. M. Choi; C. Y. Ku; S. H. Chen. *J. Phys. Chem. B,* **1999**, 103, (25), p5347.

[79] P. Mukerjee. *Colloid Surf. A-Physicochem. Eng. Asp.,* **1994**, 84, (1), p1.

[80] U. Batra; W. B. Russel; M. Pitsikalis; S. Sioula; J. W. Mays; J. S. Huang. *Macromolecules,* **1997**, 30, (20), p6120.

[81] S. R. Bhatia; W. B. Russel; J. Lal. *J. Appl. Crystallogr.,* **2000**, 33, (1), p614.

[82] G. J. Fleer; M. A. C. Stuart; J. M. H. M. Scheutjens; T. Cosgrove; B. Vincent, *Polymers at Interfaces.* **1993**, Chapman & Hall: London, New York.

[83] S. A. Hagan; S. S. Davis; L. Illum; M. C. Davies; M. C. Garnett; D. C. Taylor; M. P. Irving; T. F. Tadros. *Langmuir,* **1995**, 11, (5), p1482.

[84] W. Liang; T. F. Tadros; P. F. Luckham. *J. Colloid Interface Sci.,* **1992**, 153, (1), p131.

[85] S. T. Milner; T. A. Witten. *Macromolecules,* **1992**, 25, (20), p5495.

[86] M. A. C. Stuart; T. Cosgrove; B. Vincent. *Adv. Colloid Interface Sci.,* **1986**, 24, (2-3), p143.

[87] C. Washington; S. M. King. *Langmuir,* **1997**, 13, (17), p4545.

[88] C. Washington; S. M. King; R. K. Heenan. *J. Phys. Chem.,* **1996**, 100, (18), p7603.

[89] H. F. Eicke; M. Gauthier; R. Hilfiker; R. Struis; G. Xu. *J. Phys. Chem.,* **1992**, 96, (12), p5175.

[90] H. F. Eicke; C. Quellet; G. Xu. *Colloids & Surfaces,* **1989**, 36, (1), p97.

[91] G. Fleischer; F. Stieber; U. Hofmeier; H. F. Eicke. *Langmuir,* **1994**, 10, (6), p1780.

[92] R. Hilfiker; H. F. Eicke; C. Steeb; U. Hofmeier. *J. Phys. Chem.,* **1991**, 95, (3), p1478.

[93] M. Odenwald; H. F. Eicke; W. Meier. *Macromolecules,* **1995**, 28, (14), p5069.

[94] C. Quellet; H. F. Eicke; G. Xu; Y. Hauger. *Macromolecules,* **1990**, 23, (13), p3347.

[95] R. Struis; H. F. Eicke. *J. Phys. Chem.,* **1991**, 95, (15), p5989.

[96] S. Fusco; A. Borzacchiello; P. A. Netti. *J. Bioact. Compat. Polym.,* **2006**, 21, (2), p149.

[97] J. Bergenholtz. *Curr. Opin. Colloid Interface Sci.,* **2001**, 6, (5-6), p484.

[98] J. Bergenholtz; N. Willenbacher; N. J. Wagner; B. Morrison; D. van den Ende; J. Mellema. *J. Colloid Interface Sci.,* **1998**, 202, (2), p430.

[99] J. F. Brady. *J. Chem. Phys.,* **1993**, 99, (1), p567.

[100] S. L. Elliott; W. B. Russel. *J. Rheol.,* **1998**, 42, (2), p361.

[101] D. R. Foss; J. F. Brady. *J. Rheol.,* **2000**, 44, (3), p629.

[102] R. A. Lionberger; W. B. Russel. *J. Rheol.,* **1997**, 41, (2), p399.

[103] P. N. Pusey; W. Vanmegen. *Nature,* **1986**, 320, (6060), p340.

[104] P. N. Pusey; W. Vanmegen. *Phys. Rev. Lett.,* **1987**, 59, (18), p2083.

[105] W. B. Russel; D. A. Savill; W. R. Schowalter, *Colloidal Dispersions.* **1989**, Cambridge University Press: Cambridge, England.

[106] V. Trappe; V. Prasad; L. Cipelletti; P. N. Segre; D. A. Weitz. *Nature,* **2001**, 411, (6839), p772.

[107] J. S. Higgins; H. C. Benoit, *Polymers and Neutron Scattering.* **1994**, Oxford: Clarendon Press.

[108] D. Stauffer, *Introduction to Percolation Theory.* **1985**, Taylor and Francis Inc.: Philadelphia.

[109] F. Chambon; H. H. Winter. *Polym. Bull.,* **1985**, 13, (6), p499.

[110] H. H. Winter; F. Chambon. *J. Rheol.,* **1986**, 30, (2), p367.

[111] J. E. Martin; D. Adolf. *Annu. Rev. Phys. Chem.,* **1991**, 42, p311.

[112] M. Rubinstein; R. H. Colby; J. R. Gillmor. *Abstr. Pap. Am. Chem. Soc.,* **1989**, 197, p82.

[113] F. Chambon; H. H. Winter. *J. Rheol.,* **1987**, 31, (8), p683.

[114] W. Vanmegen; S. M. Underwood. *Phys. Rev. E,* **1994**, 49, (5), p4206.

[115] T. G. Mason; D. A. Weitz. *Phys. Rev. Lett.,* **1995**, 75, (14), p2770.

[116] K. N. Pham; A. M. Puertas; J. Bergenholtz; S. U. Egelhaaf; A. Moussaid; P. N. Pusey; A. B. Schofield; M. E. Cates; M. Fuchs; W. C. K. Poon. *Science,* **2002**, 296, (5565), p104.

[117] F. Mallamace; P. Gambadauro; N. Micali; P. Tartaglia; C. Liao; S. H. Chen. *Phys. Rev. Lett.,* **2000**, 84, (23), p5431.

[118] V. Trappe; D. A. Weitz. *Phys. Rev. Lett.,* **2000**, 85, (2), p449.

[119] P. Sollich. *Phys. Rev. E,* **1998**, 58, (1), p738.

[120] P. Sollich; F. Lequeux; P. Hebraud; M. E. Cates. *Phys. Rev. Lett.,* **1997**, 78, (10), p2020.

[121] D. Vlassopoulos; G. Fytas; S. Pispas; N. Hadjichristidis. *Physica B,* **2001**, 296, (1-3), p184.

[122] S. R. Bhatia; A. Mourchid; M. Joanicot. *Curr. Opin. Colloid Interface Sci.,* **2001**, 6, (5-6), p471.

[123] S. R. Bhatia; A. Mourchid. *Langmuir,* **2002**, 18, (17), p6469.

CHAPTER 2

COUNTERION EFFECTS IN AOT SYSTEMS

2.1 Background

The simplest microemulsion systems are composed of a surfactant, water and oil. Aerosol OT, which is sodium bis(2-ethylhexyl) sulfosuccinate and simply called AOT, is a model surfactant that can form nanometer size reverse micelles and microemulsion water droplets in many oils (Fig. 2-1). In this chapter, for clarity we will use NaAOT to refer to the surfactant with a sodium counterion. NaAOT has been extensively studied and has important applications in drug delivery, enhanced oil recovery, cosmetics, detergency, and so on. It has been found that the type of counterion, solvent, solvent content, droplet volume fraction and temperature all have important effects on the droplet size, shape, structure and properties of AOT-based microemulsion systems.

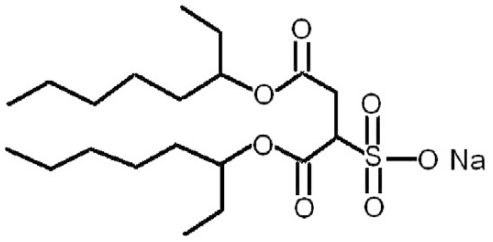

Figure 2-1. Chemical structure of NaAOT.

As reviewed by Chen [1] and more recently by Moulik and Paul [2], NaAOT microemulsions display a simple dependence of droplet size and volume fraction on composition. Specifically, the droplet size increases linearly with *X*, the molar ratio of water to surfactant [3]. Because of this linear dependence of droplet size on *X,* a monotonic increase in viscosity with *X* is expected. However, at constant volume fraction

and temperature, the low shear viscosity of NaAOT microemulsions exhibits a well-known maximum as a function of X. The position of the peak, $X = 8$, is insensitive to volume fraction and temperature, but the magnitude increases with volume fraction. Bergenholtz et al. [4] showed that this maximum in viscosity could be related to an apparent maximum in the attraction between droplets near $X = 8$.

Batra et al. [5] explored the origin of the maximum in viscosity more thoroughly. Through dilute viscometry, dynamic light scattering, and static light scattering, they showed a direct connection between the viscosity maximum and a maximum in interdroplet attraction around $X = 8$. A microscopic explanation of these phenomena was offered via a model for fluctuations in net charge on the droplets. As the amount of water in the system, or X, is increased, the sulfosuccinate group becomes hydrated, releasing its counterion into the droplet. Exchange of surfactants and counterions between droplets then could result in a pair of droplets with opposite charge. This leads to an interdroplet attraction that increases with X until hydration is complete. Batra et al [5] take the probability of counterion release as proportional to the probability of the head group having a certain number of associated waters, X_m. A value of $X_m > 6$ is assumed, presumably because the Na^+ counterion requires 5-6 water molecules to complete its first hydration shell [6]. In this model, the amount by which X_m exceeds 6 is related to the energetics of binding.

This mechanism suggests that the interactions between droplets and the dependence of the viscosity on X may depend on the hydration behavior of the counterion. Three other commonly-studied counterions for the 2-diethylhexyl sulfosuccinate surfactant are Ca^{2+}, Mg^{2+} and K^+. Recent Monte Carlo simulations have suggested that, by contrast with Na^+

which has a hydration number of either 5 or 6, the hydration number of K^+ displays a distribution ranging from 5-10 [6]. Neutron diffraction studies have suggested that the water molecules in the K^+ hydration shell are also more disordered than those in the Na^+ hydration shell [7]. The hydration number for Ca^{2+} has been reported as 6-7 [8].

Counterion substitution is known to have other important effects on the structure and properties of microemulsion systems with AOT-based surfactants. Eastoe et al. studied the effect of counterion radius on the oil-water interfacial tension and droplet radius with n-heptane as the oil [9]. This group also studied the effect of divalent counterions (Mg^{2+}, Ca^{2+}, Co^{2+}, Ni^{2+}, Cu^{2+}, Zn^{2+}) on the structure and properties of dilute microemulsions with cyclohexane as oil [10], and the effect of counterion (M^{n+}) size and charge on the structure of the aggregates in water-in-oil microemulsions with cyclohexane as oil, in which M^{n+} is Na^+, K^+, Rb^+, Cs^+, Mg^{2+}, Ca^{2+}, Co^{2+}, Ni^{2+}, Cu^{2+}, Zn^{2+} and Cd^{2+} [11]. They found the hydration radius of counterions has more of an impact on the structure than the charge. For example, $Ca(AOT)_2$ was found to form spherical aggregates similar to NaAOT [11]. Petit et al. studied the structure of bimetallic (Co^{2+}, Cu^{2+}, Cd^{2+}) AOT aggregates with isooctane as the oil and found strong structural changes with increasing water content. The maximum value of the molar ratio of water to AOT was found to be less than 7 for bimetallic AOT but is 60 for NaAOT. Higher water content usually leads to a phase transition to a lamellar system [12]. Eastoe et al. found that the phase behavior, interparticle structure, and dynamics of AOT microemulsions in low-density alkanes are dependent on the alkane density but the intraparticle structure shows independence on the chain length and density of alkanes [13]. Huang et al. studied the critical transition driven by the alkyl carbon number of oil and found the microemulsion with decane as oil is

"almost critical" [14]. They also found the attractive interparticle interactions arising from the overlapping of the surfactant tails could explain the dependence of phase behaviors on the chain length of the oil [15]. Other investigators studied the effect of temperature, the chain length of oil, water content, volume fraction of droplets and added salts on aggregate number and reaction rate constant of AOT/water/oil systems using time-resolved fluorescence probing [16].

Since AOT microemulsions with decane as the oil display critical behavior [14], many studies have been carried out on the AOT/water/n-decane reverse microemulsion system. As mentioned above, Bergenholtz et al studied its viscosity, microstructure and interparticle potential [4], and Batra et al studied its viscosity anomaly and charge fluctuations in dilute systems with $X < 20$ [5]. Other investigators have systematically investigated the viscosity, phase diagram and microstructure of $Ca(AOT)_2$/water/n-decane systems versus NaAOT/water/n-decane systems [16-18].

2.2 Objective of Project

The objective of this project is to examine the effects of counterion substitution, specifically K^+, Ca^{2+}, and Mg^{2+}, on the phase stability, viscosity, and interactions in AOT/water/n-decane systems using viscometry, and test the "charge fluctuation" model of the viscosity anomaly proposed previously. The behavior of KAOT, $Ca(AOT)_2$ and $Mg(AOT)_2$ is compared to that of the NaAOT system and discussed in the context of the charge fluctuation model of Batra et al. [5]. Although other groups have performed detailed studies of the impact of counterion substitution on the self-assembly, structure, and droplet interactions in AOT microemulsions [16-18], to our knowledge there have

been no studies that have connected the maximum in viscosity to interdroplet interactions for any counterions other than Na^+. Finally, because the charge fluctuation model was developed for spherical droplets, it is important to note here that we are restricted in this study to systems that form spherical droplets over a wide range of values of X and volume fraction ϕ. Several other potential counterions, such as Co^{2+}, Ni^{2+}, Cu^{2+}, Zn^{2+}, are not suitable because they undergo a transition from rodlike aggregates to spherical aggregates as X increases [16-18], and any change in viscosity with X will be impacted by this morphological change.

Below, we describe the synthesis of KAOT, $Ca(AOT)_2$, and $Mg(AOT)_2$, investigation of the viscosity and interparticle interactions of different microemulsion systems using capillary viscometry, and investigation of the microstructures using dynamic light scattering (DLS).

2.3 Materials and Methods

KAOT, $Mg(AOT)_2$ and $Ca(AOT)_2$ are prepared from NaAOT purum(Sigma-Aldrich), using previously described methods [10, 11, 19]. Microemulsions were formulated by mixing dried and recrystallized surfactant with water and decane at fixed volume fraction ϕ, calculated from the specific volumes, and then diluting with decane and filtering through 0.22 μm Millipore membrane syringe filters into the Ubbelohde capillary viscometers. The values of X cited are the stoichiometric ones, neglecting the small amount of water of hydration ($\Delta X < 0.5$ for KAOT and $Ca(AOT)_2$, $\Delta X < 1$ for $Mg(AOT)_2$) that normally cannot be removed from the surfactant easily. Measurements of the viscosity were performed in capillary viscometers at a fixed temperature T=30°C

maintained within ±0.1°C with a Neslab R211 constant temperature water bath. Three repeat runs of each sample were performed, with the standard deviation between runs in the range of 0.02–0.08% for all samples. Capillary viscometers of size 0C, 1C, and 1 were used, corresponding to capillary radii ~ 1.0 mm. This is much larger than the size of the AOT microemulsion droplets, which have radii in the range 2.0–5.0 nm [5], and thus we do not expect any edge effects from the capillary walls. The phase stability was studied in oven at different temperatures. Some of the solution samples are filtered into tubes for droplet size measurement using Argon laser (wavelength λ=514.5nm) for dynamic light scattering at 30ºC.

2.4 Results and Discussion

2.4.1 Phase stability (T = 20 –50°C, ϕ = 0.02 – 0.2).

$Ca(AOT)_2$/water/n-decane systems are monophasic solutions at 30°C with $5 \leqslant X \leqslant 22$. The waterless system, which is just the $Ca(AOT)_2$/n-decane binary system, appears as a white solid-like system and partially melts to become transparent when the temperature rises to 50°C, in good agreement with prior results [18]. If some amount of water is added, the solid-like system becomes a transparent solution. For X = 15 or 17.5, the system will separate into two transparent phases below 25°C. The phase boundary is difficult to determine and is sensitive to temperature. For $15 > X > 5$, the system appears as a stable, transparent, single phase in this range of temperature.

KAOT/water/n-decane systems appear as monophasic solutions at $X < 10$. Some small droplets are separated from bulk solution at $X > 10$ at room temperature and lower temperatures. The droplets will disappear when temperature rises to 30°C.

$Mg(AOT)_2$/water/n-decane systems appear as monophasic solutions at $X \leqslant 5$. For $X \geqslant 6$, the system is separated into two phases, a thin solution and a thick viscous system. It shows a significant change in the microstructure around $X = 6$. For $6 < X < 10$, both of the two phases are transparent. For $X > 10$, the upper phase is transparent and the bottom one is a white opaque solid. At $X = 6$, the phase boundary was found to disappear when temperature rise above 35°C.

2.4.2 Viscosity ($T = 30$°C, $\phi = 0.02 - 0.2$)

For dilute microemulsions, viscometry data can be interpreted using virial expansions to derive information on microstructure and interactions [2]. For example, for particles with an adhesive hard sphere interparticle potential, the dependence of viscosity on droplet volume fraction can be shown to be:

$$\eta_r = \frac{\eta_0}{\mu} = 1 + 2.5\phi + \left(6.0 + \frac{1.9}{\tau}\right)\phi^2 + O(\phi)^3 \quad (1)$$

Here, η_0 is the low-shear viscosity, μ is the solvent viscosity, η_r is referred to as the reduced viscosity, and $1/\tau$ is the stickiness parameter, related to interparticle attractions.

Another typical approach is to analyze data in terms of the intrinsic viscosity $[\eta]$ [5]:

$$\eta_r = 1 + [\eta]\phi + k_H[\eta]^2\phi^2 + O(\phi^3) \quad (2)$$

where $[\eta]$ is the intrinsic viscosity and k_H is the Huggins coefficient. Comparing eqs.(1) and (2), it can be seen that these two parameters reflect the hydrodynamic volume of individual droplets and pair interactions, respectively. For the hard sphere system with purely repulsive interactions, we expect a value of 2.5 for $[\eta]$ and a value of 1.0 for k_H, with the value of k_H increasing if interparticle attractions are present. Since

$$[\eta] = \lim_{\phi \to 0} \frac{\eta_r - 1}{\phi} \tag{3}$$

plotting data as the reduced viscosity, η_{sp} (where $\eta_{sp} = (\eta_r - 1)/\phi$) versus ϕ for $0 \le X \le 22$ allows $[\eta]$ and $k_H[\eta]^2$ to be determined from the slope and intercept, respectively.

To interpret our results in terms of the charge fluctuation model, the most relevant information to derive from the viscometry data is the interdroplet attraction, which can be expressed in terms of either k_H or $1/\tau$. The value of k_H as determined by Eq. (2) can be very sensitive to any errors in $[\eta]$, which can lead to artifacts in the apparent dependence of k_H on other physical parameters. Thus, in analyzing our data, we chose to express the interparticle attraction in terms of $1/\tau$ rather than k_H, since this can be directly determined from the data independent of $[\eta]$, via Eq. (1). In addition, we extrapolated our results at low ϕ to obtain values of $[\eta]$ via Eq. (3) and determined k_H using Eq.(2) for a comparison. As discussed below, the values of $[\eta]$ given by Eq. (3) are close to the hard-sphere value, 2.5, for most samples (Table 2-1). Equation (1) utilizes the low-shear viscosity, and use of capillary viscometry itself assumes that the fluid is Newtonian and hence that the viscosity is independent of shear rate. The shear rate that the sample experiences in the capillary will depend on the time for the sample to flow through the viscometer, which in turn depends on the viscosity of the sample. For all of our samples, the flow time was in the range 100–1000 s. This corresponds to a shear rate that is $O(1)$ s^{-1} for all our samples. For the sample compositions that we examine ($X < 25$ and $\phi < 0.2$), we do not expect any non-Newtonian effects. Detailed rheological experiments of AOT/water/isooctane microemulsions suggest that shear-thinning effects are only observed at for samples with much higher water content, $X > 70$ [20]. Thus, for analysis of our data, we assume that

the viscosities obtained from capillary viscometry are equivalent to the low-shear viscosity and that they can be analyzed using Eqs. (1)–(2).

Ca(AOT)$_2$/water/n-decane system. The relative viscosity of Ca(AOT)$_2$/water/n-decane systems initially increases with increasing X, reaches a maximum at X = 15, and then decreases with further increases of water amount or X (Figure 2-2). Similar to NaAOT, the position of the maximum does not depend on ϕ, but the magnitude increases with ϕ.

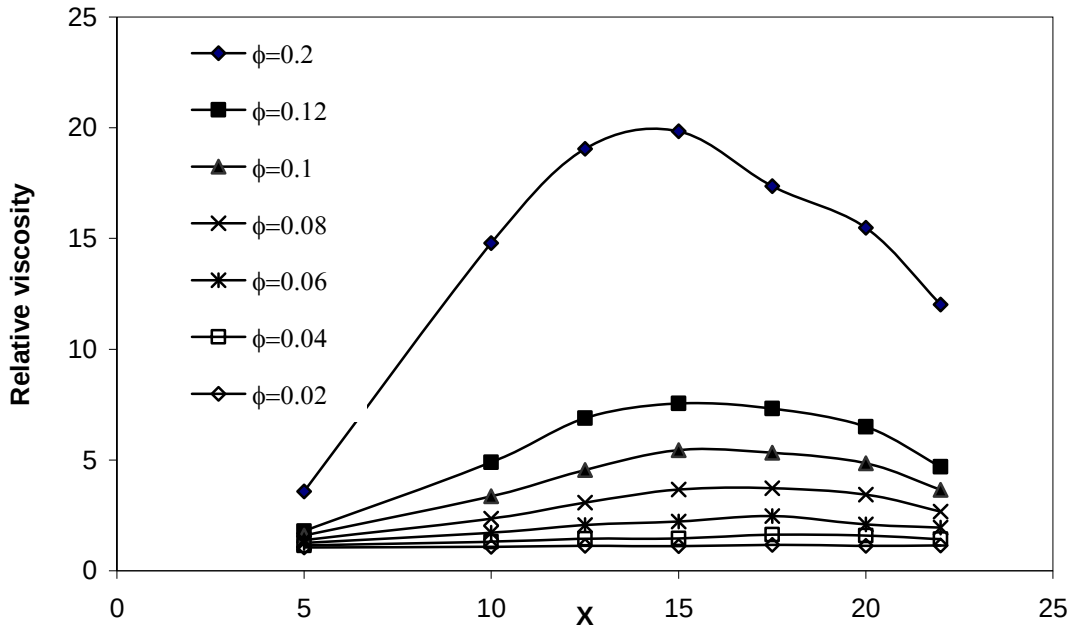

Figure 2-2. Relative viscosity η_r versus X, the molar ratio of water to Ca(AOT)$_2$, at fixed ϕ for the Ca(AOT)$_2$/water/n-decane system. Lines are guides for the eye.

A plot of η_{sp} versus ϕ for the Ca(AOT)$_2$/water/n-decane system at fixed X (Figure 2-3) allows the intrinsic viscosity $[\eta]$ to be determined from the intercept. The resulting intrinsic viscosity values at each X fall between 2.3 and 2.7 (Table 2-1). These values suggest that the droplets are either spherical or close to spherical, and that the surfactant tails are likely collapsed, with little penetration of decane into the surfactant layer. It is interesting that we obtain a value of $[\eta]$ close to the hard sphere value, in spite of the fact

that others have reported ellipsoidal droplets for the $Ca(AOT)_2$/water/*n*-decane system [18]. In addition, these values of $[\eta]$ suggest that the viscosity behavior we observe is not due to any type of change in the morphology or self-assembly of the system, such as observed in rodlike micelles that may change in aspect ratio or grow into wormlike micelles with changes in ionic strength.

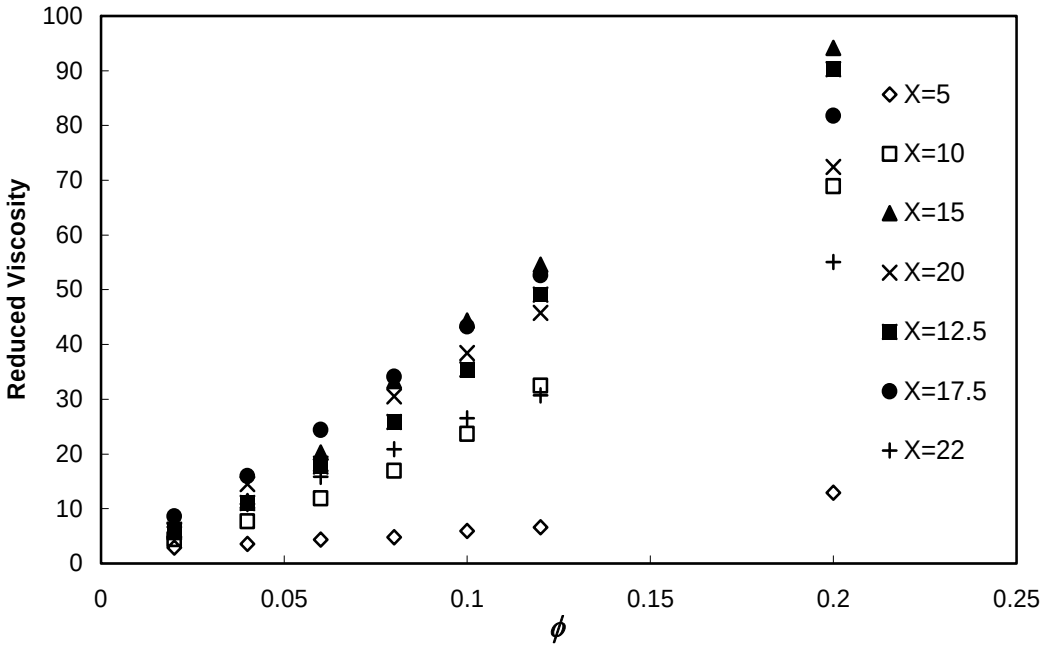

Figure 2-3. Reduced viscosity η_{sp} versus ϕ for the $Ca(AOT)_2$ system.

Table 2-1. Intrinsic viscosity of $Ca(AOT)_2$/water/n-decane, KAOT/water/n-decane, and $Mg(AOT)_2$/water/n-decane microemulsions as a function of *X*, the molar ratio of water to surfactant.

	X								
Surfactant	0	2.5	5	10	12.5	15	17.5	20	22
KAOT	3	--	2.6	2.5	--	2.4	--	2.3	--
$Ca(AOT)_2$	--	--	2.3	2.4	2.5	2.6	2.7	2.5	2.6
$Mg(AOT)_2$	2.8	3.0	3.9	--	--	--	--	--	--

The corresponding k_H values at each X are very high and reach a maximum of nearly 80 at X = 15 (Figure 2-4). Figure 2-5 shows η_r versus ϕ for the $Ca(AOT)_2$/water/*n*-decane system at fixed X along with quadratic fits to the data. Figure 2-5 includes data at very low ϕ (0.005–0.1) that are not shown in Figure 2-2 and 2-3; these data allow us to obtain more accurate values of fit parameters. In all cases, the data fit a quadratic form very well.

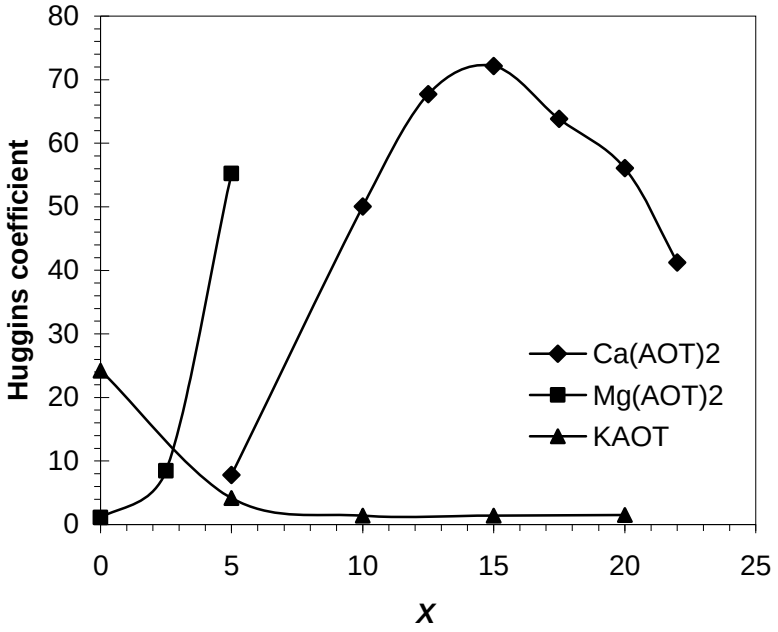

Figure 2-4. Huggins coefficient k_H versus X, the molar ratio of water to surfactant. Lines are guides for the eye.

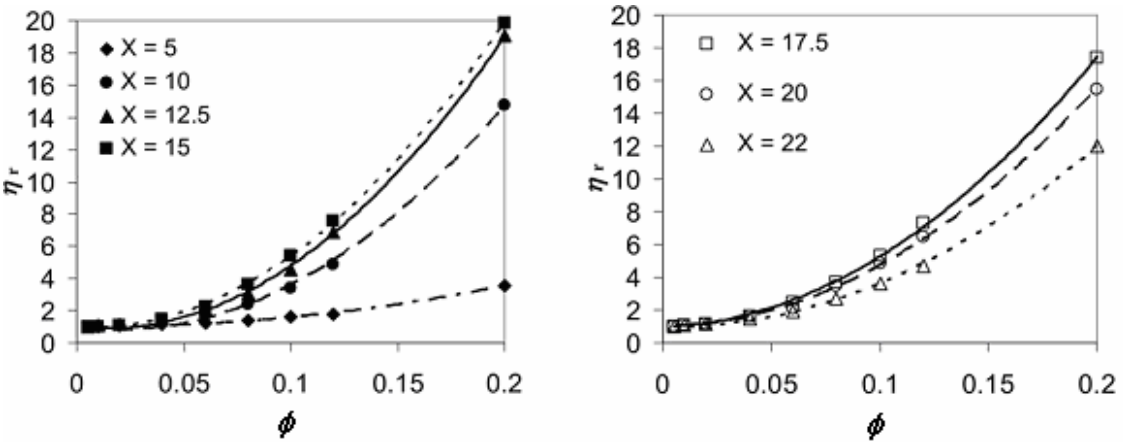

Figure 2-5. Relative viscosity η_r versus ϕ for the $Ca(AOT)_2$ system. For clarity, data at different X are shown on separate graphs for values below (left) and above (right) the viscosity maximum. Lines are fits to $\eta_r = 1 + 2.5\phi + (6.0 + 1.9/\tau)\phi^2$. Symbols and lines are as follows: $X = 5$, filled diamond and dot-dashed line; $X = 10$, filled circle and dashed line; $X = 12.5$, filled triangle and solid line; $X = 15$, filled square and dotted line; $X = 17.5$, open square and solid line; $X = 20$, open circle and dashed line; and $X = 22$, open triangle and dotted line.

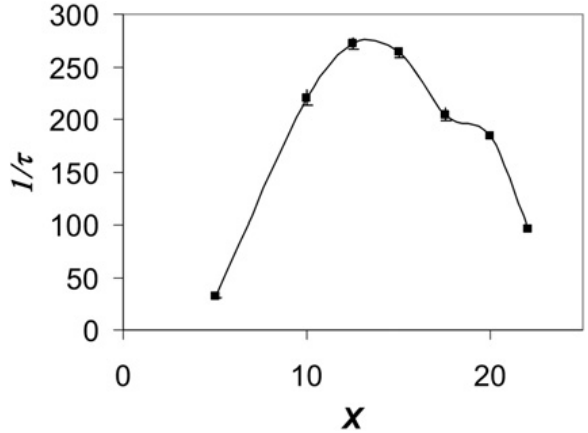

Figure 2-6. Stickiness parameter for $Ca(AOT)_2$/water/*n*-decane microemulsions versus X, the molar ratio of water to surfactant. The line is a guide for the eye.

Figure 2-6 shows the values of $1/\tau$ that can be derived from the data, along with uncertainties based on the goodness of fit. The relative uncertainty in the $1/\tau$ values are 2–5%. The values of $1/\tau$ are very high and reach a maximum at $X = 12.5$ (Figure 2-6). Again, similar to the NaAOT system, the droplet interactions appear to mirror the viscosity maximum, with a maximum attraction at a value of X near the viscosity maximum.

One interesting feature is the high value of k_H or $1/\tau$ for $Ca(AOT)_2$ microemulsions, suggesting strong attractive interactions between droplets. Corresponding values for the NaAOT system are in the range 1.0-10.0 [5]. Values of k_H for the NaAOT system are in the range 1.0–10.0, which would roughly correspond to $1/\tau$ values in the range 0.1–30.0 assuming that the droplets can be described as adhesive hard spheres [5]. The high values may be a consequence of approximating the interdroplet potential by a simple adhesive hard sphere model; if this is not an adequate description of the potential, the data must be interpreted in terms of qualitative trends only. Bergenholtz et al. [4] found that a square well model could not provide quantitative agreement between values for the interdroplet attraction derived from SANS and viscometry. However, these high values may also suggest strong interactions in the $Ca(AOT)_2$ system than in the NaAOT system. This may be related to the divalent counterion. When the Ca^{2+} counterion is released and surfactant exchange occurs between droplets, the resulting pair of oppositely charged droplets will each have a higher net charge than in the Na^+ case, resulting in a stronger electrostatic attraction.

According to the charge fluctuation model [5], the position of the maximum is dependent on X_m, which should be a function of both the number of water molecules needed for hydration and the binding energetics. Values for the hydration number of Ca^{2+} have been reported to be similar to or slightly higher than Na^+. The strength of binding for the (Ca^{2+})-$(AOT^-)_2$ pair is also likely to be much higher than the (Na^+)-(AOT^-) pair, due to stronger electrostatic interactions with the divalent cation. Thus, it is consistent with the model to expect that the maximum in viscosity would occur at a higher value of X.

KAOT/water/n-decane system. The relative viscosity of KAOT/water/n-decane systems demonstrates distinct behavior from $Ca(AOT)_2$ and NaAOT systems (Figure 2-7). At fixed ϕ, the relative viscosity of KAOT/water/n-decane systems has a maximum value at $X = 0$ (the waterless KAOT/n-decane system). The relative viscosity then decreases sharply to form a plateau as water content increases. A plot of η_{sp} versus ϕ for the KAOT/water/n-decane system at fixed X (Figure 2-8) allows determination of the intrinsic viscosity $[\eta]$ and the Huggins coefficient k_H from the intercept and slope, respectively. A plot of η_r versus ϕ for the KAOT/water/*n*-decane system at fixed X (Figure 2-9) allows determination of $1/\tau$. The relative uncertainties in the values of $1/\tau$ are in the range 2–6%, based on the goodness of fit. The intrinsic viscosity (Table 2-1) has a value of 3.0 for the waterless system, dropping to the hard sphere value for $X > 5$. The value of k_H (Figure 2-4) for the KAOT/water/n-decane system is roughly 24 for $X = 0$ but drops quickly to 1.4-1.5 as water content increases. This suggests that there are only weak attractive interactions between droplets for the hydrated systems. However, the lack of strong attractive interactions and a viscosity maximum in this system do support the idea that there is a connection between the viscosity maximum observed in NaAOT and $Ca(AOT)_2$ and the maximum in the interparticle attractions seen in those systems.

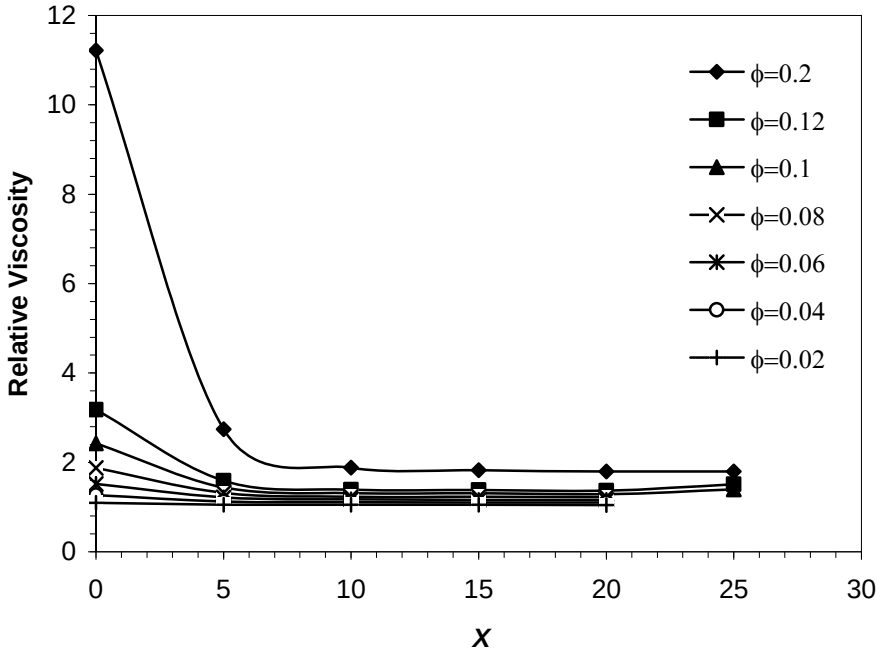

Figure 2-7. Relative viscosity η_r changes with X, molar ratio of water to KAOT. Lines are guides for the eye.

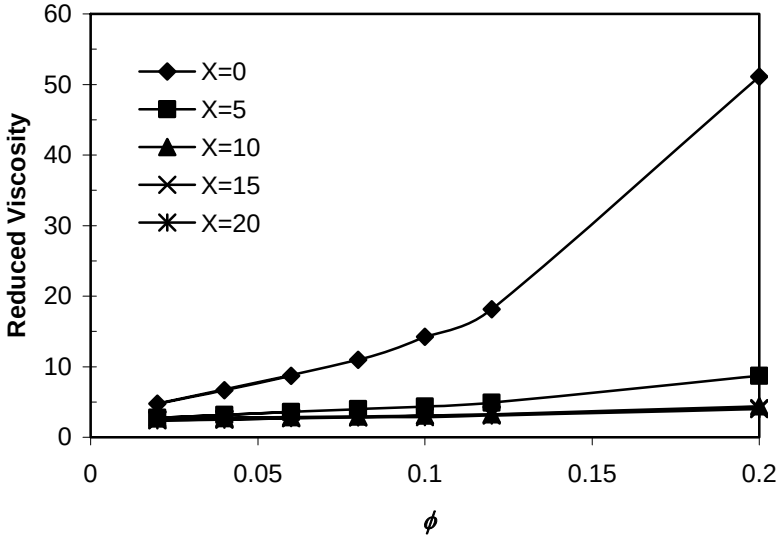

Figure 2-8. Reduced viscosity η_{sp} changes with ϕ, the volume fraction of droplet to total solution of KAOT. Lines are guides for the eye.

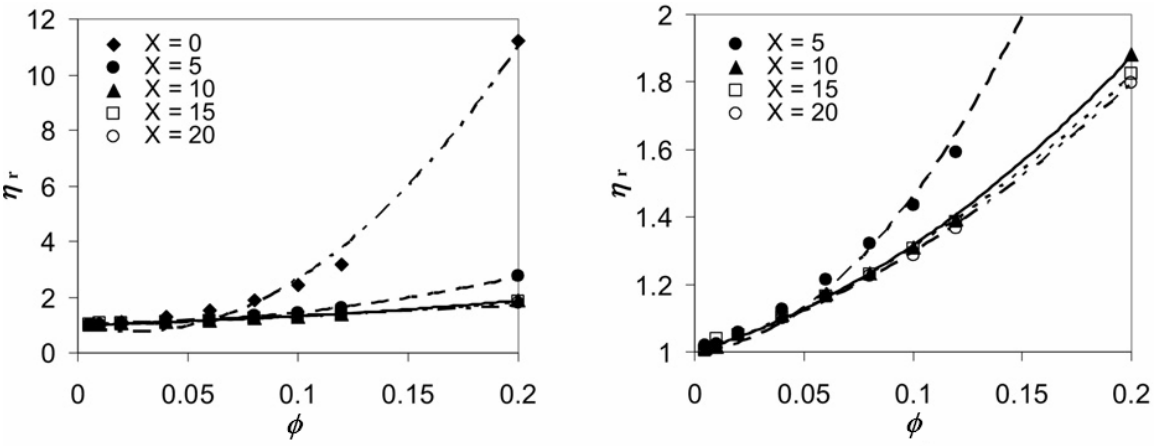

Figure 2-9. Relative viscosity η_r versus ϕ for the KAOT system. For clarity, data for the higher values of X are expanded on the right. Lines are fits to $\eta_r = 1+2.5\phi+(6.0+1.9/\tau)\phi^2$. Symbols and lines are as follows: $X = 0$, filled diamond and dot-dashed line; $X = 5$, filled circle and dashed line; $X = 10$, filled triangle and solid line; $X = 15$, open square and dotted line; $X = 20$, open and dot-dashed line.

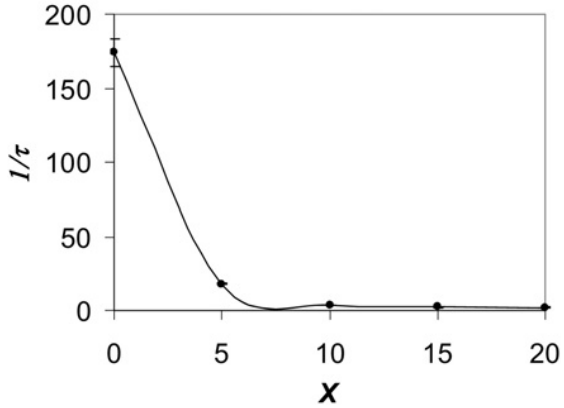

Figure 2-10. Stickiness parameter for KAOT/water/*n*-decane microemulsions versus X, the molar ratio of water to surfactant. The line is a guide for the eye.

The microscopic explanation of the difference between KAOT system and other systems is less clear. Some studies have implied that the interaction between K^+ and the sulfosuccinate group in AOT is not as strong as that between Na^+ and the sulfosuccinate group, due to the larger size of the K^+ counterion [10, 11], but in the context of the charge fluctuation model, this seems to imply that that X_m should be closer to the hydration number of the K^+ counterion, not that the maximum would disappear. The origin may lie

in the hydration behavior of the potassium counterion. As mentioned above, Monte Carlo simulations have shown that the hydration number of K^+ displays a probability distribution ranging from 5-10, as opposed to Na^+ in which the hydration number has a distinct value of either 5 or 6 [6]. In addition, analysis of the energetics in these simulations have shown that the waters in the first hydration shell of Na^+ have a strong interaction with the cation and a weak interaction with the rest of the solvent, whereas the waters in the first hydration shell of K^+ have interactions of nearly the same magnitude with the counterion and the rest of the solvent [6]. If this is the case, the interdroplet interactions and the overall behavior of the KAOT system would likely be insensitive to the amount of water in the system. In fact, this is precisely what we observe, although there are significant differences between the waterless system and $X = 5$, all of our measured and derived parameters for the KAOT system plateau for $X > 5$.

$Mg(AOT)_2$/water/n-decane system. From Figure 2-11 and 2-12, the relative viscosity and reduced viscosity of the $Mg(AOT)_2$ system change quickly with water content. Its relative viscosity increases sharply with water content below $X \leqslant 5$. The intrinsic viscosity of $Mg(AOT)_2$ system increases slightly from below 3 to above 3 with water content increasing. Here only the monophasic systems at $X = 0$, 2.5 and 5 were diluted for the investigation of Huggins coefficient and stickiness parameter (Figure 2-13).

Systems above $X = 5$ were separated into two phases. The upper one has almost same viscosity as the pure n-decane. The bottom one shows the features of a lamellar system and appears as a white soft deposit that does not flow easily. This suggests that the hydration of Mg^{2+} ion is very strong and the surfactants accumulate in the bottom phase at high water content.

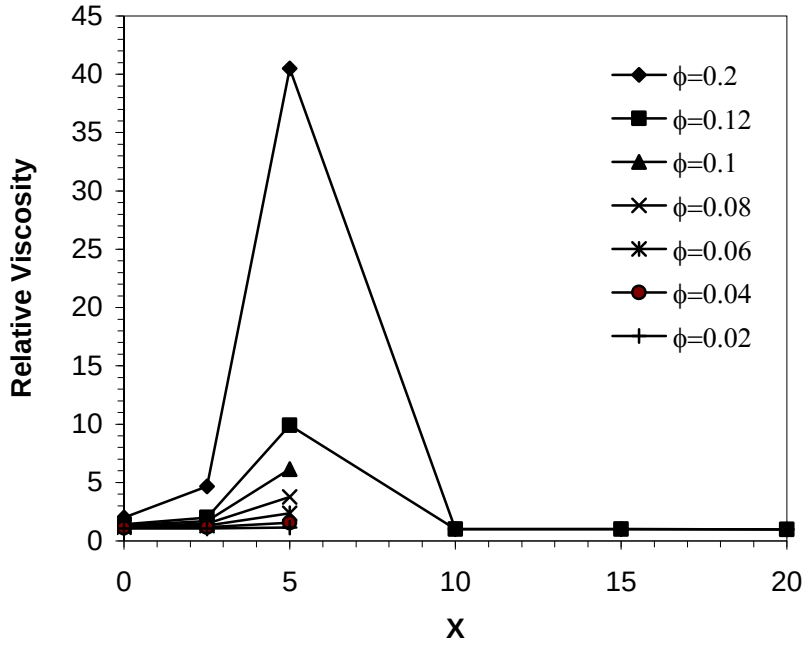

Figure 2-11. Relative viscosity η_r changes with X, molar ratio of water to $Mg(AOT)_2$. Lines are guides for the eye.

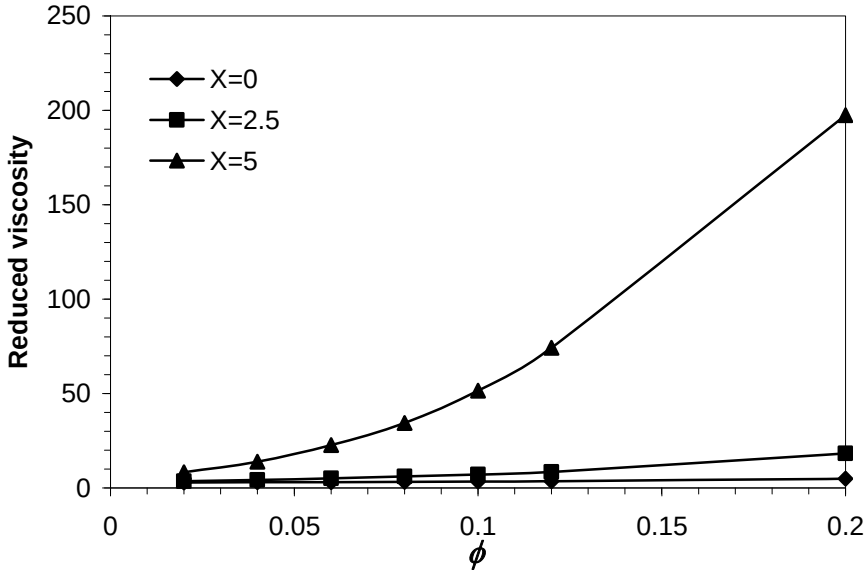

Figure 2-12. Reduced viscosity changes with ϕ, the volume fraction of droplet to total solution of Mg(AOT)*2*. Lines are guides for the eye.

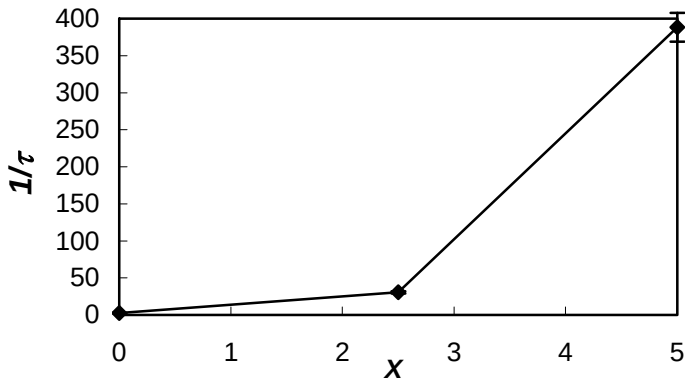

Figure 2-13. Stickiness parameter for $Mg(AOT)_2$/water/*n*-decane microemulsions versus *X*, the molar ratio of water to surfactant. The line is a guide for the eye.

2.4.3 Dynamic light scattering (DLS) (λ=541.5nm, θ=60º, *T*=30ºC)

Dynamic Light Scattering (DLS) is a good method for measuring droplet size and translational diffusion coefficient of microemulsion droplets. The scattering vector of dynamic light scattering is:

$q = (4\pi n_0/\lambda)sin(\theta/2)$

where q is scattering vector, n_0 is the refractive index of the solvent, θ is the scattering angle, λ is wavelength [2].

The translational diffusion coefficient D_T and average hydrodynamic radius R_h of the microemulsion droplets can be obtained from scattering intensity correlation function, Brownian motion principles and Stokes-Einstein Equation [2]:

$$R_h = \frac{k_B T}{6\pi\eta D_T}$$

where k_B is Boltzmann constant, η is the viscosity of solvent.

Figure 2-14 shows a transition for the hydrodynamic radius of $Ca(AOT)_2$/water/n-decane microemulsion droplets at *X*=12 or so, similar to the behavior of NaAOT systems [5]. For the KAOT/water/n-decane system, Figure 2-15 shows droplet size increases

rapidly with water content at high volume fraction but almost does not change with water content at low volume fraction. Figure 2-16 shows droplet sizes of $Mg(AOT)_2$/water/n-decane microemulsion increase quickly with water content at fixed volume fractions.

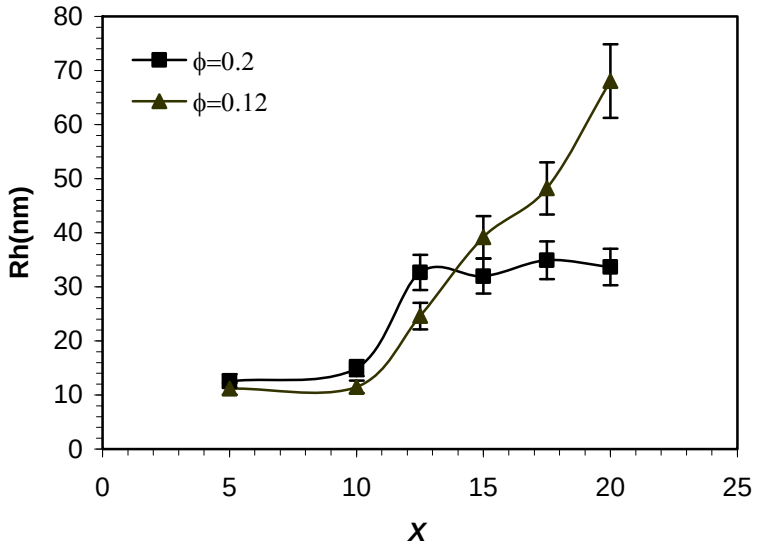

Figure 2-14. Average hydrodynamic radius of $Ca(AOT)_2$/water/decane microemulsion droplets. Lines are guides for the eye.

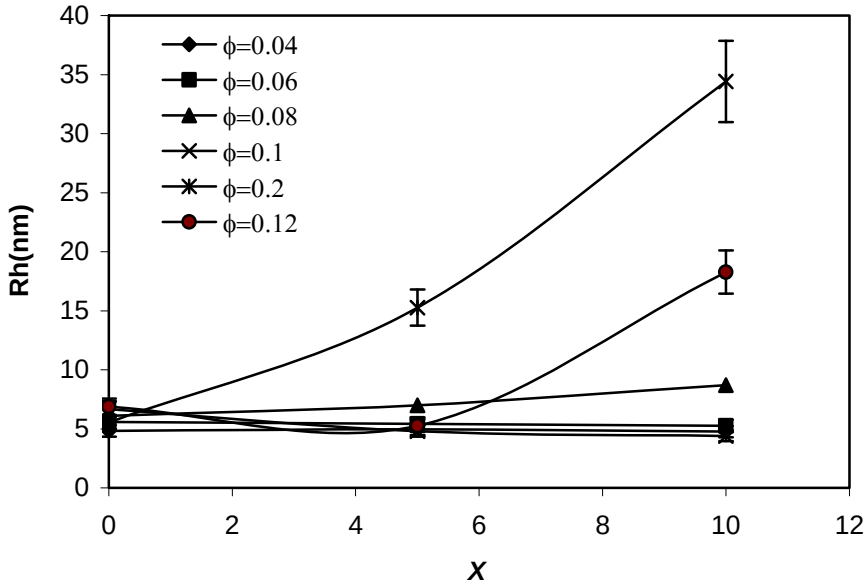

Figure 2-15. Average hydrodynamic radius of KAOT/water/decane microemulsion droplets. Lines are guides for the eye.

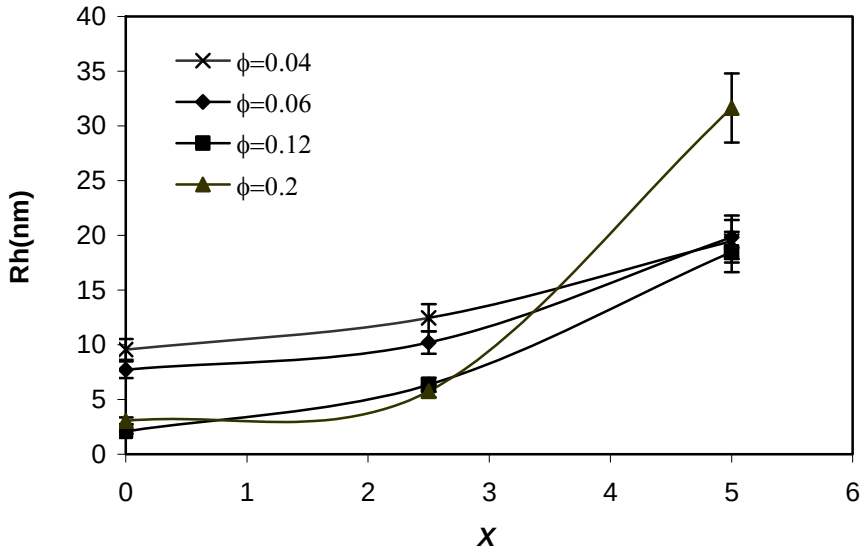

Figure 2-16. Average hydrodynamic radius of $Mg(AOT)_2$/water/decane microemulsion droplets. Lines are guides for the eye.

These results suggest that the hydration capability of the counterion plays an important role in the droplet size and the viscosity behavior. In the series we have examined, Mg^{2+} has the strongest hydration capability and K^+ has the weakest hydration capability. So water content has more obvious effects on the droplet sizes of $Ca(AOT)_2$ and $Mg(AOT)_2$ systems.

2.4.4 Effects of Water Content

Water content plays an important role in the phase stability and microstructure. For divalent counterions, there is a trend to form cylindrical aggregates when water content increases [12]. We observe similar behavior (Table 2-1 and Figure 2-4) in $Ca(AOT)_2$ and $Mg(AOT)_2$ systems, the intrinsic viscosities of increase with water content (Table 2-1). Spherical droplets are present if the hydration radius R_h of counterion < 3.0 Å, and cylinder shape droplets are present if R_h >3.0 Å because the R_h will affect the interaction

between counterion and hydrated SO_3^- group as some authors stated [12]. The R_hs of Na^+, K^+, Mg^{2+} and Ca^{2+} are 1.6Å, 1.1Å, 3.1Å and 2.7Å respectively [11]. As Table 2-1 shows, $Mg(AOT)_2$, $Ca(AOT)_2$ and KAOT systems all have a structure transition when they switch from the waterless binary systems to ternary systems with water since all the hydration radius of counterion increases with addition of water. As Figure 2-3 shows, the $Mg(AOT)_2$ system containing water has a stronger interaction than waterless system. However the KAOT system has reverse behavior and its intrinsic viscosity also decreases with addition of water. The shape fluctuation may also make contribution to interaction.

The results of DLS experiments provide some explanations. At constant volume fraction, the surfactant content decreases slowly and water content increase sharply, and the droplet size increases with water content except KAOT systems, shown in Figure 2-14 – Figure 2-16. The swelling of the droplets increases the possibility of penetration of solvent or overlapping of surfactant tails, leading to a stronger interaction and higher viscosity. But when the swelling grows to some degree, the droplets merge into larger droplets. This merging will decrease the amount of droplets and their interaction surface area, leading to the decrease of the viscosity. In low volume fraction KAOT systems, the droplet size does not change too much with water content. It shows K^+ has very low hydration capacity. The large droplet can be stabilized only in high volume fraction KAOT systems. It suggests that the bicontinuous structures exit in high water content systems, especially in KAOT and $Mg(AOT)_2$ systems.

2.4.5 Effects of Temperature

The three kinds of systems in this work have different sensitivities to temperature. KAOT and $Ca(AOT)_2$ systems are more sensitive than $Mg(AOT)_2$. Compared with the insensitivity of $M(AOT)_2$/water/cyclohexane to temperature and the less sensitivity of NaAOT/water/cyclohexane to temperature [10], this shows that the sensitivity may partially arise from the long chain of n-decane that can penetrate into the tails of AOT.

2.4.6 Effects of Ion Hydration and Mobility

We have compared the viscosity behavior of NaAOT, KAOT, $Ca(AOT)_2$, and $MgAOT)_2$ with each other, and discussed the effects of ion charge, hydrodynamic ion radius, water and volume fraction on the viscosity, and tried to use charge fluctuation model to explain the viscosity anomalies. The charge fluctuation model suggested a possible origin of viscosity anomaly. At present, there are two existing mechanisms to describe charge fluctuations in microemulsion [2] (Figure 2-17). One mechanism is hopping, indicating surfactant ions hop from one droplet to another one. The other one is that ions transport by fusion and fission. The asymmetric shape of droplets or deviation from spherical shape may also affect the viscosity, which is indicated by the intrinsic viscosity.

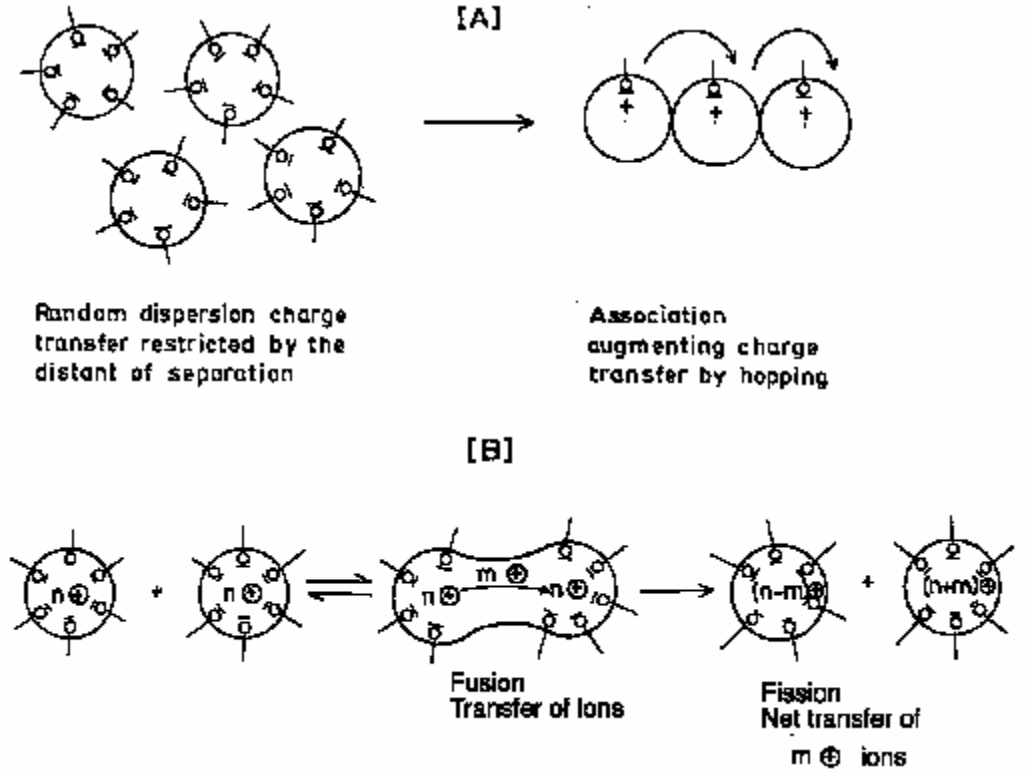

Figure 2-17. [A]. Hopping mechanism. Ions hop in the direction indicated by the curl heads. [B]. Ion transport by fusion and fission. *n* cations in the droplets. *m* cations are involved in the transfer process. (Source: Ref [2])

However, the viscosity behavior of KAOT microemulsion system is not explained thoroughly. So we need to more carefully consider the nature of the ions. The two mechanisms of charge fluctuation are both related to an important property, the mobility of ions. The mobility of ions is related to the ion bindings with other ions or water molecules. The ion bindings are related to electrostatic force, hydrogen bonds, and VDW forces in the systems. We have discussed the relationship between viscosity anomaly and the hydration of cations, and also discussed the particular hydration capacity of K^+ and its interaction strength with the hydration water and bulk water. Table 2-2 shows Ca^{2+} and Mg^{2+} have much larger hydration energy than K^+ and Na^+.

Table 2-2. Enthalpy of Hydration (H_{hyd} kJ/mol) of some typical ions.
(http://www.science.uwaterloo.ca /~cchieh/cact/ applychem/hydration.html and ref. [21])

Ion	$\boldsymbol{H_{hyd}}$	**Ion**	$\boldsymbol{H_{hyd}}$	**Ion**	$\boldsymbol{H_{hyd}}$
H^+	-1130	Al^{3+}	-4665	Fe^{3+}	-4430
-	-	-	-	F^-	-505
Li^+	-520	Be^{2+}	-2494	Cl^-	-363
Na^+	**-406**	**Mg^{2+}**	**-1921**	Br^-	-336
K^+	**-322**	**Ca^{2+}**	**-1577**	I^-	-295
Rb^+	-297	Sr^{2+}	-1443	**NO_3^-**	**-329**
Cs^+	-276	Ba^{2+}	-1305	ClO_4^-	-238
-	-	-	-	**HSO_4^-**	**-289**
Cr^{2+}	-1904	Mn^{2+}	-1841	Fe^{2+}	-1946
Co^{2+}	-1996	Ni^{2+}	-2105	Cu^{2+}	-2100
Zn^{2+}	-2046	Cd^{2+}	-1807	Hg^{2+}	-1824

Here we need to introduce other helpful concepts for possible understanding of the distinct viscosity behavior between KAOT and the others. Small ions with high charge density will cause strong electrostatic ordering of surrounding waters and breaking of hydrogen bonds, so this type of ions are called kosmotropes - order maker, such like Mg^{2+}, Ca^{2+}, and Na^+ [22]. For large ions with low charge densities, their surrounding waters are largely hydrogen bonded and disordered, so they are called chaotropes - disorder maker, such like K^+ [22]. This is in agreement with Monte Carlo simulations of the hydration number of K^+ and hydration energetics in the above discussions. Another important concept, screening-binding effects, indicates that hydrated water shell weakens the electrostatic forces between cations and anions [23]. This may play a key role in the release of surfactant ions during hydration of cations, which affects the mobility of both anions and cations.

Freda et al found the addition of water into NaAOT/water/CCl_4 system would increase

the mobility of the polar heads and then the overall molecule mobility from dielectric measurements and neutron scattering [24]. Fioretto et al and D'Angelo et al used infrared and dielectric spectroscopy to investigate the dynamics-hydration relationship in NaAOT/water/CCl_4, $Ca(AOT)_2$/water/CCl_4, and $Cu(AOT)_2$/water/CCl_4 systems, and observed that hydration can dilute the interaction between charged groups and enhance the individual mobility [25-28]. These results are helpful to understand the viscosity anomaly and charge fluctuation in our microemulsion systems.

However, the mobility of KAOT as a function of water/KAOT ratio is not reported. From Table 2-2, if we assume the hydration energy of SO_3^- is similar to NO_3^- and HSO_4^-, there may be a competition between the K^+ and AOT^-, especially after K^+ is hydrated by low amount of water. The mobility of hydrated AOT^- may be much less than the anhydrated AOT^- anion. In NaAOT, $Ca(AOT)_2$, and $Mg(AOT)_2$ microemulsions, AOT^- may not be hydrated until the cations are completely hydrated. This difference may help us to explain the distinction between KAOT and the other three surfactants. K. Sameshima et al. suggested that all the O atoms of SO_3^- form hydrogen bonds with H_2O when [water]/[AOT] is above 5 [29].

In summary, the screening effects of hydration water shell and the mobility of ions may be the key to discover the mechanism of viscosity anomaly in AOT microemulsion systems and even all the ionic surfactant-based microemulsion systems. And if these are true, it is possible to predict the performance of other ions with similar ion charge density and similar hydration energy. So a future work on mobility of KAOT as a function of water/KAOT molar ratio would be suggested.

In addition, for the hopping mechanism in Figure 2-17, there may be an effect from

solvent. Long chain oils like decane may have more drag force than the short chain oils like CCl_4 or cyclohexane. This may cause a lower interparticle interaction in short chain oils. It would be another meaningful future work to investigate the effects of solvent on the charge fluctuation.

2.5 Summary

In this study KAOT, $Ca(AOT)_2$ and $Mg(AOT)_2$ were synthesized from NaAOT, and then viscometry and dynamic light scattering were used to investigate the phase behavior, viscosity, interparticle interaction, and microstructure of $Ca(AOT)_2$/water/n-decane, $Mg(AOT)_2$/water/n-decane, and KAOT/water/n-decane microemulsions. These systems demonstrate distinct behavior in terms of viscosity and particle interactions. $Ca(AOT)_2$/water/n-decane systems demonstrate a maximum in relative viscosity, intrinsic viscosity, and interdroplet attraction as a function of the molar ratio of added water to surfactant, X, at a fixed volume fraction ϕ. This behavior is similar to that of NaAOT/water/n-decane systems. The maximum occurs at a higher volume fraction. The relative viscosity, stickiness parameter $1/\tau$ and Huggins coefficient k_H for the $Ca(AOT)_2$/water/n-decane system demonstrates a maximum near X = 12.5~15. These features of the $Ca(AOT)_2$/water/n-decane system are similar to the behavior of the NaAOT/water/n-decane system, which displays a maximum in viscosity and a maximum in droplet attraction at X = 8 [4, 5].

These anomaly phenomena may contribute to the transition of droplet size and the charge fluctuation model. Molecular rearrangement or ion exchange on surfactant interface leads to a charge fluctuation. Smaller ion radius and higher charge can lead to stronger interaction because of charge fluctuation. K^+ shows a weaker interaction with

water, and Ca^{2+} and Mg^{2+} shows a stronger interaction with water than Na^{+}, both leading to a phase separation more easily at high water content systems than NaAOT systems. NaAOT and $Ca(AOT)_2$ systems have some similar behaviors in terms of viscosity and microstructure. The ionic and hydrodynamic radius of counterion plays a more important role in the behaviors of viscosity, microstructure, and droplet shape than its charge. With n-decane as solvent, the microemulsion systems show some sensitivity to temperature which may arise from the long chain of n-decane, showing some effects of solvent. The mobility of KAOT as a function of water/KAOT ratio may be the key to explain the distinct viscosity anomaly in KAOT systems.

Bibliography

[1] S. H. Chen. *Annu. Rev. Phys. Chem.,* **1986**, 37, p351.

[2] S. P. Moulik; B. K. Paul. *Adv. Colloid Interface Sci.,* **1998**, 78, (2), p99.

[3] M. Kotlarchyk; S. H. Chen; J. S. Huang. *J. Phys. Chem.,* **1982**, 86, (17), p3273.

[4] J. Bergenholtz; A. A. Romagnoli; N. J. Wagner. *Langmuir,* **1995**, 11, (5), p1559.

[5] U. Batra; W. B. Russel; J. S. Huang. *Langmuir,* **1999**, 15, (11), p3718.

[6] M. Carrillo-Tripp; H. Saint-Martin; I. Ortega-Blake. *J. Chem. Phys.,* **2003**, 118, (15), p7062.

[7] R. Mancinelli; A. Botti; F. Bruni; M. A. Ricci; A. K. Soper. *J. Phys. Chem. B,* **2007**, 111, (48), p13570.

[8] M. F. Bush; R. J. Saykally; E. R. Williams. *Chem Phys Chem,* **2007**, 8, (15), p2245.

[9] J. Eastoe; S. Chatfield; R. Heenan. *Langmuir,* **1994**, 10, (6), p1650.

[10] J. Eastoe; G. Fragneto; B. H. Robinson; T. F. Towey; R. K. Heenan; F. J. Leng. *J. Chem. Soc.-Faraday Trans.,* **1992**, 88, (3), p461.

[11] J. Eastoe; T. F. Towey; B. H. Robinson; J. Williams; R. K. Heenan. *J. Phys. Chem.,* **1993**, 97, (7), p1459.

[12] C. Petit; P. Lixon; M. P. Pileni. *Langmuir,* **1991**, 7, (11), p2620.

[13] J. Eastoe; W. K. Young; B. H. Robinson; D. C. Steytler. *J. Chem. Soc.-Faraday Trans.,* **1990**, 86, (16), p2883.

[14] J. S. Huang; M. W. Kim. **1984**, 24, (2), p197.

[15] J. S. Huang. *J. Chem. Phys.,* **1985**, 82, (1), p480.

[16] J. Lang; A. Jada; A. Malliaris. *J. Phys. Chem.,* **1988**, 92, (7), p1946.

[17] F. Caboi; G. Capuzzi; P. Baglioni; M. Monduzzi. *J. Phys. Chem. B,* **1997**, 101, (49), p10205.

[18] P. Pitzalis; R. Angelico; O. Soderman; M. Monduzzi. *Langmuir,* **2000**, 16, (2), p442.

[19] M. Kotlarchyk; S. H. Chen; J. S. Huang; M. W. Kim. *Phys. Rev. A,* **1984**, 29, (4), p2054.

[20] J. Emsley. The elements. Clarendon Press, Oxford, 1989.

[21] J. Salamone. Polymeric Materials Encyclopedia. CRC Press, **1996**, p5812.

[22] B. Hribar; N. Southall; V. Vlachy; K. Dill. *J. Amer. Chem. Soc.*, **2002**, 124, p12302.

[23] M.Bara; A.Guiet-Bara; J. Durlach. *Magnes. Res.* **1988**, 1, p29. *Magnes. Res.* 1989, 2, p243.

[24] M. Freda; G. Onori; A. Paciaroni; A. Santucci. *J. Non-Crystal. Sol.*, **2002**, 307–310, p874.

[25] D. Fioretto, M. Freda, G. Onori; A. Santucci. *J. Phys. Chem. B* **1999**, 103, p8216.

[26] M. D'Angelo; D. Fioretto; G. Onori; L. Palmieri; A. Santucci. *Phys. Re*V. *E* **1995**, *52*, pR4620.

[27] M. D'Angelo; D. Fioretto; G. Onori; L. Palmieri; A. Santucci. *Phys. Re*V. *E,* **1996**, *54* (1), p993.

[28] D. Fioretto; M. Freda; G. Onori; A. Santucci. *J. Phys. Chem. B,* **1999**, 103(14), p2631.

[29] K. Sameshima; R. Tanaka; K. Igarashi; H. Ooshima. *J. Chem. Therm.* **2006,** 38, p662.

CHAPTER 3

NEW FLUOROCARBON-BASED MICROEMULSION GELS

3.1 Introduction

In this chapter, we explore perfluorocarbon microemulsions with triblock copolymers. These systems are of interest from both a fundamental and a practical point of view. We will use our experimental results to attempt to develop a universal description of gelation in soft attractive colloidal systems.

3.2 Background

From a fundamental standpoint, we will use these systems to develop a unifying description of the relationship between structure and rheology of soft attractive colloids. We will focus on controlling the particle potential and liquid-gel transition, and on understanding the mechanism of gelation, including the critical concentration for gel formation and relative importance of the "softness", the potential and attractive interactions. Our systems consist of microemulsion droplets with a radius of α and volume fraction ϕ, with p end-adsorbing triblock polymers per droplet. The polymers can either form loops on the particle surface, leading to a soft repulsion, or bridges between two droplets, leading to a soft attraction of Φ_{min}/kT. The polymer chains can be described by a segment length l, number of segments N, and excluded volume parameter V_{ex}. The surface coverage of chains, or chain ends per area, is given by $n_p = p/(2\pi\alpha^2)$, and the polymer layer thickness is given by L_a, which is a function of N, l, n_p, and V_{ex} [1-3]. The

repulsive force arising from the polymer loops can be shown [2, 3] to depend on $L_a^2 n_p$; thus, we will use $L_a^2 n_p$ as a measure of the softness of our systems.

We will formulate solutions with differing values of droplet concentration, polymer concentration, and polymer molecular weight to vary ϕ, p, and N, respectively. Small-angle neutron scattering (SANS) and small-angle x-ray scattering (SAXS) will be used to quantify the interactions and elucidate the solution structure, providing values for L_a, $\Phi_{\min}/kT$, and ϕ_{eff}. Rheological experiments then will be performed to characterize the gel transition in our systems as a function of ϕ_{eff}, $\Phi_{\min}/kT$, and $L_a^2 n_p$. We envision developing a universal description of the viscoelasticity, analogous to Eq. (1-3) and Eq. (1-4), in terms of critical values for ϕ_{eff}, $\Phi_{\min}/kT$, and $L_a^2 n_p$.

Our overall vision and relationship to previous results is summarized in Table 3-1.

Table 3-1. Liquid-gel Transitions in different colloidal systems and relevant parameters.

Particle interactions	**Liquid-gel phase transitions**	**Relevant parameters**
Hard spheres [3-5]	Glass formation	ϕ - particle volume fraction
Soft spheres [6, 7]	Glass formation	ϕ_{eff} -effective volume fraction
Hard attractive spheres [8-13]	Glass formation or attractive aggregation (" jamming transitions")	ϕ -particle volume fraction $\Phi_{\min}$ - strength of attraction
Soft attractive spheres	Glass formation or attractive aggregation (" jamming transitions")	ϕ_{eff} -effective volume fraction $\Phi_{\min} / kT$ - attraction strength $L_a^2 n_p$ -softness

From a practical point of view, we will focus on perfluorocarbon systems that are of interest for biomedical uses. The unique properties of PFCs, including their biocompatibility and high capacity for dissolved gases, are reviewed in Chapter 1. Some perfluorocarbons (PFCs) are known to be able to form microemulsions with water and fluorinated surfactants [14-16]. Perfluorooctylbromide (PFOB) is one such PFC. PFOB

has several biomedical applications. It is known to enhance tumor echogenicity, and hence has been used as a contrast material for CT, MRI and ultrasound imaging, especially for hepatosplenography and tumor-imaging [16-18]. PFOB emulsions are also used for oxygen carriers in cell culture and cell-based devices, for example in bio-artificial liver systems [19] and in cell encapsulation matrices [20].

The structure and rheology of PFC-based products can impact their use in the above applications. For example, in PFC emulsions, the size of PFC droplets influences oxygen transport, and for cell encapsulation applications, it is important that the system be a mechanically robust gel. However, it is difficult to form stable elastic gels of PFOB that can be used in clinical settings. In general, the difficulty arises from fluorocarbons' high fluidity, high hydrophobicity, and the low capability to dissolve common gelation agents [14]. A few types of PFC-based gels have been reported, but these have mainly been emulsions (water-in-fluorocarbon or fluorocarbon-in-water) that are only kinetically stable [21-33]. Fluorinated polyethoxylated alcohols can be formed as water-in-fluorocarbon emulsion gels with 50-98% water content [24, 25, 33]. Fluorocarbon-in-water emulsion gels have been reported to be formed from a variety of light and heavy linear and cyclic fluorocarbons [29, 30] or formed by adding a thickener to the aqueous phase of a emulsion [23, 26]. Gels in organic media can be formed by cooling the $F(CF_2)_n(CH_2)_mH$ diblock solutions below T_g or formed from mixtures of fluorocarbon, phospholipids, semifluorinated alkane and small amount of water [21-23, 26, 28-30, 32]. Gels in a continuous water medium also can be formed by cooling some fluorocarbon vesicle systems below crystal-liquid crystal phase transition temperature [31]. The rheological properties and structure of some PFC-based emulsion gels have been

investigated by Stébé and coworkers [24, 25, 27, 33, 34]. Some authors studied fluorocarbon-based binary emulsion systems with triblock copolymers as emulsifier [35, 36].

3.3 Objective of Project

Our aim is to make use of triblock copolymers, mainly PEO-PPO-PEO, such as Pluronic® F127, $(EO)_{101}$-$(PO)_{56}$-$(EO)_{101}$, to control the phase behavior and rheological properties of PFOB-based microemulsion solutions, and in so doing create stable microemulsion gels with tunable elasticity. We will utilize water-in-fluorocarbon microemulsions. We predict that the hydrophilic PEO endblocks will enter the water cores of the microemulsion droplets, while the relatively hydrophobic PPO chains will reside in the continuous fluorocarbon phase. The target structure is shown as Figure 3-1. The PPO midblocks may either form loops on the droplet surface or bridges between droplets, and in so doing increase the effective volume fraction of droplets. Chains that bridge droplets serve as transient "crosslinks," creating a networked structure and providing an attractive force between droplets, while loops contribute a soft repulsion between droplets. Thus, the targeted systems can be considered as soft attractive colloidal systems.

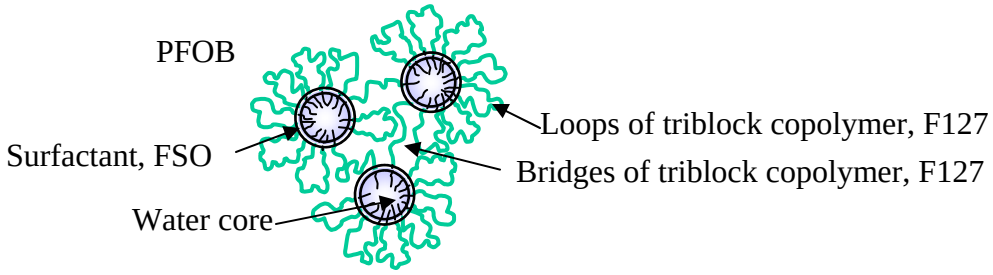

Figure 3-1. Scheme of PFOB/FSO/water with triblock copolymers. The copolymers form loops and bridges on microemulsion droplets with PFOB as solvent and water as droplet core. Dark circles indicate surfactant layer.

3.4 Materials and Experiments

Materials. PFOB, Pluronic® F127 (abbreviated as F127), and Zonyl® FSO-100 (F-$(CF_2)_{7.5}$-$(CH_2CH_2$-$O)_8$-H, abbreviated as FSO) were obtained from Sigma Aldrich. Deuterium Oxide (D_2O, 99.8 atom% D) and fluorescein isothiocyanate (FITC) were obtained from Acros Organics. Pluronic® F68, F87, F98, F108, and Pluronic® R 25R4 were obtained from BASF. Nanopure water was used in all sample preparation, except SANS samples which were prepared with D_2O.

Sample Preparation. Previously published phase diagrams of water, FSO, and perfluorocarbons suggest that stable water-in-oil microemulsions may be formed at room temperature with 1:1 ratios of water to PFC, and at FSO concentrations in the range of 10-22 wt% [37]. Unless otherwise noted, for all samples described herein, the concentration of FSO was kept constant at 15 wt%, with varying amounts of PFOB, water, and F127. Aqueous solutions of F127 in nanopure water were prepared by dissolving F127 in water at concentrations of 0.5 – 12 wt%, stirring for one day, then resting for one day to remove air bubbles. These solutions were then mixed with PFOB and FSO, stirred for 5 hours at room temperature, and then held still at for 5 hours for equilibration and to remove air bubbles. It was found that F127 did not dissolve directly in PFOB. This suggests that in our final samples, all F127 triblocks are associated with microemulsion droplets, or in other words, there are no F127 micelles in the continuous PFOB phase.

We refer to samples using the following nomenclature: ϕ = 0.58, 4 wt% F127. The volume fraction of droplets, ϕ, assumes ideal mixing and is calculated as the volume of

the aqueous phase plus the volume of FSO over the total volume. This is consistent with how ϕ is defined in other work on microemulsions with added block copolymers [38-46]. The water-in-oil microemulsion structure was verified by SANS, as described below. The stated concentration of triblock polymer, 4 wt% F127, is the concentration of F127 relative to the aqueous phase, *not the overall concentration in the sample.*

Rheology. A TA AR2000 stress-controlled rheometer was used to investigate the storage modulus, loss modulus, and viscosity. The linear viscoelastic region was determined by a stress sweep, and then the storage modulus *G'* and loss modulus *G"* are obtained by performing a frequency sweep. Viscosities were obtained by steady flow experiments at low shear rate. Temperature sweeps were used to investigate the thermal properties of the rheology from 10ºC to 35ºC.

Small Angle X-ray Scattering (SAXS). Samples were transferred into 0.1mm thickness quartz capillary tubes and sealed using epoxy, then placed in a SAXS vacuum channel for testing. The SAXS experiments were conducted on a Molecular Metrology SAXS instrument at the W.M. Keck Nanostructures Laboratory at the University of Massachusetts Amherst. The instrument generates X-rays with a wavelength of λ = 1.54 Å and utilizes a 2-D multiwire detector with a sample-to-detector distance of 1.5 m. For transparent samples, SAXS data were collected for 50 minutes. For opaque samples, it took 4 hours to obtain enough scattering contrast. The intensity was reduced and normalized by the Polar® software.

Confocal Microscopy. A Leica DM-IRBE confocal optical microscopy was used to investigate sample homogeneity and possible phase separation at the microscale. Samples

were prepared as above, with the hydrophilic dye FITC added to the aqueous phase at a concentration of 20 ppm prior to sample mixing.

Small Angle Neutron Scattering (SANS). Scattering experiments were conducted at the NG-3 beamline with a wavelength of 6 Å, at the National Center for Neutron Research (NCNR), National Institute for Standards and Technology (NIST), Gaithersburg, MD [47]. Samples for SANS were prepared as above, except H_2O was replaced by D_2O. Samples were loaded into 1-mm thick quartz cells. Some samples were centrifuged to remove air bubbles before loading the cells to the slots of SANS facility. The sample to detector distances were 4 m and 13.18 m for high *q* and low *q* value, and the spectra were collected for 5 minutes and 3 minutes respectively. The combined *q* range is from 0.001 $Å^{-1}$ to 0.2 $Å^{-1}$. Spectra were obtained at 25 °C for investigation of composition effects and from 10^{o} C to 32^{o} C for temperature effects. There are 5 minutes of equilibrium for each temperature. Data reduction and normalization were performed using standard techniques [48] and all SANS data reported in this work are on an absolute scale. The scattering length densities for all materials used in this SANS experiments are given in Table 3-2.

Table 3-2. Scattering length density (SLD) of the materials in SANS experiments.

Materials	SLD($Å^{-2}$)
H_2O	-5.6e-7
D_2O	6.33e-6
$C_8F_{17}Br$	3.64e-6
FSO	7.29e-7
$-CH_2CH_2O-$	5.66e-7
$-CH_2CHCH_3O-$	3.43e-7
$F-(CF_2)_{7.5}$ -	~ 4e-6
F127	~ 4.86e-8

3.5 Results and Discussion

3.5.1 Formation and Stability of Microemulsions

Previously published phase diagrams for the PFOB/water/FSO system show formation of a water-in-oil microemulsion, but unfortunately these phase diagrams are for $T > 40^{o}$C [37]. For biomedical applications, it is desirable to have stable systems at temperatures ranging from ambient temperature to physiological conditions (i.e., 25^{o}C – 34^{o}C). Thus, it was necessary to first verify the temperature and concentration space over which stable, transparent solutions were formed.

Samples with 15 wt% FSO, $\phi = 0.58$, and 0 – 12 wt% F127 were found to form stable, transparent systems at ambient temperatures. The transparent, stable nature of these samples suggests that a microemulsion is formed, and this was verified with SANS, as described below. Qualitatively, the samples appear to be liquid for 0 – 1 wt% F127 and gels for higher triblock concentrations (Figure 3-2).

Figure 3-2. Transparent, stable liquids and gels formed with the addition of F127 to a microemulsion at $\phi = 0.58$ and 15 wt%FSO. From left to right, samples contain 0, 0.5, 1, 2, 4, 6, 8, and 12 wt% F127. Samples are at $T = 21$ºC.

Confocal microscopy was used to confirm that there was no phase separation in these samples on the microscale. Figure 3-3 shows micrographs of samples with the hydrophilic dye FITC at varying ϕ and 4 wt% F127. No phase separation can be seen for

samples at ϕ = 0.58. Interestingly, samples at lower ϕ display evidence of phase separation for the 4 wt% F127 system.

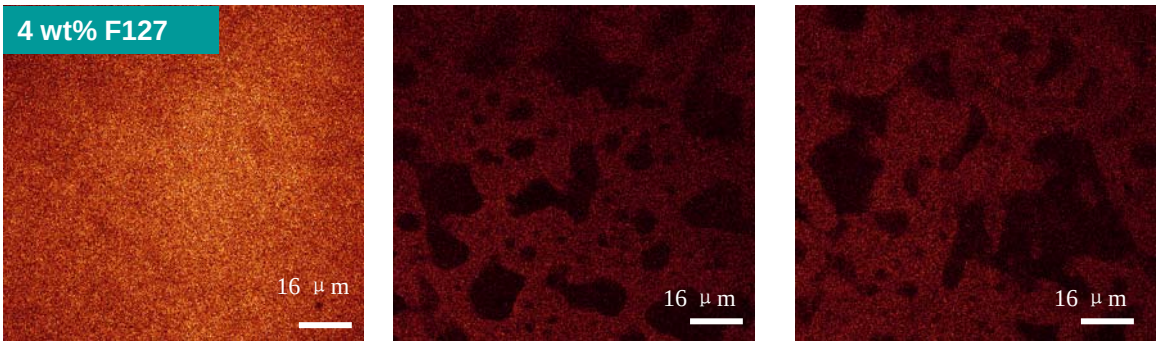

Figure 3-3. Samples of ϕ = 0.25 – 0.58, 4 wt% F127, T = 25°C. Samples at lower ϕ show evidence of phase separation.

Figure 3-4. Effects of FSO concentration on systems of ϕ = 0.58, 4 wt% F127, T = 25°C.

Samples at higher and lower FSO concentrations were found to be opaque at room temperature (Figure 3-4). At certain FSO concentrations, samples became clear at elevated temperatures. We did not perform detailed structural studies of the opaque phases, but work of Schubert and Kaler [37] suggests that the opaque phases may correspond to a lamellar liquid crystal.

Because we wished to focus on stable systems with a droplet microstructure, the majority of our SANS, SAXS, and rheology studies reported below focus on systems with an FSO concentration of 15 wt% and $\phi = 0.58$.

3.5.2 Microstructure: SANS and SAXS Studies

Sample SANS spectra on systems with $\phi = 0.58$ and varying amounts of F127 are shown in Figure 3-5. Spectra range from the neat microemulsion (0 wt% F127) to 12 wt% F127. Spectra are characteristic of scattering from spherical objects. Moreover, the sharpening of the primary peak and appearance of higher-order peaks as the amount of F127 increases suggests some ordering of droplets at higher F127 concentrations. The SANS spectra do not have sufficient resolution to determine the nature of the ordering in systems at higher F127 concentrations. However, SAXS confirms that the structure is that of hexagonally close-packed droplets, with a d-spacing of about 30 nm, where $d=2\pi/q_{max}$ (Figure 3-6).

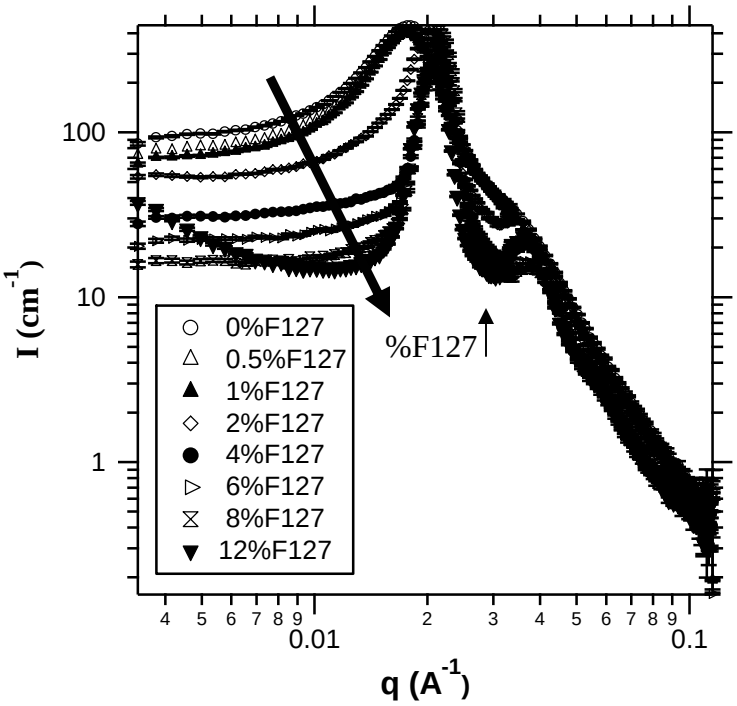

Figure 3-5. SANS spectra of $\phi = 0.58$, 0 – 12 wt% F127, $T = 25$ºC.

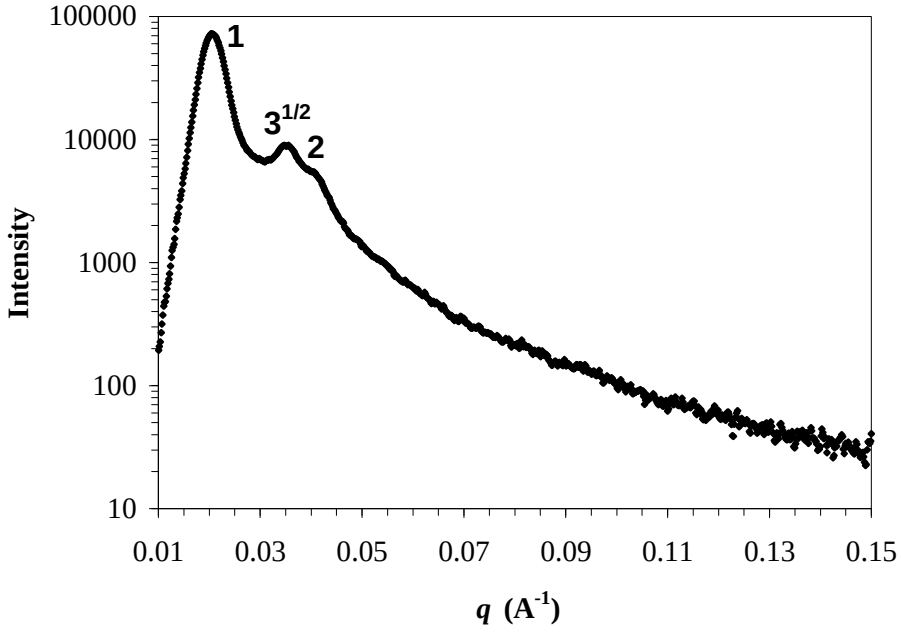

Figure 3-6. SAXS spectrum of $\phi = 0.58$, 4 wt% F127, $T = 25$ºC.

SANS spectra were fit using established data-fitting routines [48]. The scattered intensity can be expressed as [48]:

$$I = N_0 P(q) S(q) \quad (1)$$

where $P(q)$ is the form factor, $S(q)$ is the structure factor, and N_0 is the number density of the scatters. As mentioned above, the spectra are characteristic of spherical scatterers. Thus, we choose use a core-shell form factor for our systems (Figure 3-7):

$$P(q) = \frac{scale}{V_s}\left[\frac{3V_c(\rho_c - \rho_s) j_1(qr_c)}{qr_c} + \frac{3V_s(\rho_s - \rho_{solv}) j_1(qr_s)}{qr_c}\right]^2 + bkg \quad (2)$$

where $j_1(x) = (\sin x - x\cos x)/x^2$, $r_s = r_c + t$, $V_s = (4\pi/3)r_s^3$, and $V_s = (4\pi/3)r_s^3$. Polydispersity in the core size was accounted for by averaging over a Schulz distribution of radii [49], and fitting algorithms available from NIST accounted for smearing due to instrument resolution. We implemented a version of this model with a constant core/shell ratio, rather than a constant shell thickness [50-52]. Because the ratio of water to PFOB is 1:1 in our samples, it is necessary to verify that we have water-in-oil droplets, rather than oil-in-water droplets. We attempted to fit our data assuming both scenarios. Only the water-in-oil microemulsions gave us physically reasonable values for the fit parameters; assuming oil-in-water microemulsions often led to negative values for the core radius and/or the shell thickness. Thus, fits of our scattering data confirm that we have microemulsions comprising water-in-oil droplets.

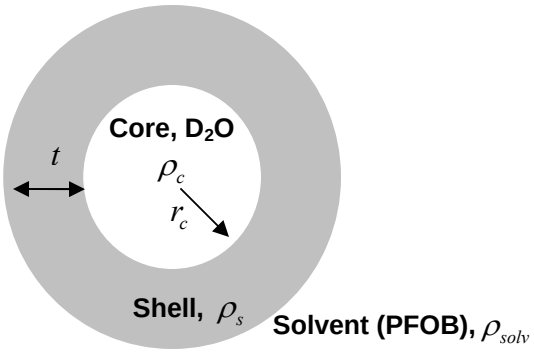

Figure 3-7. Parameters in core-shell form factor.

The structure factor *S(q)* contains the information about spatial arrangement of the particles relative to an arbitrary origin. For an isotropic solution, the orientational average can be calculated as [53]:

$$S(q) = 1 + 4\pi n_p \int_0^\infty [g(r) - 1] \frac{\sin qr}{qr} r^2 dr \tag{3}$$

where *g(r)* can be calculated from Ornstein-Zernicke (O-Z) equation [54]:

$$h(r) = g(r) - 1 = c(r) + n \int c(|\vec{r} - \vec{x}|) h(x) d\vec{x} \tag{4}$$

An additional closure relation between $c(r)$ and $h(r)$ is needed to solve the O-Z equation. We attempted to fit our data using three different models: a hard sphere potential with the Percus-Yevick (P-Y) closure [55, 56], a square-well potential with the mean spherical approximation [57], and a perturbation solution of the P-Y closure with a sticky hard sphere potential [58]. The most physically reasonable values for the parameters and best fits were obtained with the square-well potential:

$$u(r) = \begin{cases} \infty & r \le \sigma \\ -U_0 & \sigma < r < \lambda\sigma \\ 0 & r > \lambda\sigma \end{cases} \tag{5}$$

where λ is the range of square well defined in multiples of the particle diameter, U_0 is the square well depth [57]. There are some limitations to use of this approach; for example, it is known that use of the square-well potential with the mean spherical approximation yields the best agreement with Monte Carlo simulations of square-well fluids for $U_o < 1.5$ kT and $\phi < 0.08$ [57]. Our samples are at considerably higher volume fractions; in addition, the well depths we obtain are significantly higher than 1.5 kT for nearly all samples. Nevertheless, as this model was the only one that yielded physically reasonable results, we have used the results of data-fitting with this model to interpret our results.

Data fits are shown in Figure 3-8, and Table 3-3 lists the parameters obtained from fitting our SANS data with the polydisperse core-shell form factor and the square-well structure factor. For most samples, the droplet radius plus shell thickness is roughly half of the *d*-spacing estimated from SAXS, which is physically reasonable. At these high volume fractions, we would expect the droplets to be packed quite tightly. Both the core radius and the shell thickness increase at higher values of F127, although there is some uncertainty in this trend. This suggests that the PEO block of the F127 act to swell the water core, while the PPO midblocks increase the layer thickness surrounding each droplet. This is also physically quite reasonable.

There is a clear trend in increasing U_o, or strength of attraction, as the concentration of F127 in increased. Although the values for U_o are quite high and may not be quantitatively accurate due to limitations of the square-well model, it is clear that addition of triblock polymers induces attractions between droplets. Interestingly, the maximum attraction between droplets occurs at 6 wt% F127. Although we must be careful not to over-interpret these data, this behavior is directly mirrored in the elastic modulus, as

described further below. Close examination of the SANS spectra at 12 wt% F127 shows an upturn at low q that cannot be captured by the data fits. This may indicate some type of phase separation on the microscale; for example, formation of small domains that are richer in both droplets and F127 chains. It is known that similar types of samples display a phase separation that is equivalent to a gas-liquid transition in small molecule systems [40-46]. It is not clear what effect the formation of such a phase would have on the interdroplet attraction and rheology, but it may act to decrease the effective droplet volume fraction and F127 concentration in the majority phase.

Table 3-3. Fit parameters for systems at $\phi = 0.58$, 0 – 12 wt% F127, and $T = 25$°C, using polydisperse core-shell form factor and square-well structure factor.

%F127	r_c, nm	t, nm	U_o (kT)
0	8.4	3.0	13.2
0.5	8.4	3.0	80.8
1	8.2	3.0	107.7
2	15.5	1.7	379.2
4	13.8	3.2	631.2
6	9.9	6.5	3495.2
8	10.6	6.0	1947.7
12	11.7	6.2	2033.2

(Continued on the next page)

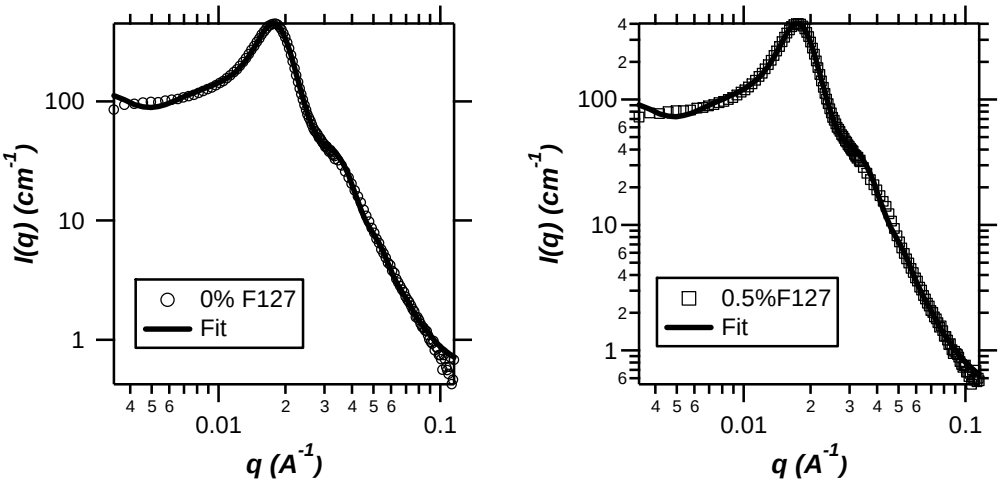

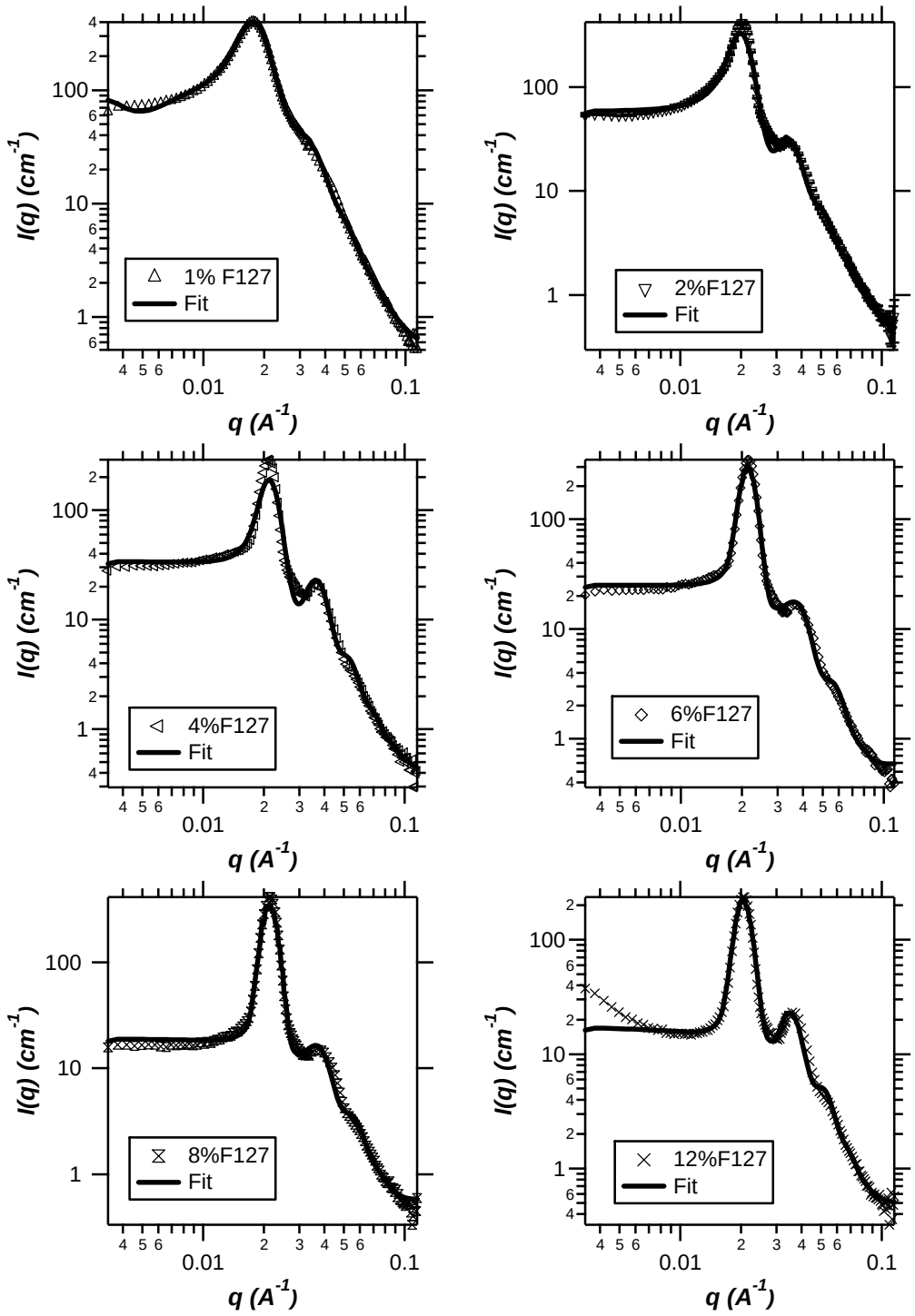

Figure 3-8. SANS spectrum and fitting of $\phi = 0.58$, 0 – 12 wt% F127, $T = 25°C$.

3.5.3 Rheology and Analysis of Structure-Rheology Relationships

As suggested in Figure 3-2, samples undergo a transition from liquids to gels as F127 concentration is increased. This was quantified through oscillatory rheology experiments. Figures 3-9, 3-10, and 3-11 show G', tan δ, and $|\eta^*|$ for samples at $\phi = 0.58$, 0 – 12 wt% F127, and $T = 20^oC$. The rheology shows formation of an elastic gel as the concentration of F127 is increased. Although F127 in aqueous solutions forms gels, the gel-liquid transition in our system occurs between 2 – 4 wt% F127, far below the gelation concentration of F127 in its neat aqueous solution, which is 16 wt% at 25ºC [59-61]. There is a non-monotonic dependence of both G' and $|\eta^*|$ on F127 concentration, with the maximum value of these parameters occurring at 6 wt% F127. As discussed above, this may be due to some sort of micro-phase separation at high F127 concentrations.

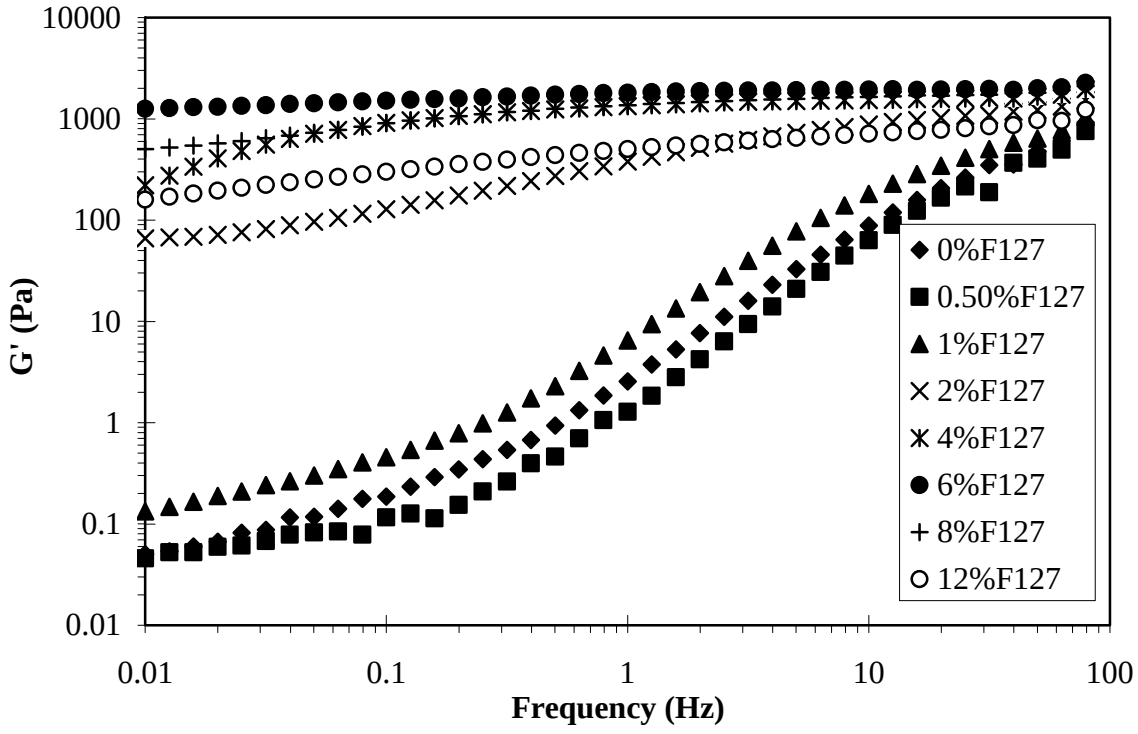

Figure 3-9. Elastic modulus, G', of samples at $\phi = 0.58$, 0 – 12 wt% F127, $T = 20$ºC.

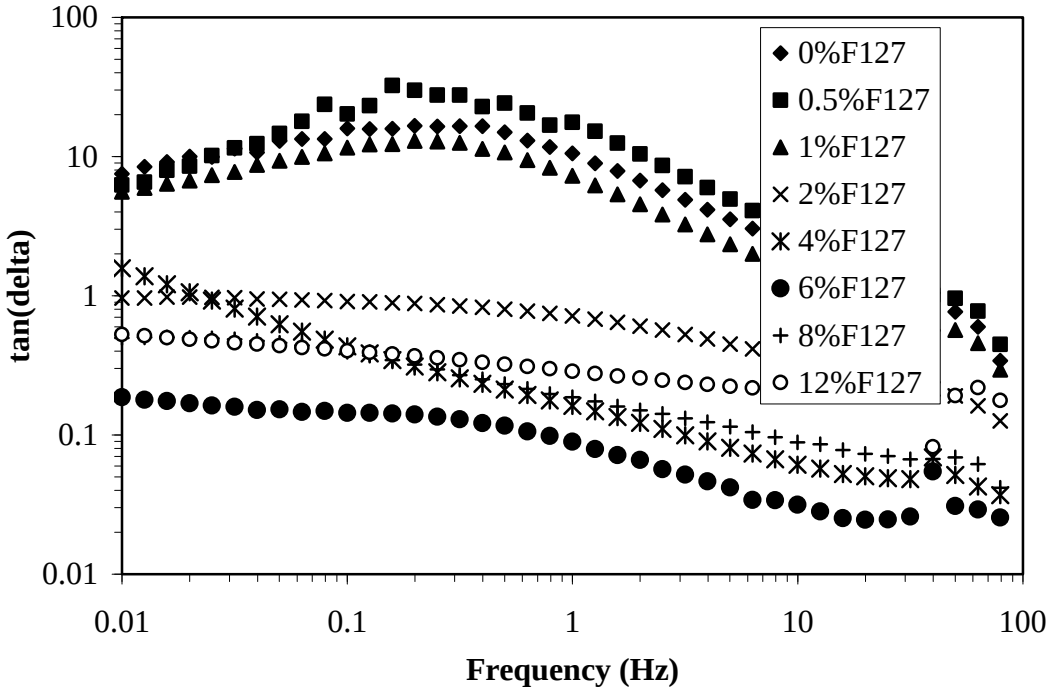

Figure 3-10. Tan δ of samples at ϕ = 0.58, 0 – 12 wt% F127, T = 20ºC.

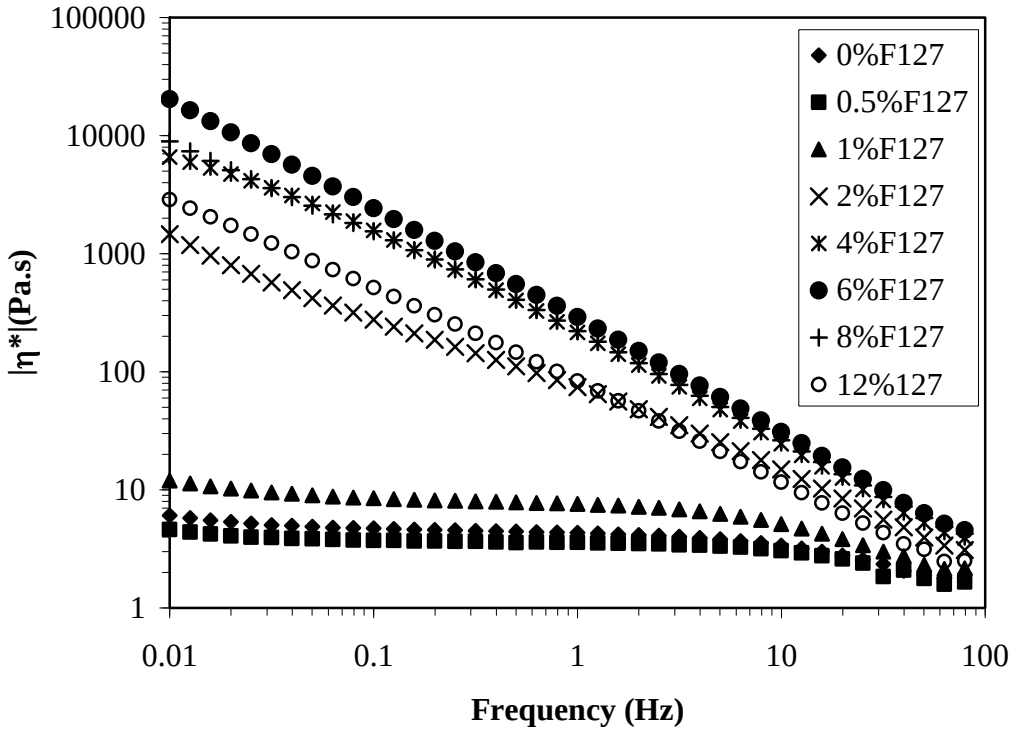

Figure 3-11. Complex viscosity of samples at ϕ = 58, 0 – 12 wt% F127, T = 20ºC.

We can use these data to determine if there are straightforward relationships between the rheology and various parameters that characterize the structure and interdroplet forces. Two commonly-used concepts in theoretical descriptions of associative polymers are the fraction of elastically effective chains, *f*, and the fraction of bridging chains. The fraction of elastically effective chains, *f*, is the fraction of chains that are connected to the infinite network. The fraction of bridging chains represents a maximum value for *f*. Theoretical descriptions of triblock copolymers attached to spherical surfaces suggest that the maximum attainable value for the fraction of bridging chains is 1/3 [62].

We can estimate the fraction of elastically effective chains from our data using results from classical rubber elasticity theory and transient network theory [63-69]:

$$G_0 = vkT \tag{6}$$

$$f = G_{0-ex} / G_{0-th} \tag{7}$$

where G_0 corresponds to high shear plateau modulus, $G_{0\text{-}ex}$ is the modulus from rheological measurement, $G_{0\text{-}th}$ is theoretical modulus with all chains effective, and v is the number density of elastically effective chains:

$$v = num_{polymer} / V_{total} \tag{8}$$

where V_{total} is the total volume of sample and $num_{polymer}$ is number of polymer chains. The average number of polymers on droplets, p, was calculated as following:

$$p = num._{polymers} / num._{droplet} \tag{9}$$

where

$$num_{droplet} = V_{total}\phi / [\frac{4}{3}\pi(r_c + t)^3] \tag{10}$$

Table 3-4 shows the results of these calculations. Parameters that characterize soft attractive potentials (Table 3-1), including the average number of elastically effective polymers per droplet, p_{eff}, the average contribution to well depth for per elastically effective polymer, $(\Phi_{\min}/kT)/p_{eff}$, the average surface coverage on a droplet, $n_p = p/(2\pi r_c^2)$, and softness, $L_a^2 n_p$, are given in Table 3-5.

Table 3-4. Number density of polymers in unit volume, v, theoretical equilibrium modulus, $G_{0\text{-}th}$, experimental equilibrium modulus, $G_{0\text{-}ex}$, and fraction of elastically effective chains, f, of ϕ = 58, 0 – 12 wt% F127 systems at 25°C.

%F127	p	v (10^{22}/m^3)	$G_{0\text{-}th}=vkT$ (Pa)	$G_{0\text{-}ex}$(Pa) (experiment)	Fraction of elastically effective chains f
0	0	0	0	59.02	NA
0.5	1.359	8.662	356.023	54.91	0.154
1	2.616	17.325	712.047	53.02	0.074
2	12.253	34.649	1424.093	71.21	0.050
4	21.782	69.299	2848.187	231.9	0.081
6	36.851	103.948	4272.280	937.1	0.219
8	48.067	138.598	5696.374	593.7	0.104
12	78.356	207.897	8544.561	575.2	0.067

Table 3-5. Effective polymer number per droplet p_{eff}, average contribution to well depth of per effective polymer, Φ_{min}/p_{eff}, surface coverage of polymer n_p, softness $L_a^2 n_p$, of ϕ =0.58, 0 – 12 wt% F127 systems at 25°C.

%F127	p_{eff}	Φ_{min}/p_{eff} (kT)	n_p (10^{-4}Å^{-2})	Softness $L_a^2 n_p$
0	NA	NA	0	0
0.5	0.210	385.587	0.305	0.0255
1	0.194	734.901	0.616	0.0572
2	0.612	618.880	0.806	0.0232
4	1.773	355.912	1.801	0.183
6	8.082	432.414	5.940	2.520
8	5.009	388.778	6.754	2.473
12	5.274	385.457	9.085	3.468

Interestingly, we find a linear relationship between the interaction strength, U_o, and both the high frequency modulus and the number of elastically effective chains per droplet (Figures 3-12 ad 3-13). To our knowledge, this is a new result that has not been shown previously for attractive colloidal dispersions.

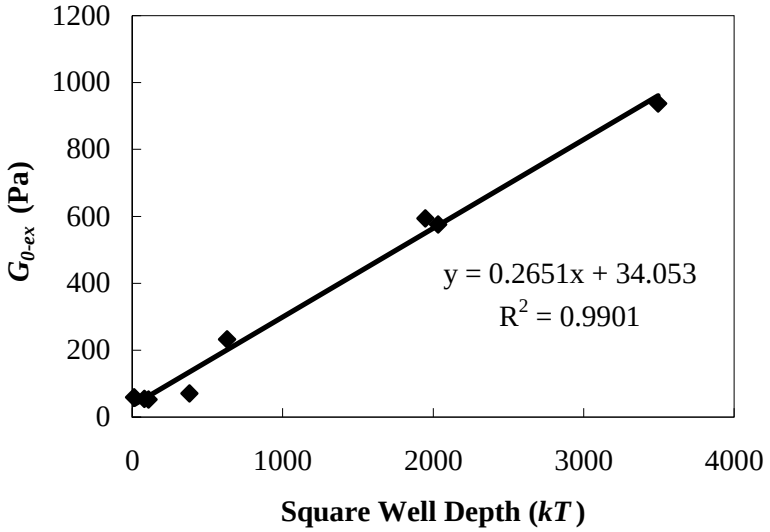

Figure 3-12. The relationship between high frequency plateau of storage modulus and square well depth. The equation is for the linear fitting trend line.

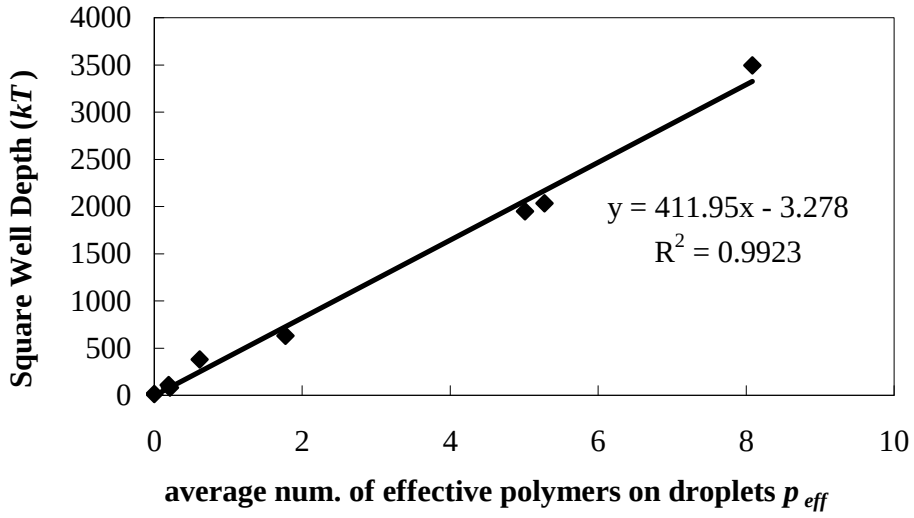

Figure 3-13. The relationship between square well depth and the average number of elastically effective polymers on droplets. The equation is for the linear fitting trend line.

As stated above, the strength of attraction exhibits a maximum at 6 wt% F127. This trend is mirrored in the behavior of the elastic modulus (Figure 3-14). This suggests that the linear relationship between elastic modulus and strength of attraction may be universal, independent of the detailed chemistry of the system.

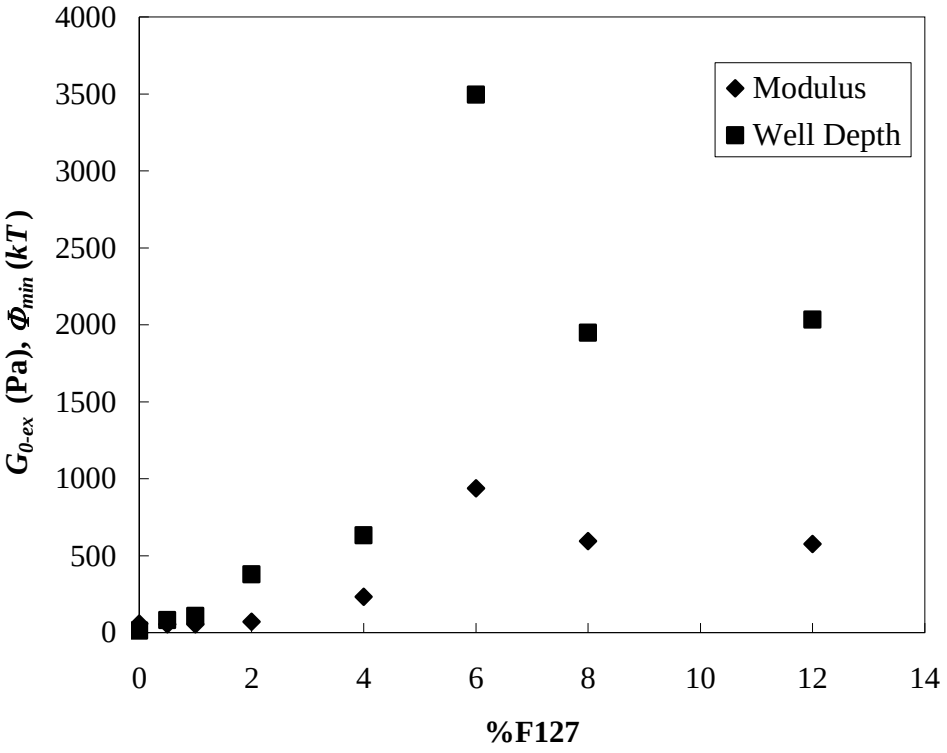

Figure 3-14. The relationships between the high frequency plateau of storage modulus and the polymer concentration, and between the attraction strength and the polymer concentration.

Unfortunately, the rheology does not display any sort of trend with regards to the degree of "softness" of the potential (Figures 3-15, 3-16). Additional experiments will need to be performed to determine if there is a better way to characterize this aspect of the potential.

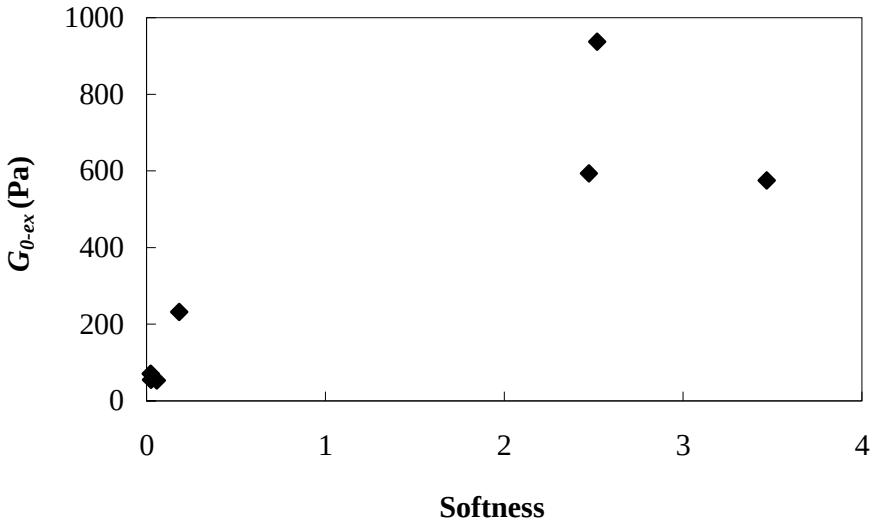

Figure 3-15. The relationship between the high frequency plateau of storage modulus and the softness.

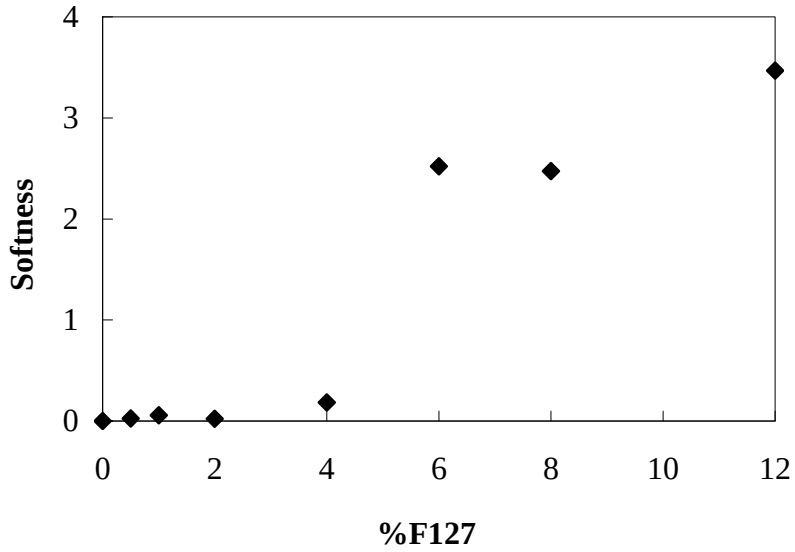

Figure 3-16. The relationship between the softness and the polymer concentration.

3.5.4 Thermoreversible Nature of Gels

Temperature sweeps performed in the range $T = 10^{o}C - 35^{o}C$ reveal the complexity of thermal effects on these systems. The systems contain triblock copolymer PEO-PPO-PEO and a surfactant of the form $(CF_2)_n$-PEO. The PPO block in F127 and the PEO

blocks in both of the two the F127 and the FSO are sensitive to temperature. Thus, it is not straightforward to predict how temperature will affect these systems.

Figure 3-17 shows the effects of temperature sweeps performed for systems with ϕ = 0.58 and 0 – 12 wt% F127 at a fixed frequency of 1 Hz. Several samples behave as liquids at room temperature (with $G'' > G'$) and form either elastic gels (with $G' > G''$) or near-critical gels (with $G' \sim G''$) at physiological temperature. Such behavior can be useful for drug delivery formations and for use of these materials in cell encapsulation and tissue engineering.

Changes in the rheology are reversible through several repeated heating and cooling cycles, as shown in Figure 3-18 for one representative sample. Although there is a small degree of hysteresis, samples that have been repeatedly heated and cooled recover their original rheological behavior. Thus, these systems are not only thermosensitive, but thermoreversible.

(Continued on the next page)

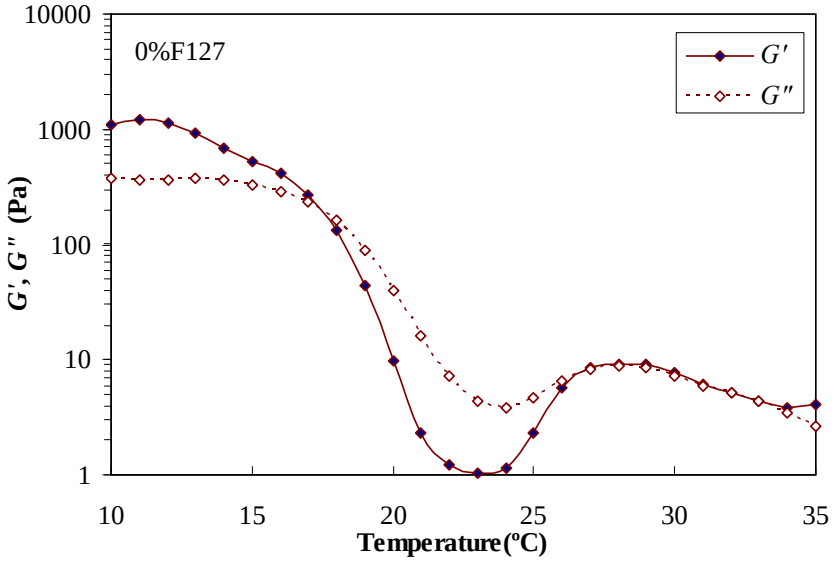

(Continued on the next page)

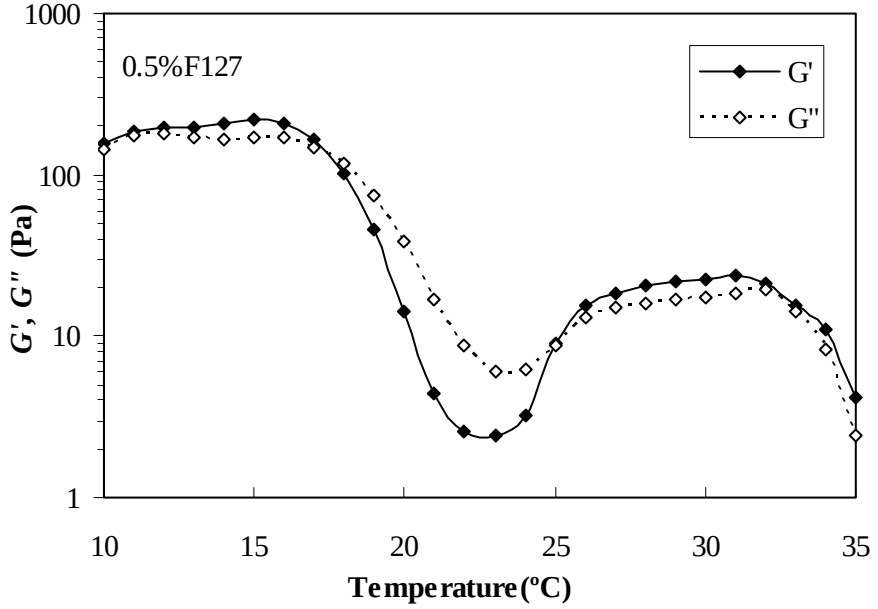

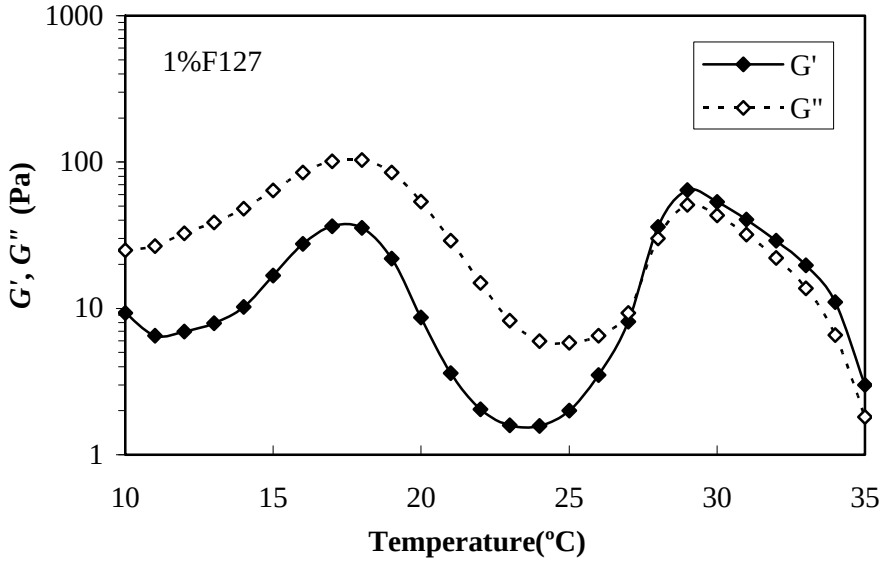

(Continued on the next page)

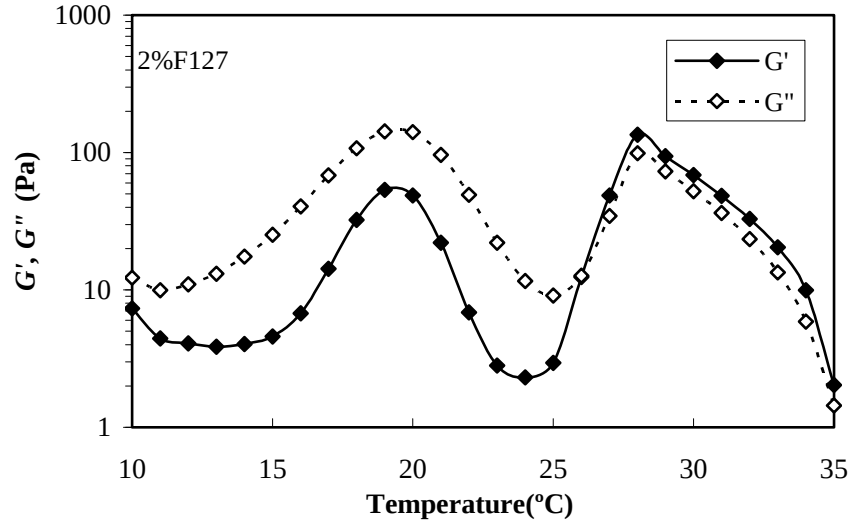

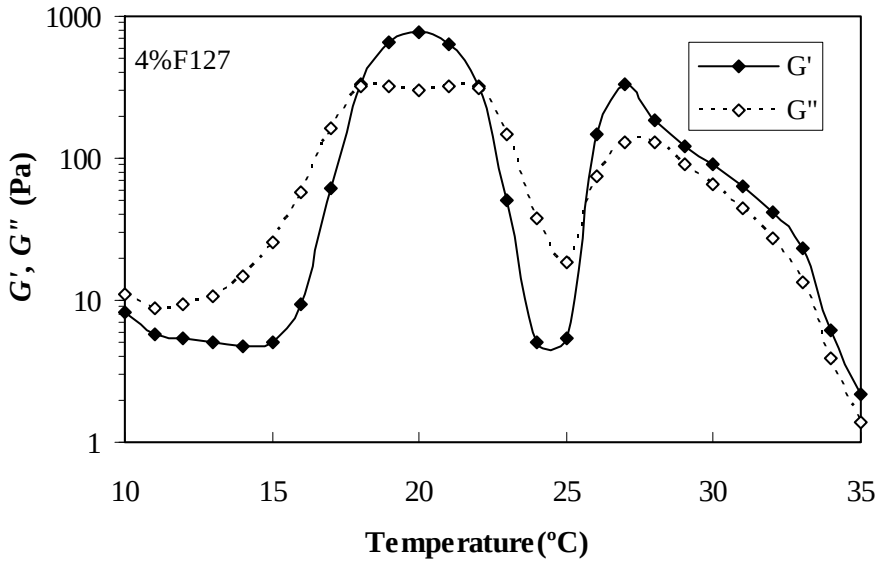

(Continued on the next page)

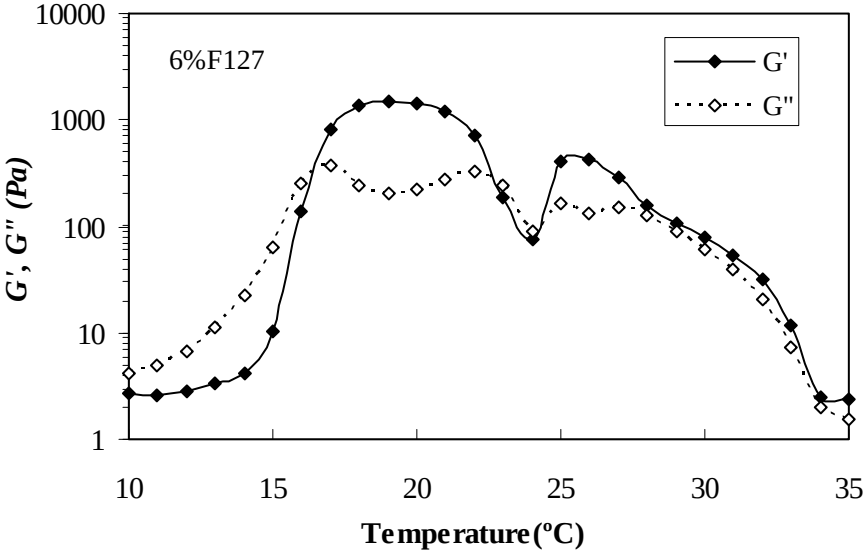

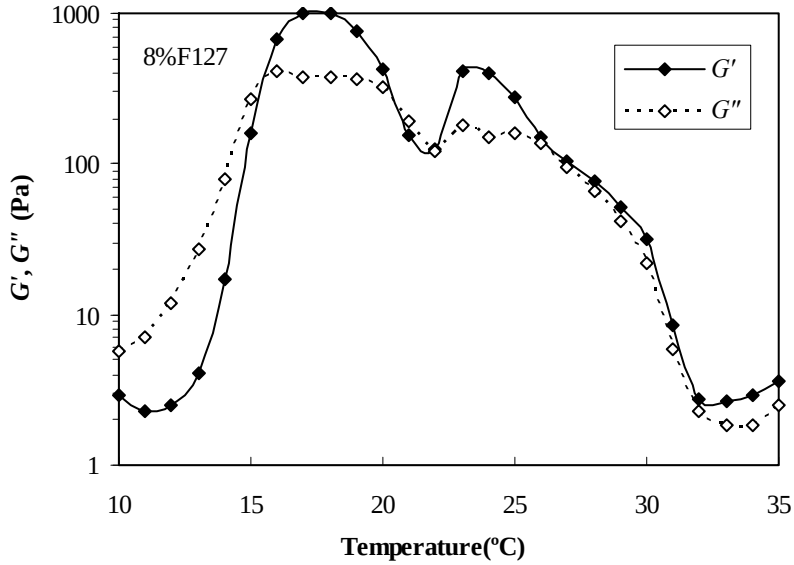

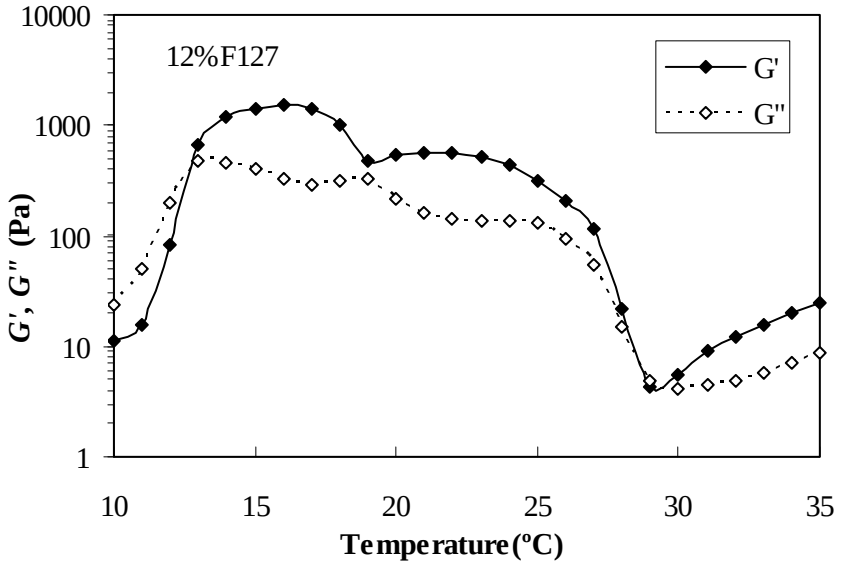

Figure 3-17. Temperature sweep (10-35ºC, equilibrium time 3minutes for each ºC, frequency 1 Hz) of the systems $\phi = 0.58$, 0 – 12 wt% F127. Solid and dashed lines are guides for the eye.

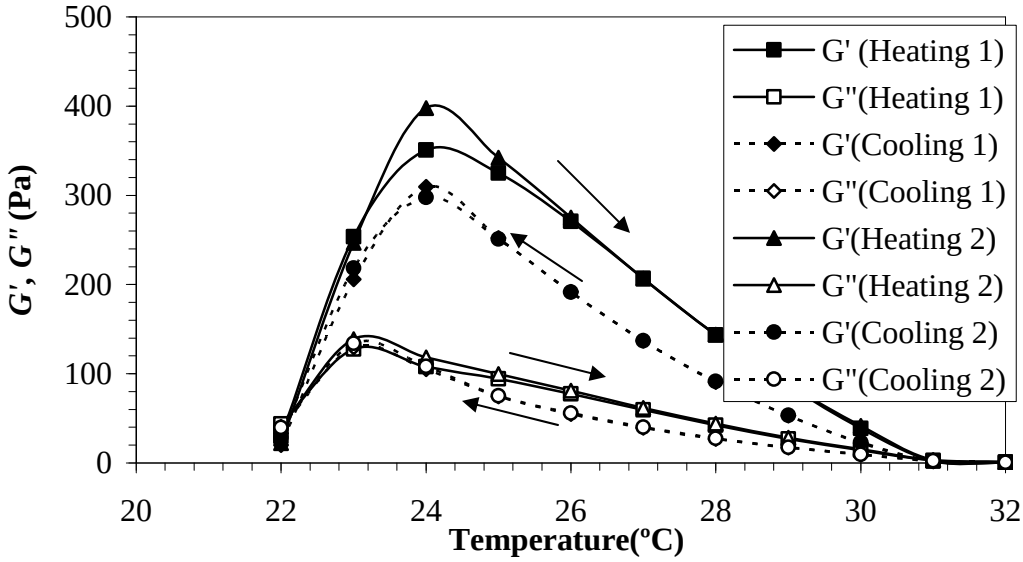

Figure 3-18. Thermoreversibility of viscoelastic moduli for $\phi = 0.58$, 4.0 wt% F127. Viscoelastic moduli from a temperature sweep at 1 Hz with an equilibrium time of three minutes for each ºC. Solid lines and dashed lines are guides for the eye.

3.5.5 Effect of Surfactant Concentration

As discussed above and shown in Figure 3-4, samples at higher and lower FSO concentrations tended to be opaque and may exhibit a transition to a lamellar phase. Although we did not perform a detailed structural characterization of these systems, we have performed preliminary rheological studies. Figure 3-19 shows that *G'* increases slowly then decreases rapidly with increasing surfactant amount. Samples at low concentrations form elastic gels, while samples at higher concentrations display liquid-like characteristics (Figure 3-20).

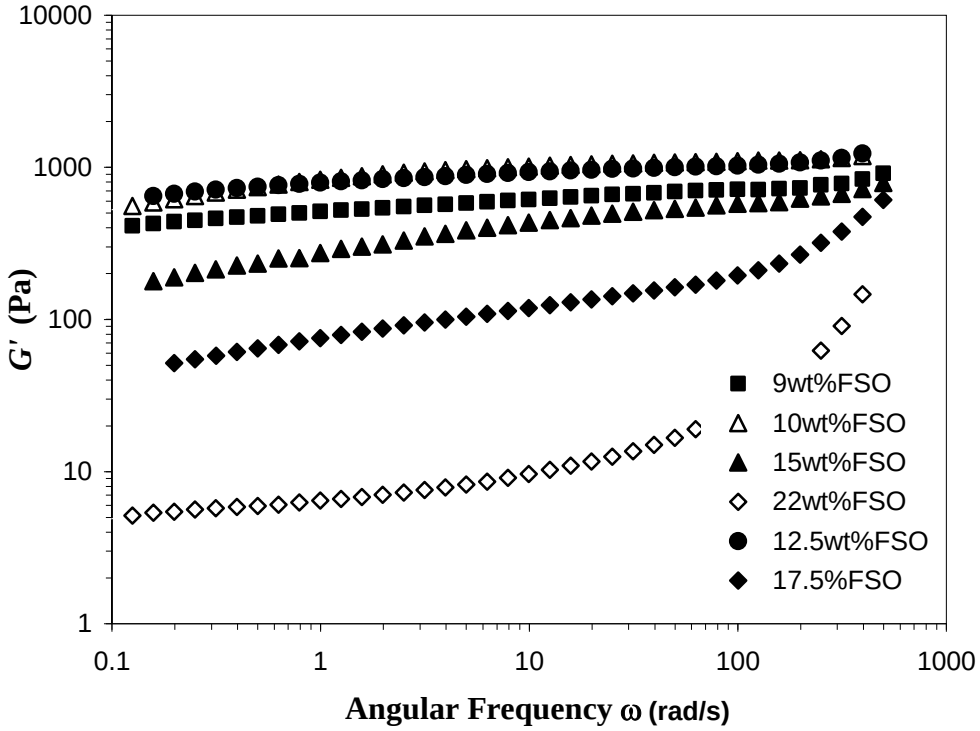

Figure 3-19. Effects of FSO on ϕ = 0.58, 4 wt %F127, and varying FSO concentration at 25ºC.

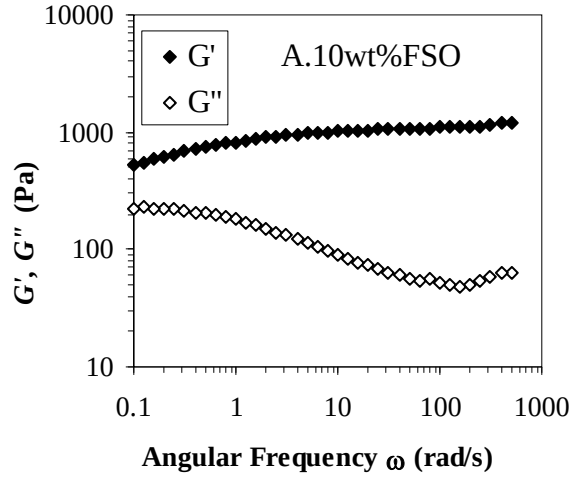

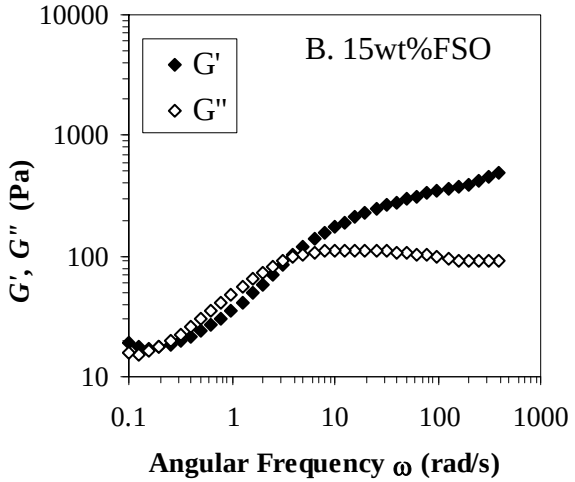

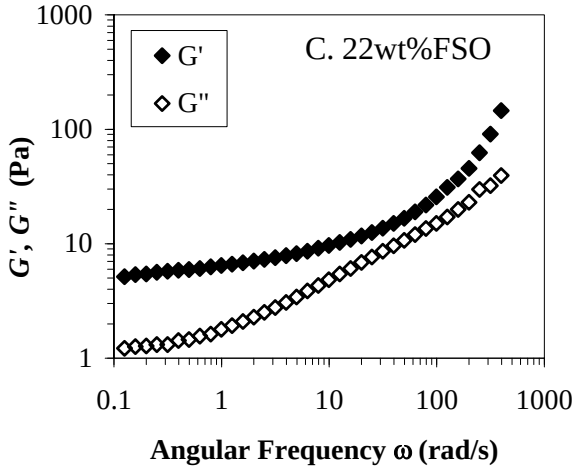

Figure 3-20. Effects of FSO on systems of 50v%PFOB/ 50v%water (4wt%F127)/ FSO (ϕ = 0.58, 4wt%F127) at 25ºC. (A)10wt%FSO, (B) 15wt%FSO, (C) 22wt%FSO.

3.5.6 Effects of Volume Fraction

The first effect of volume fraction is on the phase stability. Due to the high hydrophobicity and large density difference between water and PFOB, the systems shifting from volume ratio 1:1 are unstable. Confocal microscopy (Figure 3-3) reveals the heterogeneous micro-domains in the systems when the volume ratio of water to PFOB decreases. After a long time, some transparent liquid can be seen separating from the opaque bulk. We measured the rheology of these systems immediately after formation, before macroscopic phase separation occurred (Figure 3-21). *G''* increases systematically with ϕ but *G'* does not show a clear trend. An elastic gel is formed at both low and high ϕ.

(Continued on the next page)

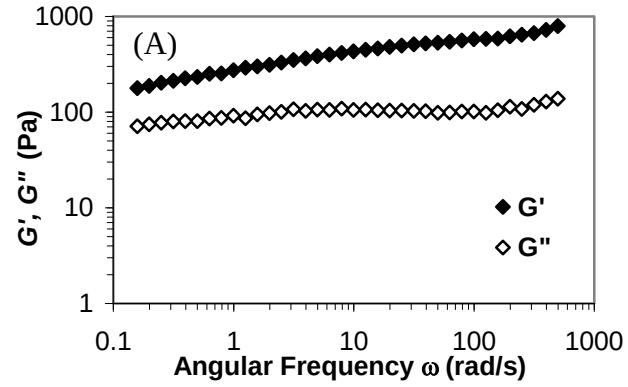

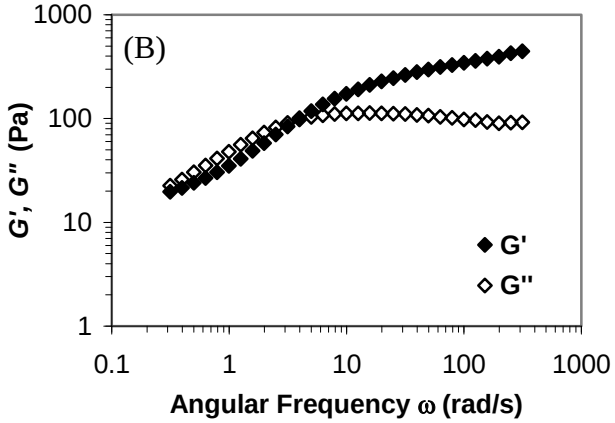

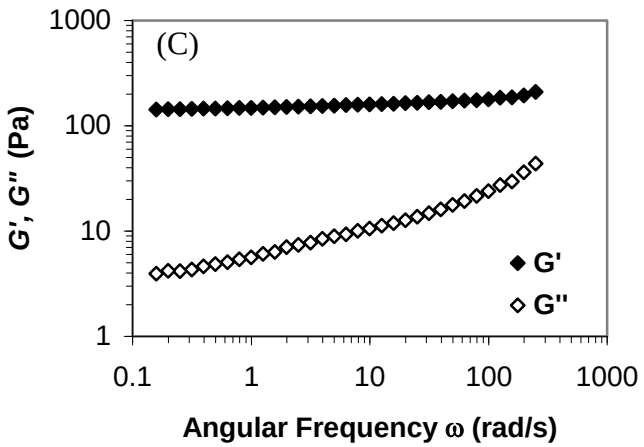

Figure 3-21. Dilution of samples at 4 wt% F127, 15 wt% FSO, T = 25ºC, and (a) ϕ = 0.58, (b) ϕ = 0.41, (c) ϕ = 0.13.

3.6 Summary

Stable elastic gels were formed with the addition of triblock copolymer F127 into the microemulsion system of PFOB/water/FSO. The rheological properties can be adjusted by composition (F127, FSO, ϕ) and temperature. The gels also have some interesting thermal behavior. They are sensitive to temperature and reversible over a range of temperature, switching from transparent to cloudy and back again within a certain range of temperature. The gels' properties observed in phase stability investigation are confirmed by rheological measurements. The results from SAXS suggested a hexagonally close-packed structure. The structures of transparent solution and gels were mainly investigated and were suggested to consist of water-in-oil microemulsion droplets. For the opaque systems, lamella or some other structure may exist. The results of best-fitting method of SANS spectra suggested a core-shell structure with water in PFOB and returned the information of interaction strength, core radius, shell thickness, and effective volume fraction. A linear relationship between high frequency storage modulus plateau

and the interaction strength was observed. No clear relationship between the softness and elastic modulus was observed.

Bibliography

[1] S. Alexander. *J. De Physique* **1977,** 38, (8), p983.

[2] J. Israelachvili, *Intermolecular and Surface Forces*. Academic Press: San Diego: **1992**.

[3] V. Trappe; V. Prasad; L. Cipelletti; P. N. Segre; D. A. Weitz. *Nature* **2001,** 411, (6839), p772.

[4] P. N. Pusey; W. Vanmegen. *Phys. Rev. Lett.* **1987,** 59, (18), p2083.

[5] W. Vanmegen; S. M. Underwood. *Phys. Rev. E* **1994,** 49, (5), p4206.

[6] P. Sollich. *Phys. Rev. E* **1998,** 58, (1), p738.

[7] P. Sollich; F. Lequeux; P. Hebraud; M. E. Cates. *Phys. Rev. Lett.* **1997,** 78, (10), p2020.

[8] J. Bergenholtz; M. Fuchs. *Phys. Rev. E* **1999,** 59, (5), p5706.

[9] L. Fabbian; W. Gotze; F. Sciortino; P. Tartaglia; F. Thiery. *Phys. Rev. E* **1999,** 60, (2), p2430.

[10] L. Fabbian; W. Gotze; F. Sciortino; P. Tartaglia; F. Thiery. *Phys. Rev. E* **1999,** 59, (2), pR1347.

[11] J. S. Higgins; H. C. Benoit, *Polymers and Neutron Scattering*. Oxford: Clarendon Press: **1994**.

[12] F. Mallamace; P. Gambadauro; N. Micali; P. Tartaglia; C. Liao; S. H. Chen. *Phys. Rev. Lett.* **2000,** 84, (23), p5431.

[13] K. N. Pham; A. M. Puertas; J. Bergenholtz; S. U. Egelhaaf; A. Moussaid; P. N. Pusey; A. B. Schofield; M. E. Cates; M. Fuchs; W. C. K. Poon. *Science* **2002,** 296, (5565), p104.

[14] M. P. Krafft. *Adv. Drug Deliv. Rev.* **2001,** 47, (2-3), p209.

[15] P. LoNostro; S. M. Choi; C. Y. Ku; S. H. Chen. *J. Phys. Chem. B* **1999,** 103, (25), p5347.

[16] C. Thomas; J. Riess; M. Guichard. *Int. J. Radiat. Biol.* **1991,** 59, (2), p433.

[17] R. F. Mattrey; G. Strich; R. E. Shelton; B. B. Gosink; G. R. Leopold; T. Lee; J. Forsythe. *Radiology* **1987,** 163, (2), p339.

[18] M. R. Gherase; J. C. Wallace; A. R. Cross; G. E. Santyr. *J. Chem. Phys.* **2006,** 125, (4), p.

[19] F. S. Moolman; H. Rolfes; S. W. van der Merwe; W. W. Focke. *Biochem. Eng. J.* **2004,** 19, (3), p237.

[20] S. F. Khattak; K. S. Chin; S. R. Bhatia; S. C. Roberts. *Biotechnol. Bioeng.* **2007,** 96, (1), p156.

[21] R. Wikramanayake; R. Enick; M. Turberg. *Fluid Phase Equilib.* **1991,** 70, (1), p107.

[22] R. J. Twieg; T. P. Russell; R. Siemens; J. F. Rabolt. *Macromolecules* **1985,** 18, (6), p1361.

[23] S. Shoshan; D. Michaeli; S. Magdassi. US Pat. 5, 073, 378, **1991**.

[24] J. C. Ravey; M. J. Stebe; S. Sauvage. *Colloid Surf. A-Physicochem. Eng. Asp.* **1994,** 91, p237.

[25] J. C. Ravey; M. J. Stebe. *Progr. Colloid & Polym. Sci.* **1990,** 82, (Surfactants Macromol.: Self-Assem. Interfaces Bulk), p218.

[26] S. Magdassi; M. Royz; S. Shoshan. *Int. J. Pharm.* **1992,** 88, (1-3), p171.

[27] A. Langenfeld; V. Schmitt; M. J. Stebe. *J. Colloid Interface Sci.* **1999,** 218, (2), p522.

[28] M. P. Krafft; J. G. Riess. WO 97/03644., **1995**.

[29] M. P. Krafft; J. G. Riess. PCT WO 95/09606, **1995**.

[30] M. P. Krafft; J. G. Riess. *Angew. Chem.-Int. Edit. Engl.* **1994,** 33, (10), p1100.

[31] T. Imae; M. P. Krafft; F. Giulieri; T. Matsumoto; T. Tada. *Progr. Colloid & Polym. Sci.* **1997,** 106, p52.

[32] J. Hopken; C. Pugh; W. Richtering; M. Moller. *Makromolekulare Chemie-Macromolecular Chemistry and Physics* **1988,** 189, (4), p911.

[33] V. G. Babak; A. Langenfeld; N. Fa; M. J. Stebe. *Progr. Colloid & Polym. Sci.* **2001,** 118, (Trends in Colloid and Interface Science XV), p216.

[34] J. C. Ravey; M. J. Stebe. *Progr. Colloid & Polym. Sci.* **1987,** 73, (New Trends Colloid Sci.), p127.

[35] C. Washington; S. M. King. *Langmuir* **1997,** 13, (17), p4545.

[36] C. Washington; S. M. King; R. K. Heenan. *J. Phys. Chem.* **1996,** 100, (18), p7603.

[37] K. V. Schubert; E. W. Kaler. *Colloid Surf. A-Physicochem. Eng. Asp.* **1994,** 84, (1), p97.

[38] U. Batra; W. B. Russel; M. Pitsikalis; S. Sioula; J. W. Mays; J. S. Huang. *Macromolecules* **1997,** 30, (20), p6120.

[39] S. R. Bhatia; W. B. Russel; J. Lal. *J. Appl. Crystal.* **2000,** 33, (1), p614.

[40] H. F. Eicke; M. Gauthier; R. Hilfiker; R. P. W. J. Struis; G. Xu. *J. Phys. Chem.* **1992,** 96, (12), p5175.

[41] H. F. Eicke; C. Quellet; G. Xu. *Colloids & Surfaces* **1989,** 36, (1), p97.

[42] G. Fleischer; F. Stieber; U. Hofmeier; H. F. Eicke. *Langmuir* **1994,** 10, (6), p1780.

[43] R. Hilfiker; H. F. Eicke; C. Steeb; U. Hofmeier. *J. Phys. Chem.* **1991,** 95, (3), p1478.

[44] M. Odenwald; H. F. Eicke; W. Meier. *Macromolecules* **1995,** 28, (14), p5069.

[45] C. Quellet; H. F. Eicke; G. Xu; Y. Hauger. *Macromolecules* **1990,** 23, (13), p3347.

[46] R. Struis; H. F. Eicke. *J. Phys. Chem.* **1991,** 95, (15), p5989.

[47] C. J. Glinka; J. G. Barker; B. Hammouda; S. Krueger; J. J. Moyer; W. J. Orts. *J. Appl. Crystal.* **1998,** 31, p430.

[48] S. R. Kline. *J. of Appl. Crystal.* **2006,** 39, p895.

[49] J. B. Hayter, In *Physics of Amphiphiles-Micelles, Vesicles, and Microemulsions*, M. C. V. DeGiorgio, Ed. North-Holland: Varenna, Italy, **1983**; p 59.

[50] A. Guinier; G. Fournet, *Small-Angle Scattering of X-Rays*. John Wiley and Sons: New York, **1955**.

[51] P. Bartlett; R. H. Ottewill. *J. Chem. Phys.* **1992,** 96, (4), p3306.

[52] http://www.ncnr.nist.gov/programs/sans/data/red_anal.html

[53] S.-H. Chen; T.-L. Lin. *Methods of Experimental Physics* **1987,** 23B, p489.

[54] L. S. Ornstein; F. Zernicke. *Proc. Amst. Acad. Sci.* **1914,** 17, p793.

[55] I. Nezbeda. *Czech. J. Phys.* **1977,** 27, (3), p247.

[56] J. K. Percus; G. J. Yevick. *Phys. Rev.* **1958,** 110, (1), p1.

[57] R. V. Sharma; K. C. Sharma. *Physica A* **1977,** 89, (1), p213.

[58] S. V. G. Menon; V. K. Kelkar; C. Manohar. *Phys. Rev. A* **1991,** 43, (2), p1130.

[59] P. K. Sharma; S. R. Bhatia. *Int. J. Pharm.* **2004,** 278, (2), p361.

[60] P. K. Sharma; M. J. Reilly; S. K. Bhatia; N. Sakhitab; J. D. Archambault; S. R. Bhatia. *Colloid Surf. B-Biointerfaces* **2008,** 63, (2), p229.

[61] P. K. Sharma; M. J. Reilly; D. N. Jones; P. M. Robinson; S. R. Bhatia. **2008,** 61, (1), p53.

[62] S. R. Bhatia; W. B. Russel. *Macromolecules* **2000,** 33, (15), p5713.

[63] M. S. Green; A. V. Tobolsky. *J. Appl. Phys.* **1946,** 17, (5), p407.

[64] K. Inomata; D. Nakanishi; A. Banno; E. Nakanishi; Y. Abe; R. Kurihara; K. Fujimoto; T. Nose. *Polymer* **2003,** 44, (18), p5303.

[65] F. Tanaka; S. F. Edwards. *J. Non-Newton. Fluid Mech.* **1992,** 43, (2-3), p247.

[66] F. Tanaka; S. F. Edwards. *J. Non-Newton. Fluid Mech.* **1992,** 43, (2-3), p273.

[67] F. Tanaka; S. F. Edwards. *J. Non-Newton. Fluid Mech.* **1992,** 43, (2-3), p289.

[68] F. Tanaka; S. F. Edwards. *Macromolecules* **1992,** 25, (5), p1516.

[69] H. Tanaka; T. Okazaki; Y. Tezuka; T. Hongo; Y. Takahashi. *Polymer* **2002,** 43, (4), p1189.

CHAPTER 4

FUTURE WORK

In this chapter, we propose future work for the two projects respectively, counterion effects in AOT systems and fluorocarbon-based microemulsion gels. The proposed future work may aid in developing a more thorough understanding of the relationship between microstructure and rheological properties.

4.1 Future Work for Counterion Effects in AOT Systems

4.1.1 Ion Mobility as a Function of Water/Surfactant Molar Ratio

As discussed in Chapter 2, the viscosity anomaly may arise from charge fluctuation or a net charge transfer caused by ion exchange between droplets. There are two existing mechanisms to explain ion exchange and charge fluctuation, which are the hopping mechanism and the fusion and fission mechanism. These two mechanisms rely on the ion mobility, which is related to the degree of hydration of the ion [1-5]. Different types of ions have different hydration behavior [1]. We have observed the different viscosity behavior between KAOT microemulsion and other AOT microemulsions. In addition, K^+ is a "disorder-maker" ion and the other ions are "order-maker" ions.

We suggest an investigation of the mobility of AOT^- anions and cations in $Ca(AOT)_2$, $Mg(AOT)_2$, and KAOT water-in-decane microemulsion systems, as a function of water/AOT molar ratio using IR and dielectric spectrometry. The results may help us to build the connections from ion type to viscosity anomaly as following:

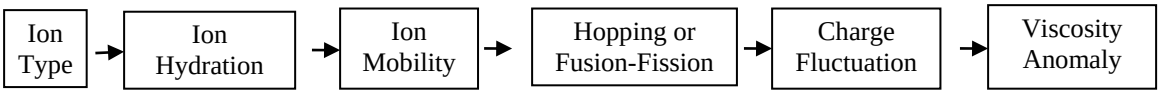

The above connections may be universal and could be used to predict the viscosity behavior and ion mobility from ion type directly.

4.1.2 Ion Mobility as a Function of Solvent

As mentioned in Chapter 2, the hopping mechanism may depend on the chemistry of the oil phase. Solvents like decane with a long chain may have more drag force than the oils like CCl_4 or cyclohexane with short chains. The drag force may be a favor for ion exchange in both the hopping mechanism and fusion and fission mechanism. This may cause a lower interparticle interaction in short chain oils. Fioretto et al and D'Angelo et al have investigated the dynamics-hydration relationship in NaAOT/water/CCl_4, $Ca(AOT)_2$/water/CCl_4, and $Cu(AOT)_2$/water/CCl_4 systems using infrared and dielectric spectroscopy [1-5].

We propose to investigate the ion mobility-hydration relation in NaAOT, $Mg(AOT)_2$, $Ca(AOT)_2$ and KAOT water-in-CCl_4 systems and compare the results with water-in-decane systems, within a wider range of water/surfactant molar ratio than the systems in ref [1-5]. This would be meaningful future work to investigate the effects of solvent on the charge fluctuation and to evaluate the mechanisms of charge fluctuation model. In this proposed future work, the influence of solvent conductivity on viscosity also may need to be concerned.

4.2 Future Work for New Fluorocarbon-based Microemulsion Gels

4.2.1 Rheology of Near the Gelation Point

The rheological properties of fluorocarbon-based microemulsion systems near the liquid-gel transition are needed to gain more for a clear understanding of polymer-induced gelation. We propose additional experiments of several samples at $\phi = 0.58$ and 2 – 6 wt% F127 to more clearly elucidate the critical polymer concentration needed for gel formation.

4.2.2 Microstructure Verification Using Cryo-EM

We found several of the SANS spectra taken at higher temperatures and varying FSO concentrations could not be fit well by one simple model, but rather could be fit very well by a combinational model with two single models for different morphologies. However, the structure indicated by models and the parameters in models needed to be physically reasonable and accurate. In order to analyze SANS data more reasonably and accurately, cryo-EM is suggested. Results may give us a visually physical idea of the microstructure in fluorocarbon-based microemulsion systems, especially the systems with complex SANS spectra which are difficult to be fit by one simple model.

4.2.3 A New Fitting Model with Multi Different SLD Shells for SANS

Our samples most closely resemble cores with several different types of “shells” with differing SLDs (e.g., the FSO layer, the F127 layer, etc.) We suggest developing a new model with multiple different SLD shells. It is difficult to analyze the concentrated systems using the present models with single shell or multiple shells with same SLD,

especially the present models also have some limitations in the values of some parameters. A reasonable and efficient closure in mathematics is also needed.

Bibliography

[1] M. Freda; G. Onori; A. Paciaroni; A. Santucci. *J. Non-Crystal. Sol.*, **2002**, 307–310, p874.

[2] D. Fioretto, M. Freda, G. Onori; A. Santucci. *J. Phys. Chem. B* **1999**, 103, p8216.

[3] M. D'Angelo; D. Fioretto; G. Onori; L. Palmieri; A. Santucci. *Phys. Re*V. *E* **1995**, 52, pR4620.

[4] M. D'Angelo; D. Fioretto; G. Onori; L. Palmieri; A. Santucci. *Phys. Re*V. *E*, **1996**, 54 (1), p993.

[5] D. Fioretto; M. Freda; G. Onori; A. Santucci. *J. Phys. Chem. B*, **1999**, 103(14), p2631.

[6] B. Hribar; N. Southall; V. Vlachy; K. Dill. *J. Amer. Chem. Soc.*, **2002**, 124, p12302.

APPENDIX

STABILITY CONCERNS OF WOOD-DERIVED PYROLYSIS BIO-OILS

1. Background

Crude bio-oil produced from bio-mass by fast pyrolysis is one of the promising renewable alternative energy sources of fossil fuel [1-2]. However, crude bio-oil is a kind of multiphase, dark brown, and very polar and reactive mixture, composed of water, acids, solid chars, alcohols, ketones, aldehydes, phenols, ethers, esters, sugars, furans, nitrogen compounds and multifunctional compounds [2-4]. This complex composition leads to the poor fuel qualities of bio-oil, such as low heating value, low volatility, instability, high viscosity, coking, corrosiveness, odor, and cold flow problems [5]. These poor qualities bring a lot of problems in applications, such as difficult burning in diesel engine, instability during long-term storage and transportation [5]. So we need to develop some economic process to upgrade the bio-oil. This work is one part of the whole project of upgrading bio-oil into fuels and chemicals with an integrated process, and focuses on the reasons of the instability and the solutions.

The instability of bio-oil is known to be caused by several polymerization reactions [6-10]. One of the appearances of instability is the significant increase of viscosity with increasing storage time. So we use the standard accelerated stability test method from Department of Energy to evaluate the stability of bio-oil. The increase rate of viscosity was the criterion. Acids and chars may be working as catalysts and the unstable chemical components may be working as reactants in the polymerizations [6-10]. So we tried to remove acids and chars, hydrogenated the unstable chemicals, compared the viscosity

increase rates and determined the major reasons of instability, and then tried to find some approaches to inhibit the polymerization reactions.

2. Materials and Experiments

2.1 Materials

Bio-oil. Crude Pine wood bio-oil (PWBO) is from Mississippi State University.

2.2 Experiments

Accelerated stability test. The samples are sealed very well with Teflon and incubated in oven at 90^{o} C for some time(8 hours, 24 hours, 2 days, etc.), and then cooled down to room temperature for rheological measurement.

Viscosity measurement. After startup of the rheometer, the bio-oil samples were loaded at room temperature to the geometry. For viscous bio-oil sample, 40mm parallel plates of rheometer ARES G2 in Engineering Lab II were applied and the viscosity was measured at 40^{o} C with solvent trap. For diluted sample, concentric cylinder of rheometer AR2000 in Polymer Science Department building was applied and the viscosity was measured at room temperature to reduce the solvent loss. All the measurement followed the standard procedure, equilibrium for 10 minutes at desired temperature and then steady state flow test at shear rate from 0.001 1/s to 10 1/s.

Filtration. The bio-oil samples were filtered by syringe filter. The pore sizes of filter mentioned in this work were 5 μm and 0.45 μm in filtration section and hydrogenation section respectively.

Neutralization. Alkali metal base, dehydrated Na_2CO_3, was used to neutralize the acidic bio-oil. The amount is a little over the TAN (total acid number).

Preparation of water soluble bio-oil (WSBO). The pine wood bio-oil (PWBO) was mixed with distilled water to separate into two phases: an aqueous rich phase (WSBO: water soluble fraction of bio-oil) and an organic rich phase (WIBO: water insoluble bio-oil fraction). The mixture was then centrifuged in a Marathon 2100 centrifuge (Fisher Scientific) at 10,000 rpm for 20 minutes to ensure the phase separation. The two phases, aqueous (top) and non-aqueous (bottom), were then separated by decanting. The weight of the aqueous fraction was measured to determine the amount of bio-oil that dissolved in water. For the experimental purpose 100 gm of bio-oil was added to 80 gm of water and mixed well. The aqueous and non-aqueous phases were separated by centrifugation followed by decanting. The resulting aqueous solution is about 39.6 wt% water soluble bio-oil (WSBO) in water. About 52.5 wt% of the PWBO was found to be water soluble.

Hydrogenation of water soluble fraction of bio-oil. Hydrogenation of the aqueous fraction of the bio-oil was carried out in a 170 ml Parr batch reactor at 125 °C and 1000 psi. About 90 gm of the aqueous fraction of the bio-oil (39.6 wt% WSBO) was loaded in the reactor along with 1.5 gm (wet basis, 50 wt% moisture content) of 5 wt% Ru / activated C catalyst (Strem Chemicals, Product No. 44-4059). The reactor was then purged at least 4-5 times with helium gas to get rid of the air present in the reaction vessel. The reactor was then purged with hydrogen at least 4-5 times to replace all the helium with hydrogen. The reactor pressure was set to 700 psi by adding hydrogen and the heating and stirring were started. Once the temperature reached 125 °C, the reactor pressure was increased to 1000 psi total by adding more hydrogen. Additional hydrogen was added to the reactor during the course of reaction to compensate for the hydrogen consumption. The total pressure was maintained at 1000 psi. The reaction was continued

for 135 minutes. The product is filtered at end using a 0.45 μm filter to remove the catalyst particle. This product was then subjected to the accelerated stability test.

Visual observation with optical microscopy. Samples were loaded to glass slide and observed using Olympus DX60 in Polymer Science Department. The micrographs were taken by Sony CCD color video camera.

3. Results and Discussion

3.1 Effects of filtration

Figure 1 and 2 gave us a basic idea and reference of viscosity increase in original PWBO without any treatment. The viscosity behaviors of treated PWBO with filtration and neutralization were compared with untreated PWBO. The efficiency of hydrogenation treatment is investigated with aqueous fraction of PWBO.

Figure 3 shows the filtration with 5μm syringe filter has some influence in the microstructure. The viscosity lines of filtered PWBO have less fluctuation than untreated PWBO at low shear rate, where the shear stress is close to inertia force and sensitive to the homogeneity, such as particle density, particle size and particle shape. However, the viscosity increase rate didn't have significant change from the comparison between Figure 2 and 4. The efficiency of filtration from visual observation could be evaluated in Figure 5 and 6. Figure 6 shows the 5 μm filter didn't remove the chars completely, there are small particles remaining in filtered PWBO. If we assume 5 μm syringe filter removed a lot of chars, this result may suggest the chars may be not a critical factor of causing viscosity increase.

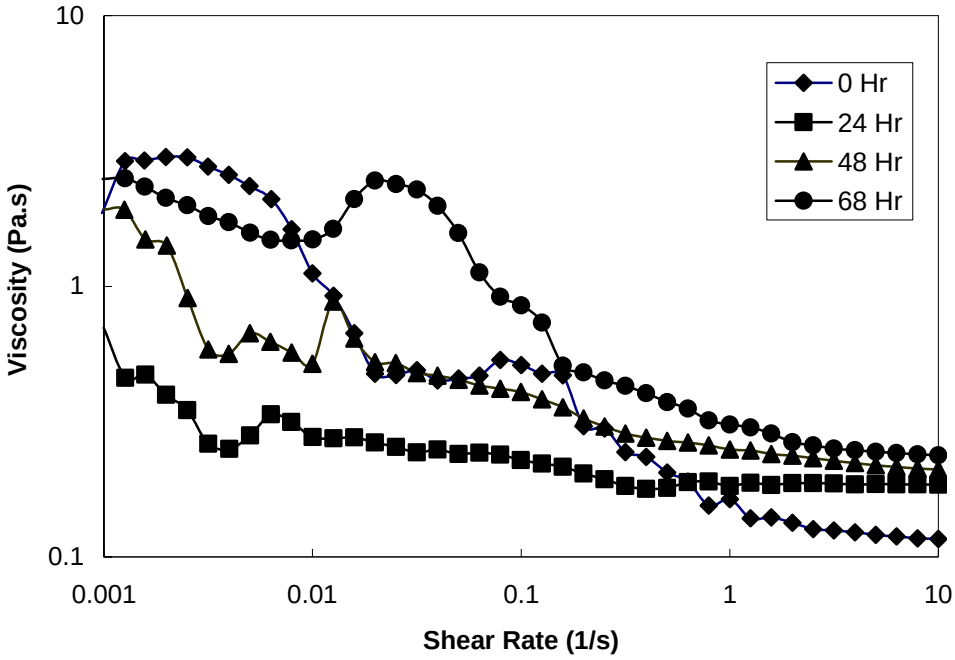

Figure A-1. Viscosity of untreated bio-oil (PWBO) versus shear rate. Lines are guides for eye.

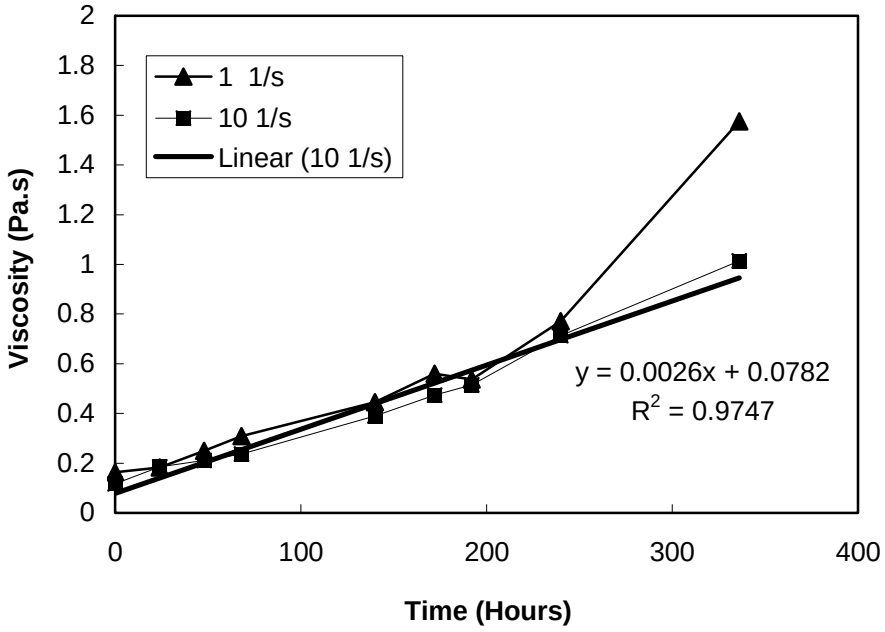

Figure A-2. Viscosity of untreated bio-oil (PWBO) versus incubation time at 90° C. The linear line is the trendline of viscosity at shear rate 10 1/s. Samples were incubated at 90° C, viscosity was measured at 40° C.

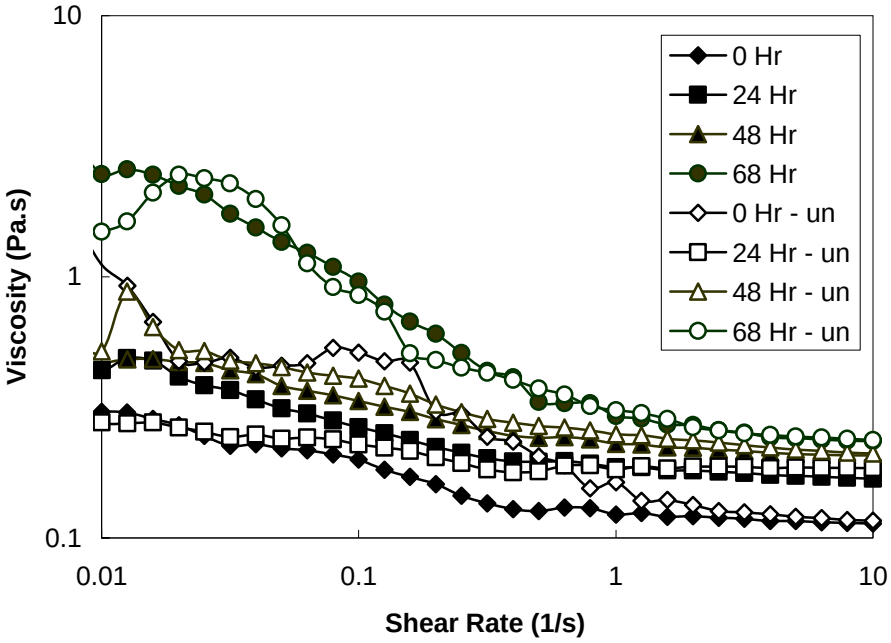

Figure A-3. Comparison of viscosity behavior versus shear rate between untreated PWBO and filtered PWBO with 5 μm syringe filter. The solids are untreated PWBO, the opens are filtered PWBO. Samples were incubated at 90° C, viscosity was measured at 40° C.

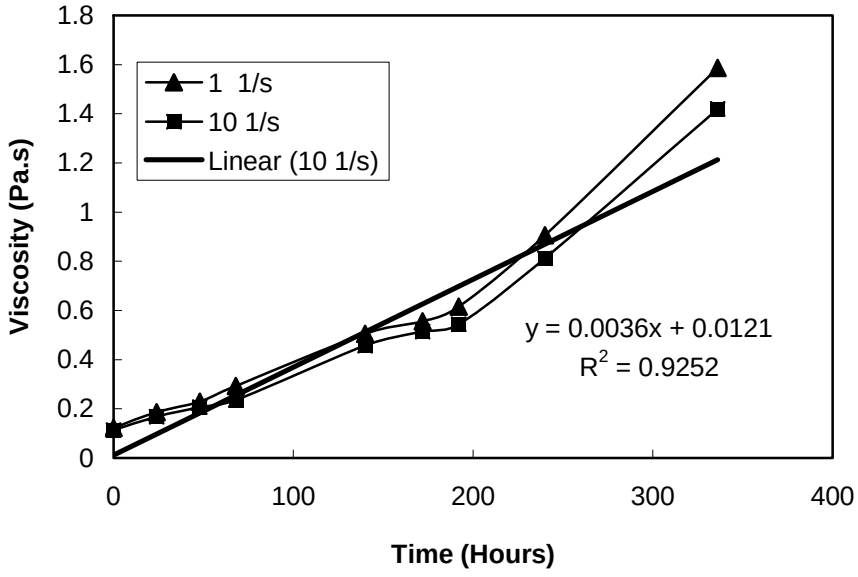

Figure A-4. Viscosity of filtered PWBO versus incubation time at 90° C. The lines are guides for eye. Samples were incubated at 90° C, and viscosity was measured at 40° C.

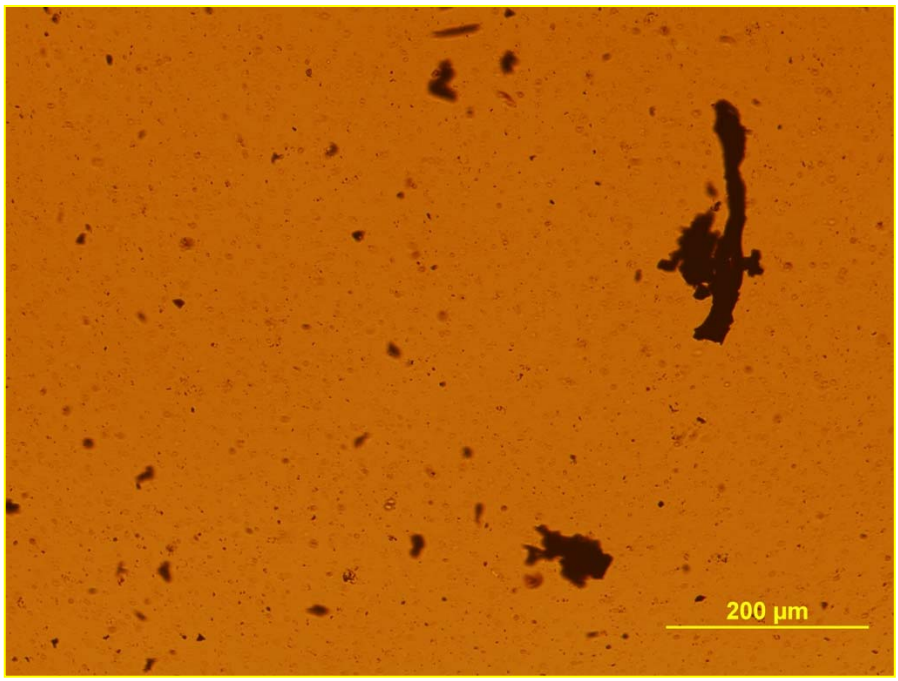

Figure A-5. Micrograph of untreated PWBO before incubation. (10X) Large particles are observed.

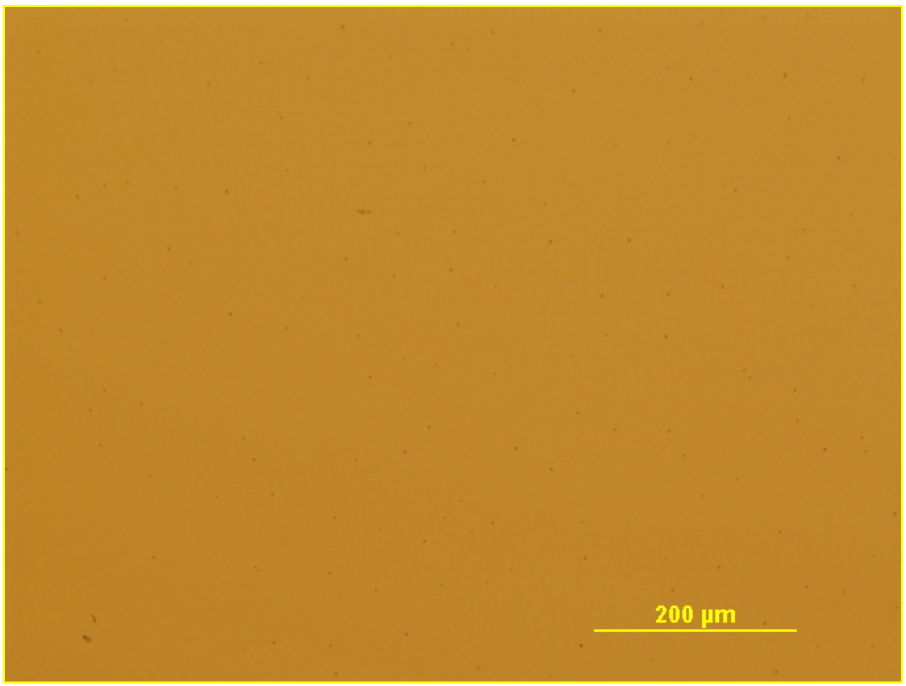

Figure A-6. Micrograph of filtered PWBO with 5 µm syringe filter before incubation. (10X) Small dot particles are observed.

3.2 Effects of neutralization

Figure 7 shows the neutralized PWBO with Na_2CO_3 still has a increase rate of viscosity which is close to untreated PWBO. So the transition from acidic to basic didn't stop the instability. The polymerization reaction may not be catalyzed by acids, or may be able to continue in basic environment.

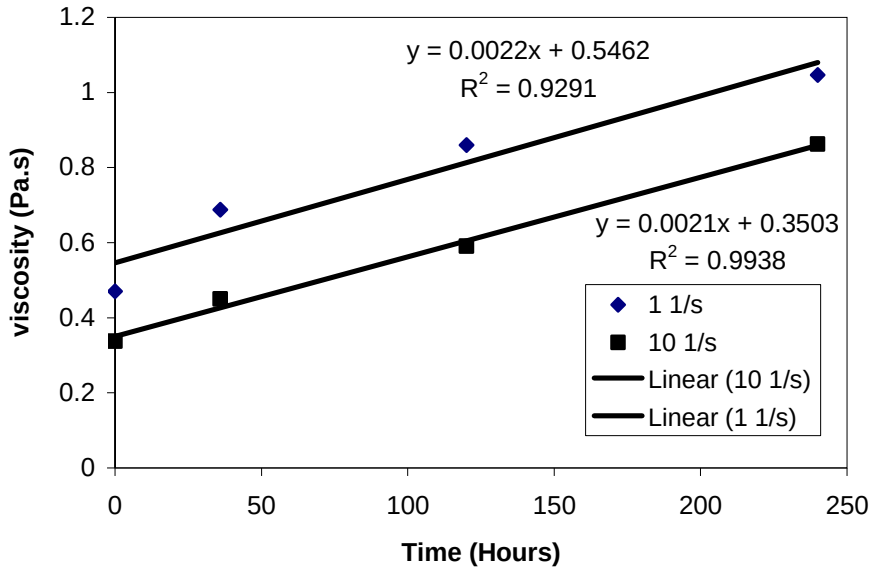

Figure A-7. Viscosity of neutralized PWBO versus incubation time. Samples were incubated at 90° C, viscosity was measured at 40° C.

3.3 Effects of hydrogenation

Figure 8 shows the viscosity of unhydrogenated WSBO has an increase trend even after some black viscous oil separated from the bulk solution (shown in Figure 10). Figure 9 shows a decrease trend of viscosity in hydrogenated WSBO, which only has a few black droplets separated from bulk solution after long time heating treatment (shown in Figure 11). The hydrogenated WSBO was filtered with 0.45 μm syringe filter. So we need to concern the effects of filtration together with the hydrogenation. A group of

experiments without the factors of filtration will show us the influence of hydrogenation directly in the future work. Table 1 listed the chemicals already know in PWBO and their products of hydrogenation treatment.

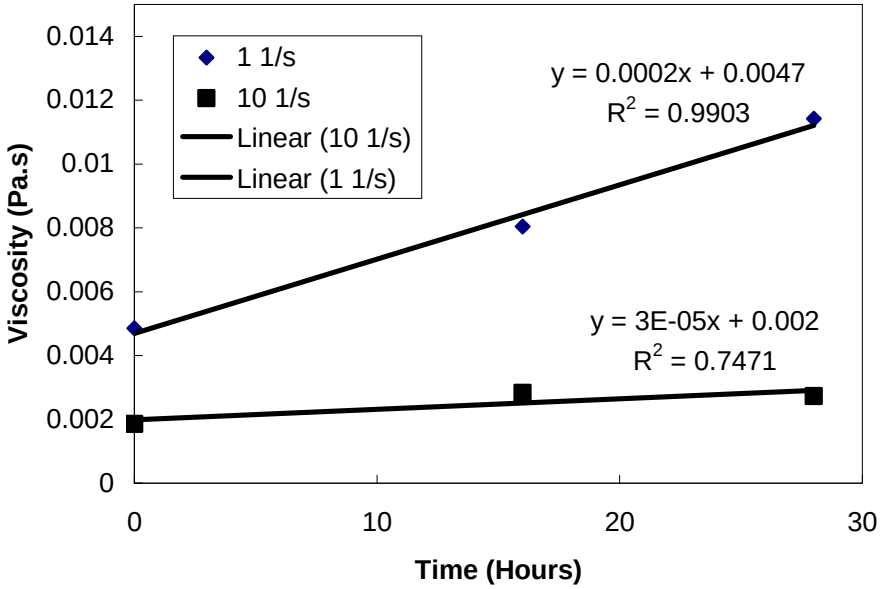

Figure A-8. Viscosity of unhydrogenated 39.6wt% WSBO (unfiltered) as a function of incubation time. Samples were incubated at 90° C, and viscosity was measured at 25° C. The linear lines are trend lines of viscosity increase.

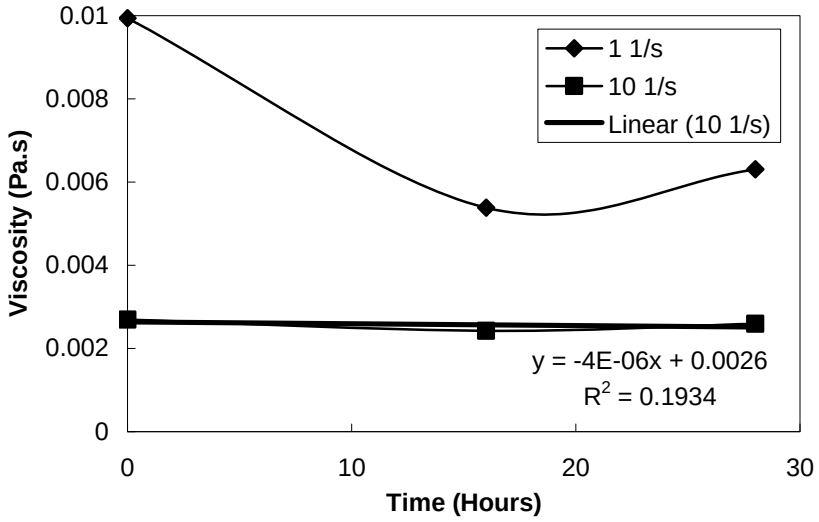

Figure A-9. Viscosity of hydrogenated 39.6% WSBO (filtered with 0.45 μm syringe filter) versus incubation time. Samples were incubated at 90° C, and viscosity was measured at 25° C. Lines are guides for eye. Linear line is the trend line of viscosity at 10 1/s.

Figure A-10. Unhydrogenated WSBO at room temperature after heating treatment. Black viscous oils at the bottom and on the wall were created during heating treatment and separated from bulk solution.

Figure A-11. Hydgrogenated WSBO at room temperature after hearting treatment. Only a few of black oil droplets were created and separated from bulk solution.

Table A-1. Some chemicals already known in PWBO and their products of hydrogenation treatment. (Continued on the next page)

No.	Reactant	Product	Type of Reaction
1	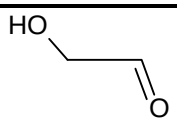 Hydroxyacetaldehyde	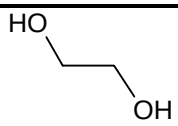 Ethylene glycol	Hydrogenation
2	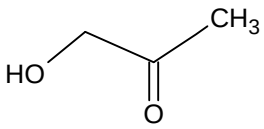 Hydroxyacetone	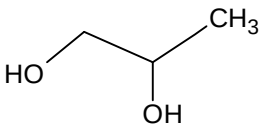 Propylene glycol	Hydrogenation

3	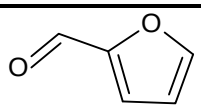 Furfural	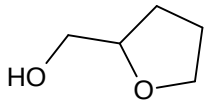 Tetrahydrofurfuryl alcohol	Hydrogenation
4	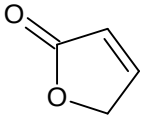 2-Furanone	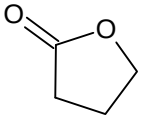 γ-Butyrolactone	Hydrogenation
5	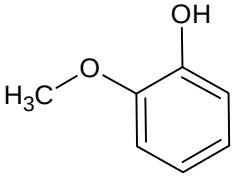 Guaiacol	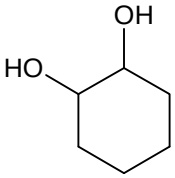 1,2-Cyclohexanediol	Hydrogenation
6	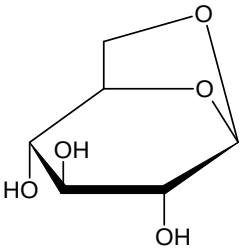 Levoglucosan	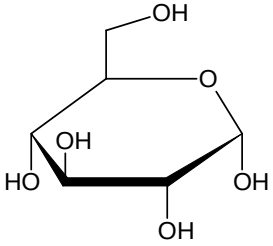 Glucose	Hydrolysis
7	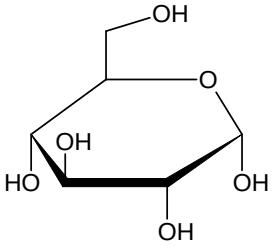 Glucose	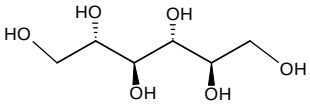 Sorbitol	Hydrogenation
8	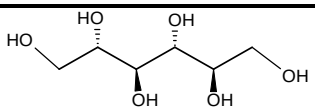 Sorbitol	Ethylene glycol, Propylene glycol & 1,4-Butanediol	Hydrogenolysis
9	CH_3-COOH Acetic acid		
10	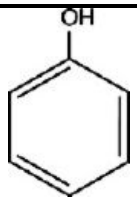 Phenol		

4. Summary

This work investigated the stability of untreated pine wood bio-oil(PWBO) and PWBO treated with filtration, neutralization and hydrogenation in terms of viscosity increase over heating treatment time. Filtration and neutralization didn't inhibit the polymerization reactions in PWBO effectively. So acids and chars may not be the main factors of instability. Hydrogenation may be a promising solution technically although its cost is high. In future work, it is necessary to investigate the polymerization mechanisms and find efficient inhibition methods.

5. Future work

The bio-oil could be considered as an emulsion system since it contains water and organic compounds, so there are a lot of hydrous micro domains and anhydrous micro domains. Most of the chemicals listed in Table 1 are unstable. The functional groups are very reactive and can cause various polymerization reactions in two kinds of micro domains. So in the future work, while investigate the removal of acids and chars, we propose to investigate the reaction mechanisms existing in the bio-oil with concerns of cationic, anionic, radical polymerization and cross-link reaction, and then find cost-effective polymerization inhibitors.

Some specific suggestions are to investigate the stability of model systems mixed by the chemicals in Table 1:

1) A model system with all the chemicals in the second column.
2) A model system with all the chemicals except acids in the second column.
3) An hydrogenated model system with all the chemicals in the second column.

4) A hydrogenated model system with all the chemicals except acids in the second column.

After heating treatment, the model systems will be analyzed using HPLC, NMR and GC/MS, and rheometer. Hopefully the changes of chemical components and functional groups can be tracked by the above instruments, and then we can gain the ideas how many kinds of polymerization reaction occurring in the systems and how to inhibit the reactions. Model systems with only a few of chemicals can also be investigated to find the more details of reactions if needed.

Bibliography

[1] G. W. Huber; S. Iborra; A. Corma. *Chemical Reviews* **2006**, 106, p4044.

[2] D. Mohan; C. U. Pittman; P. H. Steele. *Energy and Fuels* **2006**, 20, p848.

[3] A. V. Bridgwater; G. V. C. Peacocke. *Renewable and Sustainable Energy Reviews* **2000**, 4, p1.

[4] D. C. Elliott; G. F. Schiefelbein. *American Chemical Society, Division of Fuel Chemistry* **1989**, 34, p1160.

[5] S. Czernik; A. V. Bridgwater. *Energy and Fuels* **2004**, 18, p590.

[6] M.E. Boucher; A. Chaala; H. Pakdel; C. Roy. *Biomass and Bioenergy* **2000**, 19, p351.

[7] R. K. Sharma; N. N. Bakhshi. *Canadian J. Chem. Eng.* **1991**, 69, p1071.

[8] B. Scholze; C. Hanser; D. Meier. *J. Analytical and Applied Pyrolysis* **2001**, 58–59, p387.

[9] J.D. Adjaye; N.N. Bakhshi. *Fuel Processing Technology* **1995**, 45, p185.

[10] S. T. Srinivas; A. K. Dalai; N. N. Bakhshi. *Canadian J. Chemical Engineering* **2000**, 78, p343.

BIBLIOGRAPHY

A. Ceglie; K. P. Das; B. Lindman. *J. Colloid Interface Sci.,* **1987**, 115, (1), p115.

A. Guinier; G. Fournet, *Small-Angle Scattering of X-Rays*. John Wiley and Sons: New York, **1955**.

A. Langenfeld; V. Schmitt; M. J. Stebe. *J. Colloid Interface Sci.* **1999,** 218, (2), p522.

A. Na; C. Eriksson; S. G. Eriksson; E. Osterberg; K. Holmberg. *J. Am. Oil Chem. Soc.,* **1990**, 67, (11), p766.

A. V. Bridgwater; G. V. C. Peacocke. *Renewable and Sustainable Energy Reviews* **2000**, 4, p1.

B. Hribar; N. Southall; V. Vlachy; K. Dill. *J. Amer. Chem. Soc.*, **2002**, 124, p12302.

B. K. Paul; S. P. Moulik. *Curr. Sci.*, **2001**, 80, (8), p990.

B. Scholze; C. Hanser; D. Meier. *J. Analytical and Applied Pyrolysis* **2001**, 58–59, p387.

C. A. Bunton; F. Nome; F. H. Quina; L. S. Romsted. *Accounts Chem. Res.*, **1991**, 24, (12), p357.

C. Ceschin; J. Roques; M. C. Maletmartino; A. Lattes. *J. Chem. Tech. & Biotech. a-Chem. Tech.*, **1985**, 35, (2), p73.

C. E. Cooke; J. H. Schulman In *The effect of different hydrocarbons on the formation of microemulsions*, Surface Chemistry, Stockholm, 1964; Ekwall, P.; Groth, K.; Runnstrom-Reio, V., Eds. Academic Press, New York: Stockholm, 1964; pp 231.

C. J. Glinka; J. G. Barker; B. Hammouda; S. Krueger; J. J. Moyer; W. J. Orts. *J. Appl. Crystal.* **1998,** 31, p430.

C. Petit; P. Lixon; M. P. Pileni. *Langmuir*, **1991**, 7, (11), p2620.

C. Quellet; H. F. Eicke; G. Xu; Y. Hauger. *Macromolecules,* **1990**, 23, (13), p3347.

C. Solans; J. G. Dominguez; S. E. Friberg. *J. Dispersion Sci. Technol.*, **1985**, 6, (5), p523.

C. Thomas; J. Riess; M. Guichard. *Int. J. Radiat. Biol.* **1991,** 59, (2), p433.

C. Toncumpou; E. J. Acosta; L. B. Quencer; A. F. Joseph; J. F. Scamehorn; D. A. Sabatini; S. Chavadej; N. Yanumet. *J. Surfactants Deterg.*, **2003**, 6, (3), p191.

C. Tondre; A. Xenakis. *Faraday Discuss.*, **1984**, p115.

C. Washington; S. M. King. *Langmuir*, **1997**, 13, (17), p4545.

C. Washington; S. M. King; R. K. Heenan. *J. Phys. Chem.*, **1996**, 100, (18), p7603.

D. Attwood, Microemulsions. In *Colloidal Drug Delivery Systems*, Kreuter, J., Ed. Marcel Dekker, New York: **1994**.

D. C. Elliott; G. F. Schiefelbein. *American Chemical Society, Division of Fuel Chemistry* **1989**, 34, p1160.

D. F. Sears; J. H. Schulman. *J. Phys. Chem.*, **1964**, 68, (12), p3529.

D. Fioretto; M. Freda; G. Onori; A. Santucci. *J. Phys. Chem. B,* **1999**, 103, p2631.

D. Fioretto; M. Freda, G. Onori; A. Santucci. *J. Phys. Chem. B* **1999**, 103, p8216.

D. Mohan; C. U. Pittman; P. H. Steele. *Energy and Fuels* **2006**, 20, p848.

D. R. Foss; J. F. Brady. *J. Rheol.*, **2000**, 44, (3), p629.

D. Stauffer, *Introduction to Percolation Theory.* **1985**, Taylor and Francis Inc.: Philadelphia.

D. Vlassopoulos; G. Fytas; S. Pispas; N. Hadjichristidis. *Physica B,* **2001**, 296, (1-3), p184.

E. C. Donaldson; G. V. Chilingarian; T. F. Yen, *Microbial Enhanced Oil Recovery*. **1989**, Elsevier, New York: p 9.

E. Kissa, *Fluorinated surfactants and repellents.* **2001**, Marcel Dekker, New York: Vol. 97.

E. Sjoblom; S. Friberg. *J. Colloid Interface Sci.,* **1978**, 67, (1), p16.

F. Caboi; G. Capuzzi; P. Baglioni; M. Monduzzi. *J. Phys. Chem. B,* **1997**, 101, (49), p10205.

F. Chambon; H. H. Winter. *J. Rheol.,* **1987**, 31, (8), p683.

F. Chambon; H. H. Winter. *Polym. Bull.,* **1985**, 13, (6), p499.

F. Dreher; P. Walde; P. Walther; E. Wehrli. *J. Control. Release,* **1997**, 45, (2), p131.

F. M. Menger; A. R. Elrington. *J. Am. Chem. Soc.,* **1991**, 113, (25), p9621.

F. Mallamace; P. Gambadauro; N. Micali; P. Tartaglia; C. Liao; S. H. Chen. *Phys. Rev. Lett.,* **2000**, 84, (23), p5431.

F. S. Moolman; H. Rolfes; S. W. van der Merwe; W. W. Focke. *Biochem. Eng. J.* **2004,** 19, (3), p237.

F. Tanaka; S. F. Edwards. *J. Non-Newton. Fluid Mech.* **1992,** 43, (2-3), p247.

F. Tanaka; S. F. Edwards. *J. Non-Newton. Fluid Mech.* **1992,** 43, (2-3), p273.

F. Tanaka; S. F. Edwards. *J. Non-Newton. Fluid Mech.* **1992,** 43, (2-3), p289.

F. Tanaka; S. F. Edwards. *Macromolecules* **1992,** 25, (5), p1516.

G. Fleischer; F. Stieber; U. Hofmeier; H. F. Eicke. *Langmuir,* **1994**, 10, (6), p1780.

G. Gillberg; H. Lehtinen; S. Friberg. *J. Colloid Interface Sci.,* **1970**, 33, (1), p40.

G. J. Fleer; M. A. C. Stuart; J. M. H. M. Scheutjens; T. Cosgrove; B. Vincent, *Polymers at Interfaces.* **1993**, Chapman & Hall: London, New York.

G. J. T. Tiddy. *Phys. Rep.-Rev. Sec. Phys. Lett.,* **1980**, 57, (1), p2.

G. W. Huber; S. Iborra; A. Corma. *Chemical Reviews* **2006**, 106, p4044.

H. F. Eicke; C. Quellet; G. Xu. *Colloids & Surfaces*, **1989**, 36, (1), p97.

H. F. Eicke; M. Gauthier; R. Hilfiker; R. Struis; G. Xu. *J. Phys. Chem.*, **1992**, 96, (12), p5175.

H. H. Winter; F. Chambon. *J. Rheol.*, **1986**, 30, (2), p367.

H. Ohde; C. M. Wai; H. Kim; J. Kim; M. Ohde. *J. Am. Chem. Soc.*, **2002**, 124, (17), p4540.

H. Ohde; J. M. Rodriguez; X. R. Ye; C. M. Wai. *Chem. Commun.*, **2000**, (23), p2353.

H. Saito; K. Shinoda. *J. Colloid Interface Sci.*, **1967**, 24, (1), p10.

H. Saito; K. Shinoda. *J. Colloid Interface Sci.*, **1970**, 32, (4), p647.

H. Stamatis; A. Xenakis; M. Provelegiou; F. N. Kolisis. *Biotechnol. Bioeng.*, **1993**, 42, (1), p103.

H. Tanaka; T. Okazaki; Y. Tezuka; T. Hongo; Y. Takahashi. *Polymer* **2002,** 43, (4), p1189.

H. Wennerstrom; B. Lindman. *Phys. Rep.-Rev. Sec. Phys. Lett.*, **1979**, 52, (1), p1.

Http://www.ncnr.nist.gov/programs/sans/data/red_anal.html

I. Nezbeda. *Czech. J. Phys.* **1977,** 27, (3), p247.

J. B. Hayter, In *Physics of Amphiphiles-Micelles, Vesicles, and Microemulsions*, M. C. V. DeGiorgio, Ed. North-Holland: Varenna, Italy, **1983**; p 59. [4] J. Bergenholtz; A. A. Romagnoli; N. J. Wagner. *Langmuir*, **1995**, 11, (5), p1559.

J. Bergenholtz. *Curr. Opin. Colloid Interface Sci.*, **2001**, 6, (5-6), p484.

J. Bergenholtz; N. Willenbacher; N. J. Wagner; B. Morrison; D. van den Ende; J. Mellema. *J. Colloid Interface Sci.*, **1998**, 202, (2), p430.

J. Bergenholtz; M. Fuchs. *Phys. Rev. E* **1999,** 59, (5), p5706.

J. C. Ravey; M. J. Stebe. *Progr. Colloid & Polym. Sci.* **1987,** 73, (New Trends Colloid Sci.), p127.

J. C. Ravey; M. J. Stebe. *Progr. Colloid & Polym. Sci.* **1990,** 82, (Surfactants Macromol.: Self-Assem. Interfaces Bulk), p218.

J. C. Ravey; M. J. Stebe; S. Sauvage. *Colloid Surf. A-Physicochem. Eng. Asp.* **1994,** 91, p237.

J.D. Adjaye; N.N. Bakhshi. *Fuel Processing Technology* **1995**, 45, p185. [27] J. D. Desai; I. M. Banat. *Microbiol. Mol. Biol. Rev.,* **1997**, 61, (1), p47.

J. E. Bowcott; J. H. Schulman. *Zeitschrift Fur Elektrochemie,* **1955**, 59, (4), p283.

J. E. Martin; D. Adolf. *Annu. Rev. Phys. Chem.,* **1991**, 42, p311.

J. Eastoe; G. Fragneto; B. H. Robinson; T. F. Towey; R. K. Heenan; F. J. Leng. *J. Chem. Soc.-Faraday Trans.,* **1992**, 88, (3), p461.

J. Eastoe; S. Chatfield; R. Heenan. *Langmuir*, **1994**, 10, (6), p1650.

J. Eastoe; T. F. Towey; B. H. Robinson; J. Williams; R. K. Heenan. *J. Phys. Chem.,* **1993**, 97, (7), p1459.

J. Eastoe; W. K. Young; B. H. Robinson; D. C. Steytler. *J. Chem. Soc.-Faraday Trans.,* **1990**, 86, (16), p2883.

J. Emsley. The elements. Clarendon Press, Oxford, 1989.

J. F. Brady. *J. Chem. Phys.,* **1993**, 99, (1), p567.

J. G. Riess. *Colloid Surf. A-Physicochem. Eng. Asp.,* **1994**, 84, (1), p33.

J. H. Clint; I. R. Collins; J. A. Williams; B. H. Robinson; T. F. Towey; P. Cajean; A. Khanlodhi. *Faraday Discuss.,* **1993**, p219.

J. H. Schulman; D. P. Riley. *J. Colloid Sci.,* **1948**, 3, (4), p383.

J. H. Schulman; J. A. Friend. *J. Colloid Sci.,* **1949**, 4, (5), p497.

J. H. Schulman; W. Stoeckenius; L. M. Prince. *J. Phys. Chem.,* **1959**, 63, (10), p1677.

J. Hopken; C. Pugh; W. Richtering; M. Moller. *Makromolekulare Chemie-Macromolecular Chemistry and Physics* **1988,** 189, (4), p911.

J. Israelachvili, *Intermolecular and Surface Forces*. Academic Press: San Diego: **1992**.

J. K. Percus; G. J. Yevick. *Phys. Rev.* **1958,** 110, (1), p1.

J. L. Cayias; R. S. Schechter; W. H. Wade. *J. Colloid Interface Sci.,* **1977**, 59, (1), p31.

J. Lang; A. Jada; A. Malliaris. *J. Phys. Chem.,* **1988**, 92, (7), p1946.

J. M. Sarciaux; L. Acar; P. A. Sado. *Int. J. Pharm.,* **1995**, 120, (2), p127.

J. M. Wiencek; S. Qutubuddin. *Sep. Sci. Technol.,* **1992**, 27, (10), p1211.

J. S. Higgins; H. C. Benoit, *Polymers and Neutron Scattering*. Oxford: Clarendon Press: **1994**.

J. S. Huang; M. W. Kim. **1984**, 24, (2), p197.

J. S. Huang. *J. Chem. Phys.,* **1985**, 82, (1), p480.

J. Salamone. Polymeric Materials Encyclopedia. CRC Press, **1996**, p5812.

K. Inomata; D. Nakanishi; A. Banno; E. Nakanishi; Y. Abe; R. Kurihara; K. Fujimoto; T. Nose. *Polymer* **2003,** 44, (18), p5303.

K. N. Pham; A. M. Puertas; J. Bergenholtz; S. U. Egelhaaf; A. Moussaid; P. N. Pusey; A. B. Schofield; M. E. Cates; M. Fuchs; W. C. K. Poon. *Science,* **2002**, 296, (5565), p104.

K. Naoe; T. Kai; M. Kawagoe; M. Imai. *Biochem. Eng. J.,* **1999**, 3, (1), p79.

K. Sameshima; R. Tanaka; K. Igarashi; H. Ooshima. *J. Chem. Therm.* **2006,** 38,

K. Shinoda. *J. Colloid Interface Sci.,* **1967**, 24, (1), p4.

K. Shinoda. *J. Colloid Interface Sci.,* **1970**, 34, (2), p278.

K. Shinoda; T. Ogawa. *J. Colloid Interface Sci.*, **1967**, 24, (1), p56.

p662.

K. V. Schubert; E. W. Kaler. *Colloid Surf. A-Physicochem. Eng. Asp.* **1994,** 84, (1), p97.

K. Zhang; C. H. Chew; S. Kawi; J. Wang; L. M. Gan. *Catal. Lett.*, **2000**, 64, (2-4), p179.

L. Fabbian; W. Gotze; F. Sciortino; P. Tartaglia; F. Thiery. *Phys. Rev. E* **1999,** 59, (2), pR1347.

L. Fabbian; W. Gotze; F. Sciortino; P. Tartaglia; F. Thiery. *Phys. Rev. E* **1999,** 60, (2), p2430.

L. L. Schramm; D. B. Fisher; S. Schurch; A. Cameron. *Colloid Surf. A-Physicochem. Eng. Asp.*, **1995**, 94, (2-3), p145.

L. S. Ornstein; F. Zernicke. *Proc. Amst. Acad. Sci.* **1914,** 17, p793.

M. A. C. Stuart; T. Cosgrove; B. Vincent. *Adv. Colloid Interface Sci.*, **1986**, 24, (2-3), p143.

M. Antonietti; R. Basten; S. Lohmann. *Macromol. Chem. Phys.*, **1995**, 196, (2), p441.

M. Antonietti; W. Bremser; D. Muschenborn; C. Rosenauer; B. Schupp; M. Schmidt. *Macromolecules*, **1991**, 24, (25), p6636.

M.Bara; A.Guiet-Bara; J. Durlach. *Magnes. Res.* **1988**, 1, p29. *Magnes. Res.* 1989, 2, p243.

M. Baviere; P. Glenat; V. Plazanet; J. Labrid. *SPE Reserv. Eng.*, **1995**, 10, (3), p187.

M. Carrillo-Tripp; H. Saint-Martin; I. Ortega-Blake. *J. Chem. Phys.*, **2003**, 118, (15), p7062.

M. Chiang; D. O. Shah. *Abstr. Pap. Am. Chem. Soc.*, **1980**, 179, (MAR), p147.

M. D'Angelo; D. Fioretto; G. Onori; L. Palmieri; A. Santucci. *Phys. Re*V. *E* **1995**, *52*,

pR4620.

M. D'Angelo; D. Fioretto; G. Onori; L. Palmieri; A. Santucci. *Phys. Re*V. *E,* **1996**, *54* (1), p993.

M.E. Boucher; A. Chaala; H. Pakdel; C. Roy. *Biomass and Bioenergy* **2000**, 19, p351. [8]

M. F. Bush; R. J. Saykally; E. R. Williams. *Chem Phys Chem,* **2007**, 8, (15), p2245.

M. Fanun; M. Leser; A. Aserin; N. Garti. *Colloid Surf. A-Physicochem. Eng. Asp.,* **2001**, 194, (1-3), p175.

M. Freda; G. Onori; A. Paciaroni; A. Santucci. *J. Non-Crystal. Sol.*, **2002**, 307–310, p874.

M. Kotlarchyk; S. H. Chen; J. S. Huang. *J. Phys. Chem.*, **1982**, 86, (17), p3273.

M. Kotlarchyk; S. H. Chen; J. S. Huang; M. W. Kim. *Phys. Rev. A,* **1984**, 29, (4), p2054.

M. Kreilgaard. *Adv. Drug Deliv. Rev.*, **2002**, 54, pS77.

M. J. Lawrence; G. D. Rees. *Adv. Drug Deliv. Rev.*, **2000**, 45, (1), p89.

M. J. Schwuger; K. Stickdorn; R. Schomacker. *Chem. Rev.*, **1995**, 95, (4), p849.

M. Odenwald; H. F. Eicke; W. Meier. *Macromolecules,* **1995**, 28, (14), p5069.

M. P. Krafft. *Adv. Drug Deliv. Rev.*, **2001**, 47, (2-3), p209.

M. P. Krafft; J. G. Riess. *Angew. Chem.-Int. Edit. Engl.* **1994,** 33, (10), p1100.

M. P. Krafft; J. G. Riess. PCT WO 95/09606, **1995**.

M. P. Krafft; J. G. Riess. WO 97/03644., **1995**.

M. R. Gherase; J. C. Wallace; A. R. Cross; G. E. Santyr. *J. Chem. Phys.* **2006,** 125, (4), p.

M. Rubinstein; R. H. Colby; J. R. Gillmor. *Abstr. Pap. Am. Chem. Soc.*, **1989**, 197, p82.

M. S. Green; A. V. Tobolsky. *J. Appl. Phys.* **1946,** 17, (5), p407.

M. Saidi; H. Khalaf. *Hydrometallurgy,* **2004**, 74, (1-2), p85.

M. Y. Chiang; K. S. Chan; D. O. Shah. *J. Can. Pet. Technol.*, **1978**, 17, (4), p61.

N. Azemar; I. Carrera; C. Solans. *J. Dispersion Sci. Technol.*, **1993**, 14, (6), p645.

N. Kometani; Y. Toyoda; K. Asami; Y. Yonezawa. *Chem. Lett.*, **2000**, (6), p682.

N. N. Li Separating hydrocarbons with liquid membranes. US Pat. 3, 410, 794, **1968**.

P. Bartlett; R. H. Ottewill. *J. Chem. Phys.* **1992,** 96, (4), p3306.

P. K. Sharma; M. J. Reilly; S. K. Bhatia; N. Sakhitab; J. D. Archambault; S. R. Bhatia. *Colloid Surf. B-Biointerfaces* **2008,** 63, (2), p229.

P. K. Sharma; M. J. Reilly; D. N. Jones; P. M. Robinson; S. R. Bhatia. **2008,** 61, (1), p53.

P. K. Sharma; S. R. Bhatia. *Int. J. Pharm.* **2004,** 278, (2), p361.

P. Kumar; K. L. Mitta, *Handbook of Microemulsion Science and Technology*. **1999**, Marcel Dekker, New York.

P. LoNostro; S. M. Choi; C. Y. Ku; S. H. Chen. *J. Phys. Chem. B*, **1999**, 103, (25), p5347.

P. Mukerjee. *Colloid Surf. A-Physicochem. Eng. Asp.*, **1994**, 84, (1), p1.

P. N. Pusey; W. Vanmegen. *Nature*, **1986**, 320, (6060), p340.

P. N. Pusey; W. Vanmegen. *Phys. Rev. Lett.*, **1987**, 59, (18), p2083.

P. Pitzalis; R. Angelico; O. Soderman; M. Monduzzi. *Langmuir*, **2000**, 16, (2), p442.

P. Sollich; F. Lequeux; P. Hebraud; M. E. Cates. *Phys. Rev. Lett.*, **1997**, 78, (10), p2020.

P. Sollich. *Phys. Rev. E*, **1998**, 58, (1), p738.

P. Y. Chow; J. Ding; X. Z. Wang; C. H. Chew; L. M. Gan. *Phys. Status Solidi A-Appl. Res.*, **2000**, 180, (2), p547.

P. Y. Feng; X. H. Bu; G. D. Stucky; D. J. Pine. *J. Am. Chem. Soc.*, **2000**, 122, (5), p994.

R. A. Lionberger; W. B. Russel. *J. Rheol.*, **1997**, 41, (2), p399.

R. F. Mattrey; G. Strich; R. E. Shelton; B. B. Gosink; G. R. Leopold; T. Lee; J. Forsythe. *Radiology* **1987,** 163, (2), p339.

R. Hilfiker; H. F. Eicke; C. Steeb; U. Hofmeier. *J. Phys. Chem.*, **1991**, 95, (3), p1478.

R. J. Twieg; T. P. Russell; R. Siemens; J. F. Rabolt. *Macromolecules* **1985,** 18, (6), p1361.

R. K. Sharma; N. N. Bakhshi. *Canadian J. Chem. Eng.* **1991**, 69, p1071.

R. L. Blum; M. H. Robbins; L. M. Hearn; S. L. Nelson Microemulsion dilutable cleaner. US Pat. 5, 854, 187, **1998**.

R. Mancinelli; A. Botti; F. Bruni; M. A. Ricci; A. K. Soper. *J. Phys. Chem. B*, **2007**, 111, (48), p13570.

R. Muller; E. Gerard; P. Dugand; P. Rempp; Y. Gnanou. *Macromolecules*, **1991**, 24, (6), p1321.

R. N. Healy; R. L. Reed. *SPE J.*, **1974**, 14, (5), p491.

R. N. Healy; R. L. Reed. *SPE J.*, **1977**, 17, (2), p129.

R. Struis; H. F. Eicke. *J. Phys. Chem.*, **1991**, 95, (15), p5989.

R. V. Sharma; K. C. Sharma. *Physica A* **1977,** 89, (1), p213.

R. Wikramanayake; R. Enick; M. Turberg. *Fluid Phase Equilib.* **1991,** 70, (1), p107.

S. A. Hagan; S. S. Davis; L. Illum; M. C. Davies; M. C. Garnett; D. C. Taylor; M. P. Irving; T. F. Tadros. *Langmuir*, **1995**, 11, (5), p1482.

S. Alexander. *J. De Physique* **1977,** 38, (8), p983.

S. Czernik; A. V. Bridgwater. *Energy and Fuels* **2004**, 18, p590.

S. Eriksson; U. Nylen; S. Rojas; M. Boutonnet. *Appl. Catal. A-Gen.*, **2004**, 265, (2), p207.

S. F. Khattak; K. S. Chin; S. R. Bhatia; S. C. Roberts. *Biotechnol. Bioeng.* **2007,** 96, (1), p156.

S. Fusco; A. Borzacchiello; P. A. Netti. *J. Bioact. Compat. Polym.*, **2006**, 21, (2), p149.

S. H. Chen. *Annu. Rev. Phys. Chem.*, **1986**, 37, p351.

S. H. Chen; T. L. Lin. *Methods of Experimental Physics* **1987,** 23B, p489.

S. Magdassi; M. Royz; S. Shoshan. *Int. J. Pharm.* **1992,** 88, (1-3), p171.

S. Shoshan; D. Michaeli; S. Magdassi. US Pat. 5, 073, 378, **1991**.

S. Magdassi. *Colloid Surf. A-Physicochem. Eng. Asp.*, **1997**, 123, p671.

S. J. Chen; D. F. Evans; B. W. Ninham; D. J. Mitchell; F. D. Blum; S. Pickup. *J. Phys. Chem.*, **1986**, 90, (5), p842.

S. P. Moulik; B. K. Paul. *Adv. Colloid Interface Sci.*, **1998**, 78, (2), p99. [100] S. L. Elliott; W. B. Russel. *J. Rheol.*, **1998**, 42, (2), p361.

S. R. Bhatia; A. Mourchid. *Langmuir*, **2002**, 18, (17), p6469

S. R. Bhatia; A. Mourchid; M. Joanicot. *Curr. Opin. Colloid Interface Sci.*, **2001**, 6, (5-6), p471.

S. R. Bhatia; W. B. Russel; J. Lal. *J. Appl. Crystallogr.*, **2000**, 33, (1), p614.

S. R. Bhatia; W. B. Russel. *Macromolecules*, **2000,** 33, (15), p5713.

S. R. Kline. *J. of Appl. Crystal.* **2006,** 39, p895.

S. T. Milner; T. A. Witten. *Macromolecules*, **1992**, 25, (20), p5495.

S. T. Srinivas; A. K. Dalai; N. N. Bakhshi. *Canadian J. Chemical Engineering* **2000**, 78, p343.

S. V. G. Menon; V. K. Kelkar; C. Manohar. *Phys. Rev. A* **1991,** 43, (2), p1130.

S. W. Tsai; C. L. Wen; J. L. Chen; C. S. Wu. *J. Membr. Sci.*, **1995**, 100, (2), p87.

T. F. Tadros. *Intl. J. of Cosmetic Sci.*, **1992**, 14, (3), p93.

T. F. Vandamme. *Prog. Retin. Eye Res.*, **2002**, 21, (1), p15.

T. G. Mason; D. A. Weitz. *Phys. Rev. Lett.*, **1995**, 75, (14), p2770.

T. Hanaoka; H. Hayashi; T. Tago; M. Kishida; K. Wakabayashi. *J. Colloid Interface Sci.,* **2001**, 235, (2), p235.

T. Imae; M. P. Krafft; F. Giulieri; T. Matsumoto; T. Tada. *Progr. Colloid & Polym. Sci.* **1997,** 106, p52.

T. Masui; K. Fujiwara; Y. M. Peng; T. Sakata; K. Machida; H. Mori; G. Adachi. *J. Alloy. Compd.,* **1998**, 269, (1-2), p116.

T. P. Hoar; J. H. Schulman. *Nature,* **1943**, 152, p102.

U. Batra; W. B. Russel; M. Pitsikalis; S. Sioula; J. W. Mays; J. S. Huang. *Macromolecules,* **1997**, 30, (20), p6120.

U. Batra; W. B. Russel; J. S. Huang. *Langmuir,* **1999**, 15, (11), p3718.

V. E. Serga; L. D. Kulikova; B. A. Purin. *Sep. Sci. Technol.,* **1999**, 35, (2), p299.

V. G. Babak; A. Langenfeld; N. Fa; M. J. Stebe. *Progr. Colloid & Polym. Sci.* **2001,** 118, (Trends in Colloid and Interface Science XV), p216.

V. K. Vanag; I. R. Epstein. *Phys. Rev. Lett.,* **2001**, 8722, (22).

V. Trappe; D. A. Weitz. *Phys. Rev. Lett.,* **2000**, 85, (2), p449.

V. Trappe; V. Prasad; L. Cipelletti; P. N. Segre; D. A. Weitz. *Nature,* **2001**, 411, (6839), p772.

W. B. Russel; D. A. Savill; W. R. Schowalter, *Colloidal Dispersions.* **1989**, Cambridge University Press: Cambridge, England.

W. Liang; T. F. Tadros; P. F. Luckham. *J. Colloid Interface Sci.,* **1992**, 153, (1), p131.

W. Meier. *Curr. Opin. Colloid Interface Sci.,* **1999**, 4, (1), p6.

W. Ming; F. N. Jones; S. K. Fu. *Macromol. Chem. Phys.,* **1998**, 199, (6), p1075.

W. Vanmegen; S. M. Underwood. *Phys. Rev. E,* **1994**, 49, (5), p4206.

X. Zhang; F. Zhang; K. Y. Chan. *Mater. Lett.*, **2004**, 58, (22-23), p2872.

Y. L. Khmelnitsky; R. Hilhorst; C. Veeger. *Eur. J. Biochem.*, **1988**, 176, (2), p265.

Zlochowe.Ia; J. H. Schulman. *J. Colloid Interface Sci.*, **1967**, 24, (1), p115.